Experimental studies of protozoan response to intense magnetic fields and forces

by

Karine Guevorkian

Sc. M., Brown University, 2002

Sc. M., Tehran University, 1999

B. Sc., Iran University of Science and Technology, 1996

Thesis

Submitted in partial fulfillment of the

requirements for the degree of Doctor of Philosophy

in the Department of Physics at Brown University

Providence, Rhode Island

May 1, 2006

Abstract of "Experimental studies of protozoan response to intense magnetic fields and forces" by Karine Guevorkian, Ph.D., Brown University, May 1, 2006.

Intense static magnetic fields of up to 31 Tesla were used as a novel tool to manipulate the swimming mechanics of unicellular organisms. It is shown that homogenous magnetic fields alter the swimming trajectories of the single cell protozoan *Paramecium caudatum*, by aligning them parallel to the applied field. Immobile neutrally buoyant paramecia also oriented in magnetic fields with similar rates as the motile ones. It was established that the magneto-orientation is mostly due to the magnetic torques acting on rigid structures in the cell body and therefore the response is a non-biological, passive response. From the orientation rate of paramecia in various magnetic field strengths, the average anisotropy of the diamagnetic susceptibility of the cell was estimated.

It has also been demonstrated that magnetic forces can be used to create increased, decreased and even inverted simulated gravity environments for the investigation of the gravi-responses of single cells. Since the mechanisms by which Earth's gravity affects cell functioning are still not fully understood, a number of methods to simulate different strength gravity environments, such as centrifugation, have been employed. Exploiting the ability to exert magnetic forces on weakly diamagnetic constituents of the cells, we were able to vary the gravity from -8 g to 10 g, where g is Earth's gravity. Investigations of the swimming response of paramecia in these simulated gravities revealed that they actively regulate their swimming speed to oppose the external force. This result is in agreement with centrifugation experiments, confirming the credibility of the technique. Moreover,

the *Paramecium*'s swimming ceased in simulated gravity of 10 g, indicating a maximum possible propulsion force of 0.7 nN. The magnetic force technique to simulate gravity is the only earthbound technique that can create increased and decreased simulated gravities in the same experimental setup. These findings establish a general technique for applying continuously variable forces to cells or cell populations suitable for exploring their force transduction mechanisms.

This dissertation by Karine Guevorkian is accepted in its present form by

the Department of Physics as satisfying the dissertation requirement

for the degree of Doctor of Philosophy.

Date _____   _____
                                       James M Valles, Jr., Director

Recommended to the Graduate Council

Date _____   _____
                                       Thomas R Powers, Reader

Date _____   _____
                                       Jay X Tang, Reader

Approved by the Graduate Council

Date _____   _____
                                       Sheila Bonde
                                  Dean of the Graduate School

iii

Vita

Author: Karine Guevorkian

Date of birth: 9/9/1973

Place of birth: Tehran, Iran

Citizenship: French

Education

- Ph.D. in Physics, Brown University, Providence RI, USA (2006)

- Sc. M. in Physics, Brown University, Providence RI, USA (2002)

- Sc. M. in Physics, Tehran University, Tehran, Iran (February 1999)

- B. S. in Physics, Iran University of Science and Technology (1996)

Honors

- Dissertation Fellowship, Brown University (Jan. 2005-May 2005)

- Student Travel Grants for the APS March Meeting (2005, 2006)

- Goloskie Fellowship, Brown University (Summer 2001)

- Best Bachelor in Physics Award, Iran University of Science and Technology (1996)

Publications

- K. Guevorkian and J. M. Valles, Jr., Aligning *Paramecium caudatum* with static magnetic fields, Biophysical Journal, 90, 3004-3011 (2006).

- K. Guevorkian and J. M. Valles, Jr., *In situ* imaging of microorganisms in intense magnetic fields, Review of Scientific Instruments, 76, 103706 (2005).

- K. Guevorkian and J. M. Valles, Jr., Varying the effective buoyancy of cells using magnetic forces, Applied Physics Letters 84(24), pp. 4863-4865 (2004).

- J. M. Valles, Jr. and K. Guevorkian, Manipulating cells with static magnetic fields, Material Processing in Magnetic Fields. Wanda H., Schneider-Muntau H. J., editors. World Scientific Publishing Co. Pte. Ltd. (2005).

- J. M. Valles, Jr. and K. Guevorkian, Low Gravity on Earth by Magnetic Levitation of Biological Material, Journal of Gravitational Physiology 9-11 (2002).

Acknowledgments

"A single hand can not clap". The completion of my thesis would not have been possible if it weren't for the support and the friendship of the following people.

I am sincerely grateful to my advisor James Valles for his patient guidance, encouragement and excellent mentorship throughout the course of this thesis. Jim's remarkable enthusiasm toward research, his excellent teaching and his ability to create a fun atmosphere in the lab made my experience as a graduate student one to always cherish and value. I am specially thankful to him for always giving me confidence and teaching me to be patient with the referees and see the bright side of things!

Special thanks to my two wonderful committee members Jay Tang and Tom Powers who have always been available to critically read my papers and give me their invaluable comments.

I would also like to thank Brown University for supporting me through the Dissertation fellowship. Also, my acknowledgments to the DC facilities of the National High Magnetic Field Laboratory in Florida for giving me the opportunity to use their facilities. Many thanks to Charlie Vickers and the machine shop at Brown University for their meticulous work in preparing parts of my apparatus.

Contents

⋆ Parts of this thesis has been previously published

List of Tables

List of Figures

Chapter 1

Introduction

With the growing application of magnetic fields in medicine, the questions regarding the effects and side effects of magnetic fields on living organisms become of vital relevance [109, 125]. The magnetic fields used in biomagnetic experiments can be static, alternating, homogenous or inhomogeneous depending on their application. There are several experimental studies that have suggested that static homogenous magnetic fields of up to a few Tesla (T) do not interfere drastically with the biological functioning of cells [85, 110]. There is also evidence however, that magnetic fields can couple with the organelles inside a cell and alter their long term development [140, 129, 101]. Several studies have reported that intense static magnetic fields on the order of a few Tesla align living cell or cell structures in a specific orientation with respect to magnetic fields [137, 120, 54]. These orientations are attributed to the interaction of the weak diamagnetic structures inside the cell with the strong magnetic fields. Unraveling the details of these orientations can lead to an understanding of how cells' development are altered in such fields. For example, Denegre and coworkers have shown that applying intense magnetic fields of up to 17 T alters the cleavage

planes in *Xenopus Laevis* embryos [28]. The alterations were attributed to the orientation of the mitotic structures by the strong magnetic fields [28, 126, 129].

In addition to magnetic torques, inhomogeneous magnetic fields offer the capability to manipulate cells or biological structures by applying forces to them. The ability to exert magnetic forces on biomaterials came to life after Beaugnon and Tournier [7] successfully levitated water and other organic materials using magnets which could produce field-field gradients of over 15 T^2 m^{-1}. This advance created opportunities to pursue earthbound investigations of the effects of simulated low gravity on a variety of systems such as crystalizing proteins [139, 70], liquid crystals [81, 82], and others.

Magnetic levitation also has great potential for the study of the gravitational sensitivity of living cells [36, 127, 66]. Since cells inhabit aqueous solutions, the similarity of the magnetic properties of water and cell components decrease the effects of magnetic forces on them. Therefore, methods to increase the magnetic forces by adding paramagnetic buffers to the solution have been found useful [56, 17, 136].

The motivation for these studies was to investigate the effects of magnetically simulated gravities on unicellular organisms. Earth's gravity exerts relatively weak forces of less than 10 pN directly on cells in biological systems. Nevertheless, it alters bone cell differentiation [55], modifies gene expression in renal cells [46], biases the orientation of swimming unicellular organisms [44, 77, 49], and alters cell signaling [23]. However, the mechanisms by which single cells can sense such small forces is not yet clear [60, 18, 45]. Using single cell microorganisms as a starting point for such investigations is extremely useful, since they provide us with information about how cells have evolved to function in the presence of earth's gravity.

The subject of our studies was the single cell ciliate, *Paramecium caudatum*. These eukaryotic cells have been invaluable as model systems for studying the effects of various stimuli on living cells. They exhibit a variety of "tactic" and "kinetic" behaviors in imposed fields [61]. They may change their swimming direction, modify their swimming speed, or modify the rate at which they change directions in response to chemical gradients [29, 131], variations in illumination [24, 57], gravity [77, 50, 97], and electric fields [73, 130, 80]. In Chapter 3 we give an introduction to the swimming mechanics of *Paramecium*. In later chapters we discuss the effects of magnetic fields and forces on the motility of *Paramecium*.

A number of methods to simulate different strength gravity environments, such as centrifugation, have been applied to research the gravitational sensitivity of protozoa. The technique we introduce to simulate gravity employs intense inhomogeneous magnetic fields to vary the effective buoyancy of cells. It will be shown in Chapter 6 that using the Magnetic Force Buoyancy Variation (MFBV) method, we can suspend non-swimming paramecia by creating zero buoyancy [42]. We are also able to force them to sediment, and even drive them to rise.

In Chapter 7, we present the application of MFBV, with some modifications, to create a wide range of increased, decreased and inverted effective gravities for the swimming gravisensitive *Paramecium*. We have found that *Paramecium* regulates its swimming speed with the applied gravity. Their inverted response to inverted gravity confirms that these cells are sensing gravity through their buoyancy. We also measure a threshold of their sensitivity to increased simulated gravity. At ten times their normal buoyancy, they cease advancing and "stall" *in situ*. This behavior suggests a maximum propulsion force of 0.7 nN.

This gravity simulation approach provides an alternative to existing "microgravity" simulation techniques such as rotating wall vessel suspension. Hence it can be applied for long term earth bound investigations of the source of the changes in osteoblast growth [55], gene expression [46] and cell signaling [23] that are induced by microgravity.

However, several questions surrounding MFBV technique needed to be answered. For example, what is the effect of the magnetic fields employed in this study on the motility of *Paramecium*? In Chapter 5 we introduce a detailed study of these effects. We found that the swimming trajectories of paramecia are altered by magnetic fields. However, we did not detect any change in their swimming speed. The orientation of their trajectories was attributed to the magnetic torques acting on the diamagnetically anisotropic structures in the cell body. The magneto-orientation of *Paramecium* is a perfect example of how we can use magnetic fields to orient cells and learn about the forces they can exert to counterbalance the external torques.

Chapter 2

Diamagnetic levitation

2.1 Introduction

In the early 1990's, Beaugnon and Tournier [8] were the first to levitate water and other organic material using inhomogenous magnetic fields. This advance gave rise to new opportunities for the study of organic material under simulated low gravity in conditions that did not need containers [36]. Although very intense magnetic field gradients are required for the levitation of organic materials, nowadays with superconducting magnet technology, it is even possible to carry out such experiments in one's own laboratory.

The experiments presented in this thesis were performed in two magnet systems. The first one, residing in the department of Physics of Brown University, was made by American Magnetics Inc., which is referred to from now on as the AMI magnet. The second system is at the National High Magnetic Field Laboratory (NHMFL), in Tallahaassee, Florida. The specifics of each magnet will be given when the experimental setups are introduced. In this chapter I will give a general introduction to the magnetic fields and forces produced

by a typical solenoid magnet system. Then the phenomenon of magnetic levitation will be described, and finally its direct use in determining the magnetic susceptibility of matter will be presented.

2.2   Overview of magnetic fields and forces

The design of a solenoid magnet depends on the application of the magnet. For experiments that require homogenous magnetic fields, such as NMR experiments, the magnet is designed such that the field varies as little as possible around the center of the magnet. On the contrary, for experiments that need magnetic forces, such as levitation, the magnet is design to provide a large field gradient, because the magnetic force, F_B, is proportional to $(\vec{B}\cdot\vec{\nabla})\vec{B}$. Nonetheless, one can still use the latter type of magnets to perform homogenous magnetic field experiments on small samples.

Fig. 2.1 shows the field profile of the AMI magnet. As can be seen, the field (green curve) is at its maximum value at the center of the magnet and it decays as we move away from the center. The profile of the field gradient (blue curve) is also plotted to show the variation of the field along the z axis. The behavior of the magnetic force is directly related to $B(z)B'(z)$ (prime denoting the derivative in the z direction). The inset of Fig. 2.2 shows that the force is zero at the center and there are two equidistant positions from the center with the strongest magnetic force. A sample placed at the center of the magnet will not feel a magnetic force and will only be subjected to static magnetic field. This position is often used as a control position.
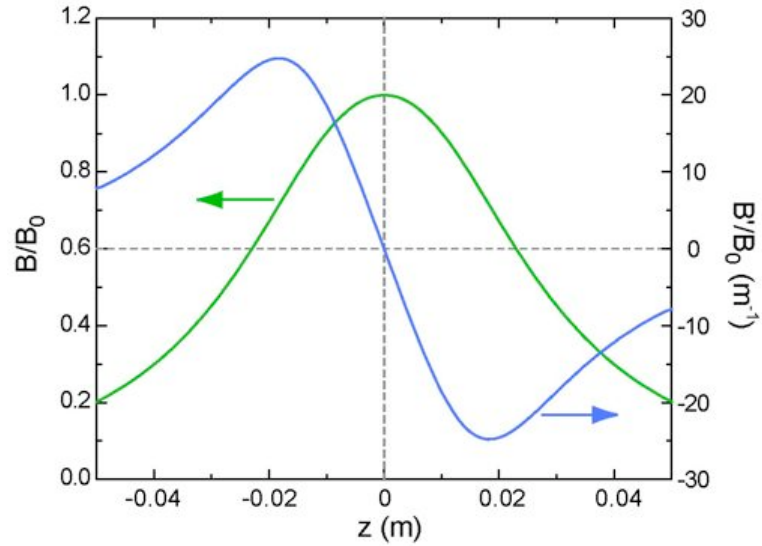
Figure 2.1: Normalized $B(z)$ and $B'(z)$ profile for AMI magnet. The values are normalized to the field strength at the center.

2.2.1 Diamagnetism and magnetic forces

Diamagnetism is an inherent property of matter. When materials are exposed to magnetic fields, the induced net magnetic moment due to the change in the motion of electrons in the valence band is such that it opposes the external magnetic field and the material is repelled by the field. This effect is very weak and is usually not observable with common magnets. Moreover, if the material has some kind of permanent magnetic moments, such as those due to the paramagnetism or ferromagnetism, then the diamagnetic response is screened and dominated by these other responses.

Contrary to common belief, biological matter does have magnetic properties. Since these materials are very weakly diamagnetic, intense magnetic fields are required to manipulate them. To acquire an idea of the magnitude of the fields and forces needed for magnetic manipulation of a biological matter, we start by calculating the potential energy per unit

volume, $U(z)$, of a weakly diamagnetic object in an axial field pointing in the z direction:

$$U_V(z) = -\frac{\chi}{2\mu_0}B^2(z) + \rho g z. \qquad (2.1)$$

The subscript V denotes per unit volume. The first term on the right is the magnetic energy of the object, where χ is the magnetic susceptibility and $\mu_0 = 4\pi \times 10^7$ H m^{-1} is the permeability of the vacuum. The second term represents the gravitational energy, where ρ is the density of the object, g is the gravitational acceleration, and z is the vertical position. Note that the magnetic susceptibility, χ, is a unit-less quantity. Its value, however, depends on the system of units used. For example $\chi(\text{SI}) = 4\pi\chi(\text{cgs})$. In the majority of this thesis, χ is in SI units, though to eliminate confusion, I will always mention the system of units used.

Using the term for energy, the force per unit volume acting on an object placed in an inhomogenous magnetic field is calculated as:

$$\vec{f}_V(z) = -\nabla U(z) = \frac{\chi}{\mu_0}B(z)B'(z)\hat{z} - \rho g \hat{z}, \qquad (2.2)$$

where $B'(z) = dB/dz$, note that the field varies only in the z direction. Figure 2.2 shows a schematic of the force direction and strength along the axis of the solenoid magnet. For a diamagnetic material placed above the center of the magnet, the total force is upwards and vice versa for the material below the center. The force per unit volume on a droplet of water as a function of position is shown in Fig. 2.2. This plot is based on the magnetic field profile of the AMI magnet at $B_0 = B(z = 0) = 9$ T. Levitation ($f_V(z) = 0$) occurs above the center of the magnet ($z > 0$) where the magnetic force is in the opposite direction of the gravitational force. The required $B(z)B'(z)$ for levitation is derived from

$$B(z)B'(z)|_{lev} = \rho g \frac{\mu_0}{\chi}. \qquad (2.3)$$
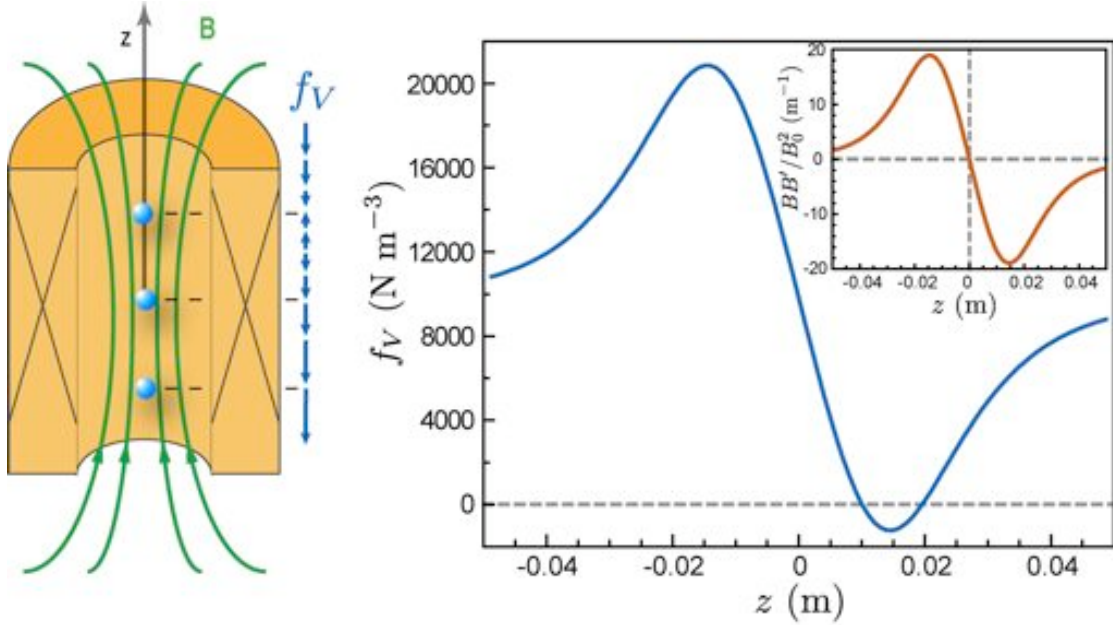
Figure 2.2: Force per volume profile for water. The levitation, $f_V = 0$, occurs at two positions, one of which is not stable

As an example of the field gradients needed to levitate biological matter we calculate the $B(z)B'(z)$ required to levitate a droplet of water. Using $\rho = 1000$ kg m^{-3}, $g = 9.81$ m s^{-2}, and $\chi = -9.04 \times 10^{-6}$ (SI), we get $B(z)B'(z)|_{lev} = -1363$ T^2 m^{-1}. This value can be achieved in the AMI magnet with $B_0 = 9$ T. As can be seen from Fig. 2.3, the levitation condition is satisfied at two vertical positions, one of which is not stable. In the next section, we will find the conditions for stable levitation and will display its application in the measurement of the magnetic susceptibility of matter.

2.2.2   Stable Levitation

The magnetic field produced by a solenoid is of the form: $\vec{B} = B(r,z)\hat{z}$ in cylindrical coordinates. The radial dependence is given by r and because there is rotational symmetry, there is no angular dependence. The radial variation of the field will create a radial force,

however small, which can potentially destabilize the levitated object by pushing it to the sides of the solenoid. Therefore, it is essential to find the conditions that create simultaneous horizontal and vertical stability [113, 10].

Starting from the potential energy:

$$U_V(r, z) = -\frac{\chi}{2\mu_0} B^2(r, z) + \rho g z. \tag{2.4}$$

For stable levitation, the energy should be minimum, therefore the force must be restoring. This gives the necessary condition for stability as

$$\oint \vec{f} \cdot d\vec{a} < 0. \tag{2.5}$$

where the integral is over a small closed surface with area unit vector $\vec{a}$. Using $\vec{f} = -\nabla U$ and the divergence theorem, $\oint f \cdot d\vec{a} = \int \nabla \cdot f dV$, we find

$$\nabla \cdot f < 0. \tag{2.6}$$

For diamagnetic materials where $\chi < 0$, the above condition using Eq. 2.4 is written as

$$\Rightarrow \nabla^2 B^2 > 0. \tag{2.7}$$

The sufficient condition for stable levitation is that the potential should increase in all directions from the levitation point. The conditions for vertical and horizontal stabilities are

$$\frac{\partial^2 B^2(r, z)}{\partial z^2} > 0 \quad \text{vertical stability} \tag{2.8}$$

$$\frac{\partial B^2(r, z)}{\partial r^2} + \frac{1}{r}\frac{\partial B(r, z)}{\partial r} > 0 \quad \text{horizontal stability}$$

We need to express these conditions in terms of the magnetic field on the axis, hence Taylor expansion of $\vec{B}$ around $r = 0$ is necessary. Instead of taking the Taylor expansion in vectorial

form, we simplify the problem by using a scalar potential. Since there is no current density $(\vec{J}(\vec{r}) = 0)$, Maxwell's equations take the form of:

$$\nabla \cdot \vec{B} = 0$$

$$\nabla \times \vec{B} = \vec{0}. \tag{2.9}$$

therefore we can introduce Φ as $\vec{B} = \vec{\nabla}\Phi$, and hence

$$\nabla^2 \Phi = 0. \tag{2.10}$$

The Taylor expansion of $\Phi(r, z)$ around $r = 0$ $(x = y = 0)$ leads to:

$$\Phi(r, z) = \Phi(0, z) + \left(\frac{\partial \Phi}{\partial x}\right)_{x=0} \Delta x + \left(\frac{\partial \Phi}{\partial y}\right)_{y=0} \Delta y$$
$$+ \frac{1}{2}\left(\frac{\partial^2 \Phi}{\partial x^2}\right)_{x=0} \Delta x^2 + \frac{1}{2}\left(\frac{\partial^2 \Phi}{\partial y^2}\right)_{y=0} \Delta y^2 + \cdots \tag{2.11}$$

The second and third terms are zero due to equilibrium conditions. Also using Eq.2.10 and the rotational symmetry condition

$$\frac{\partial^2 \Phi}{\partial x^2} = \frac{\partial^2 \Phi}{\partial y^2} = -\frac{1}{2}\frac{\partial^2 \Phi}{\partial z^2}, \tag{2.12}$$

Therefore $\Phi(r, z)$ simplifies as

$$\Phi(r, z) = \Phi(0, z) - \frac{1}{4}\left(\frac{\partial^2 \Phi}{\partial z^2}\right)_{r=0} r^2. \tag{2.13}$$

Now we can calculate B^2 using Eq. 2.13 which leads to the following expression:

$$B^2(r, z) = B^2(0, z) + \frac{1}{4}\left[B'^2(0, z) - 2B(0, z)B''(0, z)\right]r^2 \tag{2.14}$$

The stability conditions using Eq. 2.8 follow as:

$$k_v = B'^2(0, z) + B(0, z)B''(0, z) > 0 \quad \text{vertical stability} \tag{2.15}$$

$$k_h = \frac{1}{2}\left[B'^2(0, z) - 2B(0, z)B''(0, z)\right] > 0 \quad \text{horizontal stability} \tag{2.16}$$

k_v and k_h are the vertical and horizontal stability parameters. The plot of normalized k_v and k_h, for the AMI magnet is shown in Fig. 2.3. Depending on the strength of the magnetic field, we will have the following three different responses:

$$k_v > 0 \ \& \ k_h < 0 \ \text{object is levitated but pushed away from the axis} \tag{2.17}$$

$$k_v > 0 \ \& \ k_h > 0 \ \text{object is levitated on the axis}$$

$$k_v < 0 \ \& \ k_h > 0 \ \text{no levitation of the object}$$

It is useful to investigate the behavior of the potential energy landscape as a function of
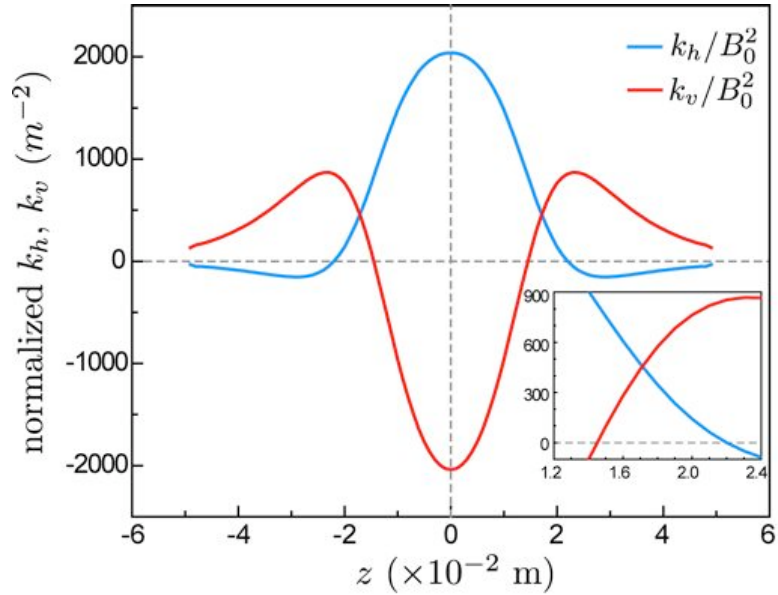
Figure 2.3: The normalized vertical and horizontal stability factors, k_v/B_0^2 and k_h/B_0^2. The inset shows the region of stable levitation.

the magnetic field. Using the expression for B^2 derived in Eq. 2.14, the total potential becomes:

$$U_V(r, z) = -\frac{\chi}{2\mu_0} \left[B^2(0, z) + \frac{1}{2} k_h r^2 \right] + \rho g z \tag{2.18}$$

Using the example of levitated water, Fig. 2.4(a) shows the energy landscape for a water

droplet in an inhomogenous magnetic field, when $B_0 = 9$ T. The minimum of the potential occurs where the levitation takes place. In Fig. 2.4(b), the contour plot of $U(r, z)$ is shown with the arrows pointing towards the lower energy position. In the next section, we will discuss how the position of the potential trap changes with changing B_0.

2.3 Drop-out method for Measuring χ

In this section we will introduce a method to measure the diamagnetic susceptibility of liquids or solids using the free levitation technique. In this technique, we first levitate the object by carefully placing it on a stick and inserting it into the magnet bore. We then remove the stick slowly. The object is (hopefully) levitated; if it is not levitated the reason might be that either B_0 is too high or too low. We adjust the B_0 and repeat until we succeed in levitating the object. In the case of liquids, we first freeze a droplet in liquid nitrogen and levitate the frozen droplet. We then wait a few seconds for the droplet to melt before carrying out the measurement.

Once the object is levitated, we reduce the magnetic field slowly, usually at a rate of 0.1 Amp s^{-1}. At some point, the droplet ceases levitating and drops out. This happens when the condition for vertical stability is no longer satisfied (refer to the lower threshold in Fig. 2.3). In other words, the potential trap moves down and then vanishes. This is shown in the sequence of images in Fig. 2.5 for a droplet of water. Since we know the exact position where the stability is lost, we can convert the current at which drop out occurs into BB', and from the levitation condition, Eq. 2.3, calculate χ of the object.

We have used this method to measure the diamagnetic susceptibility of Ficoll solutions.
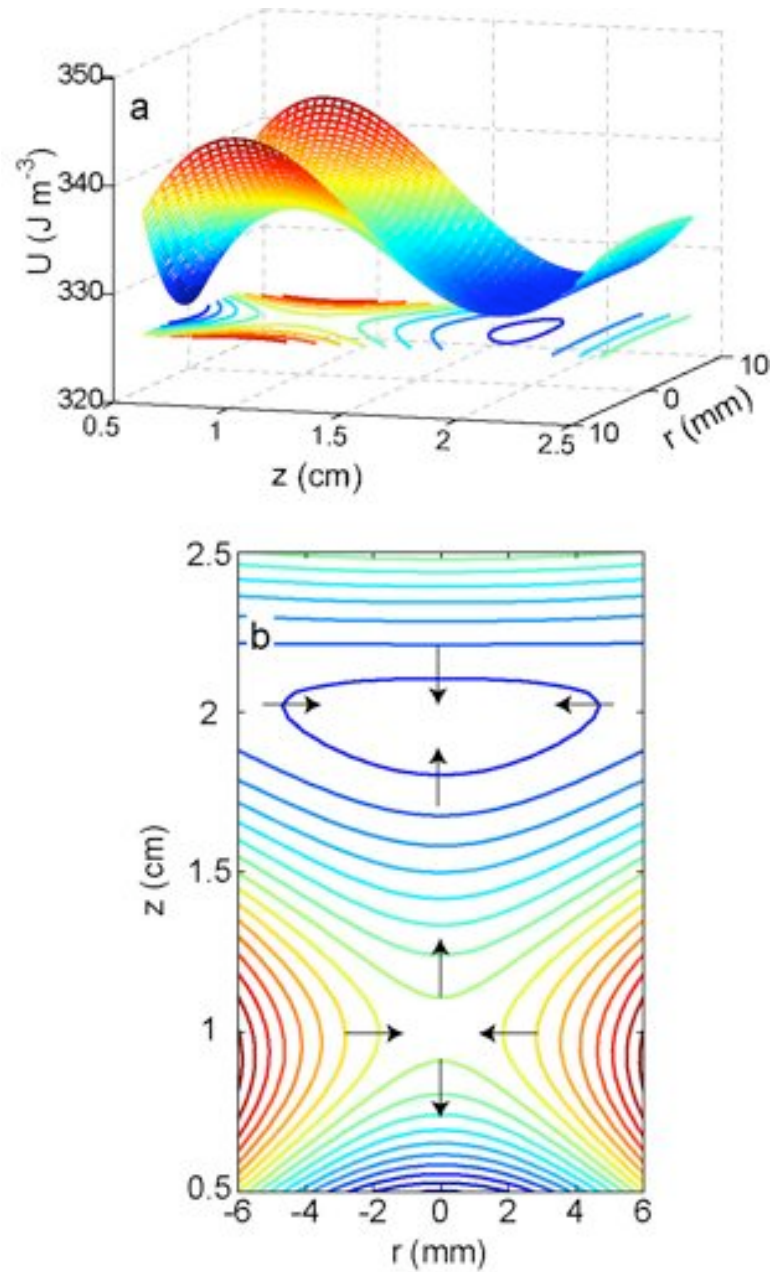
Figure 2.4: Potential energy and isopotential contours of water in inhomogenous magnetic field ($B_0 = 9$ T). (a) Potential energy landscape. (b) Potential contours. Arrows show the force direction. The contour separation is 1 J m^{-3} with the central one having $U = 328$ J m^{-3}
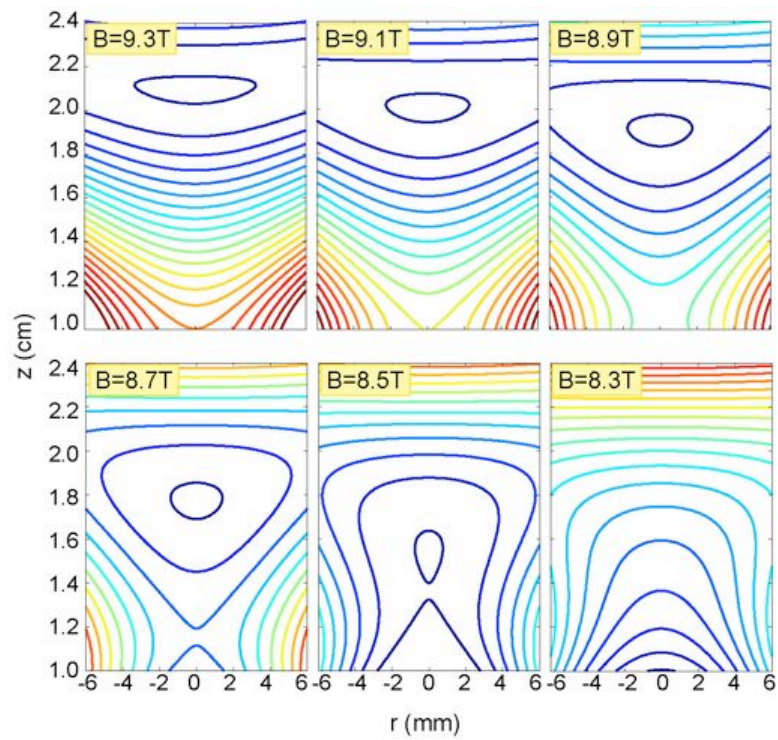
Figure 2.5: Potential contours of levitated water at various fields. As the field is lowered from the highest levitation field ($B_0 = 9.3$ T), the position of stable levitation which is the center of the closed contour, is lowered and eventually the stability condition is not met ($B_0 = 8.3$ T) and the droplet falls out

Ficoll is a water soluble polymer of sucrose, used extensively in biophysics to provide high density, high viscosity solutions. Susceptibility measurements were carried out for different concentrations of Ficoll in distilled water. The results are shown in Fig. 2.6. The fitted line gives χ_{Ficoll} as a function of concentration,

$$\chi_{Ficoll} = [-0.018C + (-9.045 \pm 0.005)] \times 10^{-6} \text{ (SI)} \tag{2.19}$$

where C is the concentration in percent. We will use this result in later chapters.
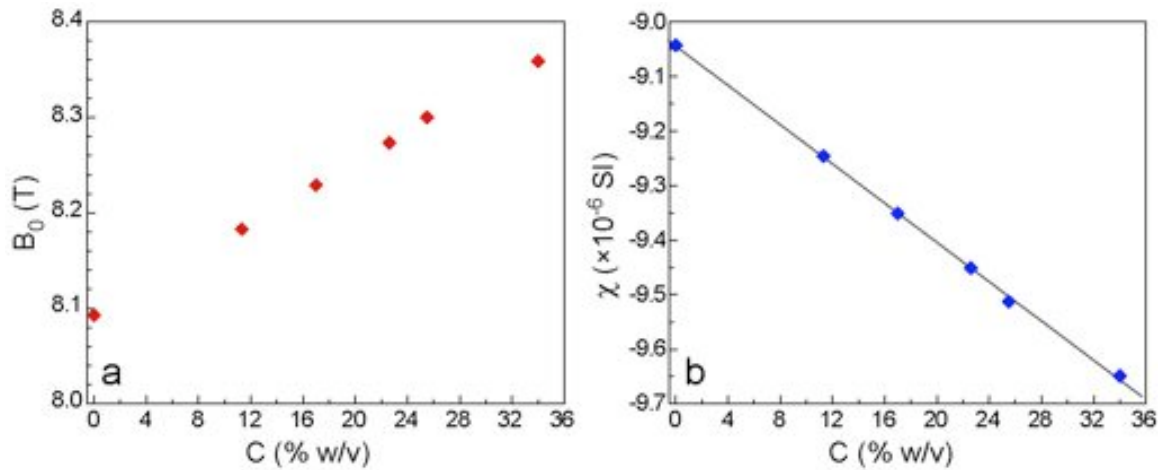
Figure 2.6: Magnetic susceptibility of Ficoll. (a) Measured drop out B_0's as a function of Ficoll concentration. (b) Calculated χ's of Ficoll as a function of concentration. All the values are scaled to χ of water

2.4 Magneto-Archimedes method for measuring χ

It is not always possible to use the drop out method for measuring χ. For example, since paramagnetic materials are attracted to the magnet $(\chi > 0)$, they can not be levitated stably. One of the useful alternative methods is based on the Magneto-Archimèdes principle [56]. A diamagnetic or paramagnetic material with known density, ρ_o, and susceptibility,

χ_o, is levitated (i.e. made neutrally buoyant) in a solution with density, ρ_{sol}, and unknown susceptibility, χ_{sol}. The total buoyant force per volume is now the superposition of the forces on the solution, plus the forces on the object,

$$f = \rho_o g - \frac{\chi_o}{\mu_0} BB' - (\rho_{sol} g - \frac{\chi_{sol}}{\mu_0} BB'). \tag{2.20}$$

Rearranging the above equation and imposing the levitation condition, $f = 0$, we obtain the unknown susceptibility in terms of the other parameters:

$$\chi_{sol} = \chi_o - \frac{\mu_0}{BB'} \Delta \rho g. \tag{2.21}$$

where $\Delta \rho = \rho_o - \rho_{sol}$.

We have used this approach to measure the susceptibility of Gadolinium-diethylene-triamine-pentaacetate (Gd-DTPA) solutions. Gd-DTPA is a paramagnetic salt that is used as an NMR contrast enhancing agent. We will discuss its application to our experiments in Chapter 7. Using the approach discussed above, we levitated a known element in various concentrations of Gd-DTPA to measure the χ of Gd-DTPA as a function of its concentration. A Bismute (Bi) shot with density 9800 kg m^{-3} and susceptibility -16.6$\times 10^{-5}$ (SI) was levitated in Gd-DTPA solutions with various concentrations in *Paramecium*'s standard solution (1 mM CaCl$_2$, 1 mM KCl, 0.1 mM MgSO$_4$, 1.5 mM MOPS, pH 7.2). The density of the solution is equal to that of water (1000 kg m^{-3}). For each measurement the position of sample cell inside the magnet was unchanged. We simply changed the solution and varied BB' until the Bi shot was levitated. The calibration was done by scaling the measured levitation BB' of Bi in water by the estimated one. Figure 2.7 shows the magnetic susceptibility of Gd-DTPA solution as a function of its concentration measured with this technique. The fitted line in Fig. 2.7 is given by:
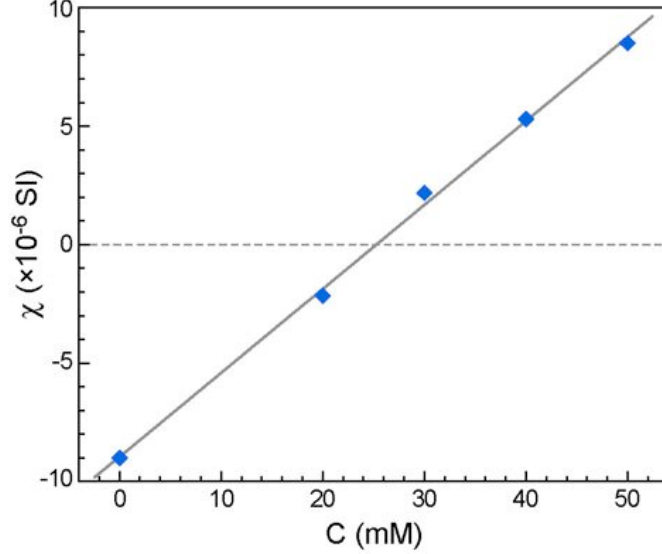
Figure 2.7: Magnetic susceptibility of Gd-DTPA at different concentrations. All values are scaled to χ of water

$$\chi = [(0.35 \pm 0.01)C - (8.95 \pm 0.32)] \times 10^{-6} \text{ (SI)} \tag{2.22}$$

where C is the concentration of Gd-DTPA in mM and χ is the magnetic susceptibility of Gd-DTPA solution in SI units. We compare the result of this measurement to the value for $\chi_{Gd-DTPA}$ that has been provided by the manufacturer. The published molar magnetic susceptibility, $\chi_{mol} = 2.8 \times 10^{-2}$ cm^3 mol^{-1} [136] which is related to the conventional unitless χ through: $\chi = \chi_{mol}\rho/MW$, where ρ is the density and MW is the molar weight of the substance. Since the magnetic properties of Gd-DTPA are mostly due the free electrons in the Gd atom, we therefore use the density and the molar weight of Gd, that is, $\rho_{Gd} = 7900$ kg m^{-3} and MW$_{Gd} = 0.157$ kg/mol, in our estimations. Hence we get $\chi_{Gd-DTPA} = 1.77 \times 10^{-2}$. For an arbitrary concentration of Gd-DTPA, χ of the solution

is calculated as:

$$\chi_{sol} \quad = \quad \frac{V_{Gd}}{V_{total}}\chi_{Gd} + \frac{V_{water}}{V_{total}}\chi_{water} \tag{2.23}$$

$$\chi_{sol} \quad = \quad [0.35C - 9.04] \times 10^{-6} \text{ (SI)} \tag{2.24}$$

where C is the mM concentration. Comparing this to our measured data given by Eq. 2.22, we find that within the measurement error the results are in good agreement.

This demonstration validates the use of magnetic levitation for measuring the magnetic susceptibility of even paramagnetic material. The application of these measurements will be clarified in Chapter 7.

Chapter 3

Paramecium caudatum

3.1 Introduction

Paramecium is a single cell eukaryote mostly found in ponds. It feeds on bacteria found in decaying vegetation. Its reactions to external stimuli such as chemical gradients and electric fields, among others, have attracted the attention of biologists for over a century. For example, the swimming speed and/or orientation of *Paramecium* change when it is exposed to chemical gradients [131, 132], heat [72], light [95] and gravity [77]. Among various species of *Paramecium*, *P. caudatum*, is the one often used in biological research because of the existing knowledge about its genetics and the availability of various mutants. They are used as a model cell for the study of signal transduction and ciliary motion in unicellular organisms.

In the work presented in this thesis we are interested in the response of swimming paramecia to static magnetic fields and magnetically simulated gravities. General introduction to *Paramecium* and the mechanisms by which it responds to external stimuli follows.

3.2 Morphology

P. caudatum has an ellipsoidal shape with a more or less circular cross section. Its posterior is slightly larger than its anterior. The length of the cell varies from 180 μm to 220 μm and the radius of its cross section is about 40 μm. The density of the cell is about 1040 kg m^{-3}.

A schematic picture of *P. caudatum* is shown in Fig. 3.1, along with its various components. The external layer, known as the cortex, is a 4 μm thick complex comprising several important structures of the cell. It is considered a "flexible cell skeleton" in that it has the ability to bend to allow cell movements, but on the other hand it can keep its shape. The cortex can be divided into three layers: (1) the plasma membrane, which is the very thin outmost layer of the cortex enveloping the whole cell, (2) the pellicle, a hexagonal array of fibers with each cilium at the center of the unit cells, and (3) the ectoplasm, the innermost layer, which is the more rigid part of the cytoplasm comprising a large array of microtubules and actin filaments. The more fluid-like part of the cytoplasm called endoplasm and contains the nuclei, the food vacuoles, the contractile vacuoles and other organelles.

3.2.1 Components in the cortex

Perhaps the most important components of the cortex are the cilia. They are the hair like structures that cover the whole cell body and are in charge of propelling the *Paramecium*. The cilia are arranged in an organized pattern which can be seen in the scanning electron micrograph of Fig. 3.2. The length of the cilia are mostly uniform, about 10-12 μm. However, the cilia at the extreme posterior part, which has an area with a radius of 10 μm are longer (16 μm). The cilia at the oral groove have variations in their length. A typical *P.*
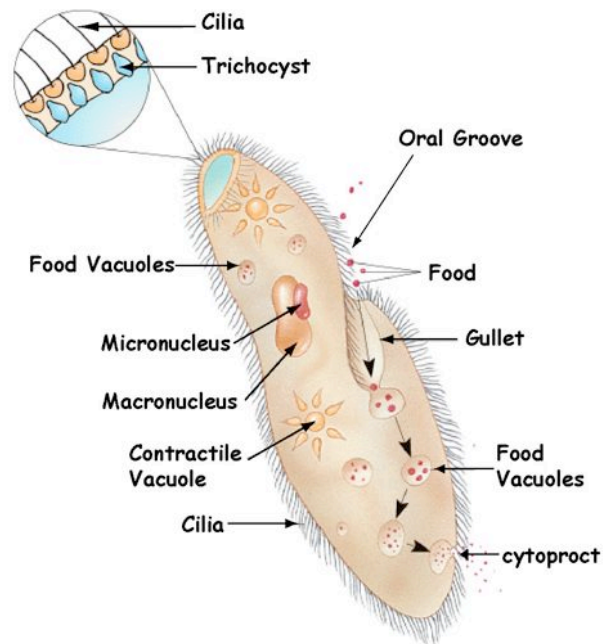
Figure 3.1: A schematic drawing of *Paramecium* showing various components of the cell. (Image by Kalle Olli, http://moritz.botany.ut.ee/ olli)

caudatum cell is covered by about 3000-4000 cilia. More information about cilia will be given in section 3.3.

Trichocystses are rigid structures that have a length of 3-4 μm and appear as fusiform. They are arranged evenly in a single layer imbedded in the ectoplasm, just beneath the cilia. They are known as extrusive organelles, which means that upon stimulation, they extrude partially or completely. It is believed that *Paramecium* fires trichocysts as a defense mechanism when mechanically injured or subjected to chemical or electrical shock. Sometimes, the trichocysts are partially or completely extruded (maximum length 40 μm) but stay attached to the membrane, and sometimes they are freed from the body. [135, 59]

The fibrillar system beneath the pellicle is comprised of two highly ordered arrays of fibrils: the interciliary fibrils that connect the ends of the cilia to one another and the

infraciliary network that provides the elasticity, contractility and mechanical support of the

cell.
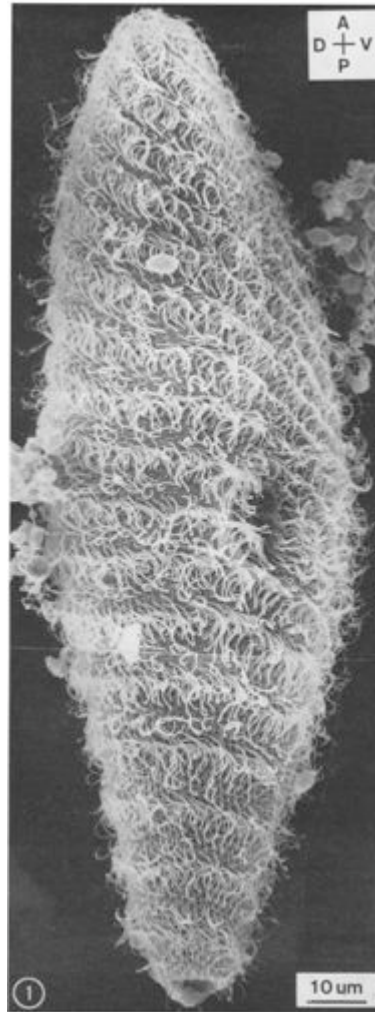
Figure 3.2: Scanning electron-micrograph of a freeze dried *Paramecium* showing the cilia covering the cell body. The oral groove can be seen on the right. A-P (anterio-posterior) and D-V (dorso-ventral). (Picture from S. L. Tamm, J. Cell. Biol. 55 (250-255), 1972)

3.2.2 Organelles in the endoplasm

Just beneath the endoplasm, two contractile vacuoles are located on the dorsal sides of

the cell. They independently contract to pump water out of the cell to keep the osmotic

pressure regulated. The filling of each vacuole takes about 8 s followed by a fast contraction of 1 s. It is not clear whether other products of metabolic activity such as carbon dioxide are also expelled by the vacuoles. [135]

Food enters the cells through a large opening on the ventral side, called the oral groove. The oral groove has a twist towards the left starting at the anterior and continuing to the middle of the cell (Fig.3.1). All surfaces around the oral groove are covered with cilia that push the food inside the gullet. Once the food concentration at the end of the gullet reaches a specific concentration, food vacuoles form (Fig.3.1). Then they disperse inside the cytoplasm and nurture the cell. Afterwards, the waste is expelled from the cytoproct located at the end of the cell.

A large number of crystals and crystalline granules are also found inside the cell. They are concentrated at both ends of the cell and distributed throughout the endoplasm. They are thought to be related to cell nutrition. They disappear when the cell is starving and reappear when food is available. The endoplasm also contains the nuclear apparatus. *P. caudatum* has a large macronucleus and one micronucleus. Both are fixed in position and do not move in the endoplasm. The macronucleus is in charge of metabolic activities, growth and morphogenesis of the cell. A *Paramecium* cell can not survive for long without a macronucleus. On the other hand, the role of the micronucleus is vague. A cell can survive and carry on its vegetative reproduction without a micronucleus for a sustained time. It has been observed that during the sexual reproduction the micronucleus is involved and a cell can not have genetic exchange through conjugation if it lacks a micronucleus. [135]

3.3 Swimming of *Paramecium*

Paramecium swims by beating its cilia and achieves speeds varying between 600-1000 μm s^{-1}. In general as the size of a swimming cell diminishes, the effect of viscous drag becomes more important. To determine the influence of viscosity on the motility of small organisms, the Reynolds number, which describes the ratio of the inertial force to the viscous force is used:

$$Re = lv\rho_s/\eta, \tag{3.1}$$

where for a microorganism, l is a characteristic dimension of the cell, v is the swimming speed, and ρ_s and η are the density and the viscosity of the solution, respectively. For a *Paramecium* swimming in water, $Re \approx 10^{-1}$, using the approximate values of $l = 80$ μm, $v = 600$ μm s^{-1}, $\rho = 1000$ kg m^{-3} and $\eta = 10^{-3}$ Pa s. This low Re number shows that the *Paramecium* can not acquire any inertia and has to overcome the effects of viscosity with every stroke. To do so, it has to employ a swimming pattern that breaks the symmetry of the motion. This is done by the two phases of the cilia beating as described in the next section.

In general, the stroke direction of the cilia is towards the posterior of the cell, which consequently pushes the *Paramecium* forward with a speed, v_p. However, as it is shown schematically in Fig. 3.3(a), the beating of cilia is oblique, to the right. This inclination makes the *Paramecium* rotate clockwise around its anterio-posterior (A-P) axis with a speed, ω_3, while it is moving forward (Fig. 3.3(b)). Moreover, the organism also rotates around its Left-Right (L-R) axis with a rotational speed ω_2 (Fig. 3.3(c)). It is believed that this is due to the more effective beating of the cilia around the oral groove [61, 93].

The superposition of the one translation and the two rotations produce a helical swimming pattern [61] as shown in Fig. 3.3(d). The rotation along the A-P axis is such that the ventral side (oral groove) is always facing the axis of the helix, this is shown by the grey pattern in Fig. 3.3(d).

Under natural conditions, for a forward moving cell, the ciliary beating direction is to the posterior-right and the frequency of beating is about 15 Hz. Various effects, such as a change in the chemical properties of the medium, or applying an external electric field, can change the beating direction and/or the frequency which will manifest in a change in the amplitude and the pitch of the helical path. To understand better the mechanism of swimming, we need to know how an individual cilium beats.

3.3.1 Cilia and metachronal coordination

A cilium has a 9+2 microtubule structure. Two central single microtubules are encircled by nine doublets, as shown in Fig.3.4. A cilium measures 12-15 μm long and about 0.25 μm in diameter. The movement of a cilium is achieved by the sliding of a few of the outer doublets with respect to the neighboring filaments through dynein arms [38, 21]. The hydrolysis of ATP molecules is the energy source for the unidirectional motion of the dynein molecular motors [108]. The beating of a cilium has two phases, the *effective stroke* and the *recovery stroke*. As the name suggests, the effective stroke is responsible for the forward movement of the organism. During this phase, the cilium is almost straight and it moves through the fluid similar to an oar. In the recovery stroke, the cilium bends while gyrating counterclockwise (viewed from above) and comes back to its original position. Figure 3.5(a) is a cartoon of the two phases of a complete stroke. Figure 3.5(b) is a photograph of the beating of the
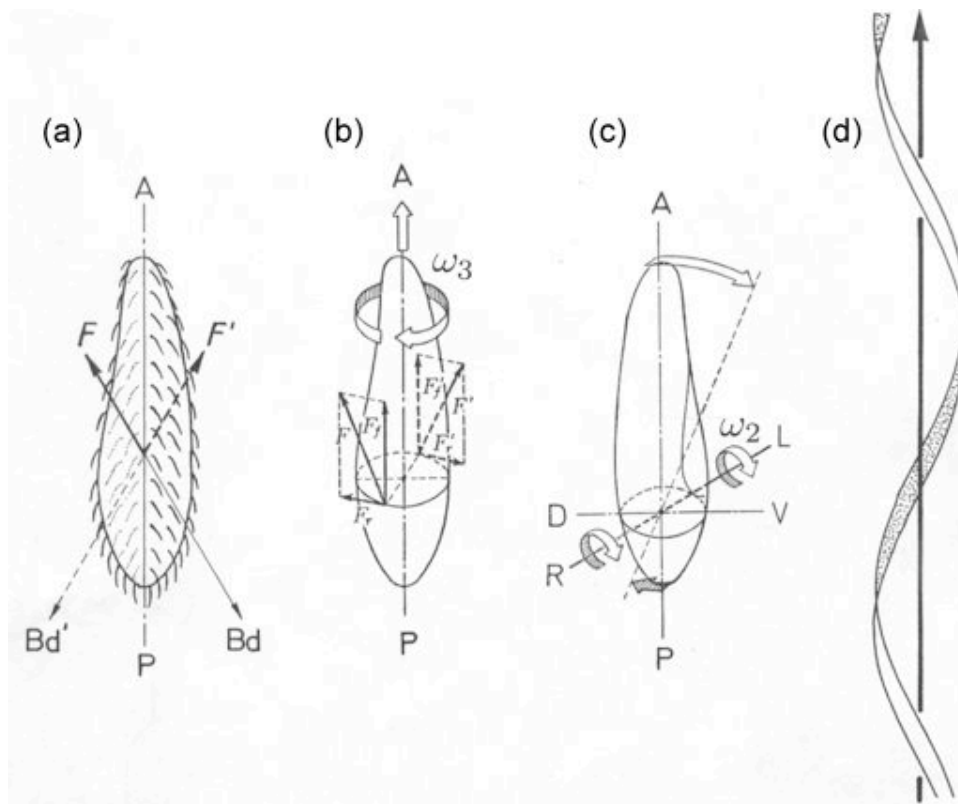
Figure 3.3: Motion of *Paramecium*. (a) The beating direction (Bd) has an angle with the Anterio-posterior (A-P) axis. Hence there is an angle between the forward propulsion force (F) with A-P axis. The dashed arrows show the back side of the cell. (b) the propulsion force has a component parallel to the A-P axis, responsible for the forward motion and a component perpendicular to the A-P axis. The latter rotates the cell around the A-P axis with velocity ω_3. (c) The variation in beating direction and strength at different parts of the cell give rise to another rotation around the Left-Right (L-R) axis. (d) Helical swimming trajectory. The Oral groove, shown as dotted pattern, is always facing the inside of the helix. (Nakaoka, *et al.*, J. of Physiol. 31 1984)

cilia. Low Re number hydrodynamic calculations of a stick reveal that the larger fluid drag on the cilium during the effective stroke compared to the fluid drag during the recovery stroke results in the organism's advance [21].
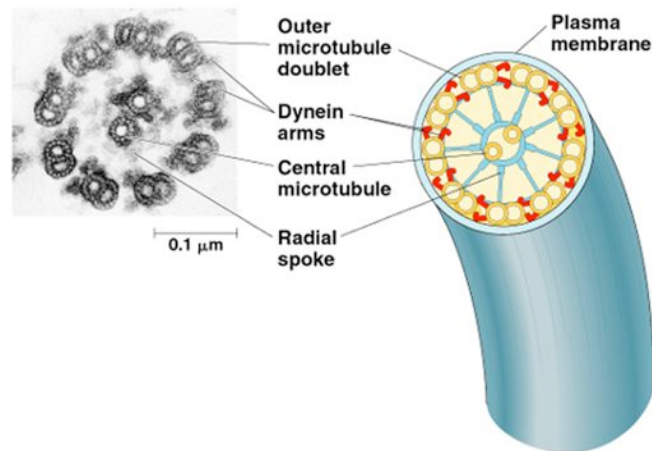
Figure 3.4: 9+2 structure of a cilium. The EM picture of the cross section of a cilium showing the microtubules and the dynein arms. On the right, a schematic of all the components of a cilium is drawn. (Picture taken from *Biology* by N. A. Campbell and J. B. Reese, copyrighted by Addison Wesley Longman Inc., 2002)

From observations of the position and shape of cilia during the effective and recovery strokes, the work done by one cilium in a whole cycle is estimated to be about 10^{-15} Joules. Interestingly, the hydrodynamic coupling of the cilia reduces the work done by each cilium during a beat cycle, as calculated by simulations. The results shows that for a row of 100 cilia, the average work done per cilium, per cycle can decrease by up to three times, depending on the interciliary spacing, compared to a single cilium. The efficiency of a cilium is expected to increase further for the realistic configuration of thousands of cilia on the surface of a cell. [40] Cilia, in general, beat in a coordinated manner such that the movement of the tip of the cilia form a wave pattern termed metachronism. This metachronal pattern is developed as a result of a constant phase difference between neighboring cilia (Fig. 3.5 (c)
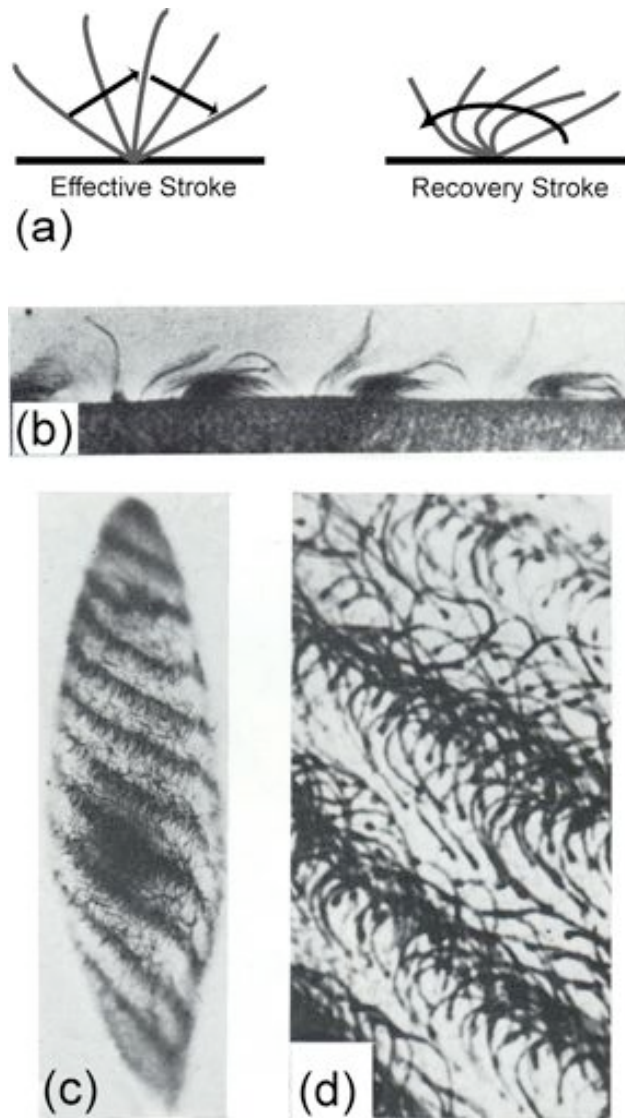
Figure 3.5: The beating of cilia. (a) A cartoon of the effective and recovery strokes. (b) Beating cycle. (c) Metachronal wave pattern. (d) The dark sections corresponding to the recovery stroke. (Figs b-d from *Paramecium, A Current Survey*, edited by W. J. Wagtendonk, 1974.)

and (d)). For *Paramecium*, the speed of the propagation of the wave is about 1 μm ms^{-1} [30] and the direction of the propagation is opposite to the direction of the power stroke and has an angle to it [59]. Local perturbations of the membrane, due to external stimulation, produce a local change in the beating of cilia that then propagates along the cell. For example, when a *Paramecium* bumps into a mechanical obstacle or a poisonous chemical environment, it swims backward by changing the direction of the cilia beating. Then, it pivots clockwise about its posterior and randomly chooses a new direction in which to swim. It repeats these steps until it escapes the trap. This behavior was first observed by Jennings, who named it the "avoiding reaction" depicted in Fig.3.6 [61]. He also observed that a "push" to the posterior of the cell increases the forward swimming speed.
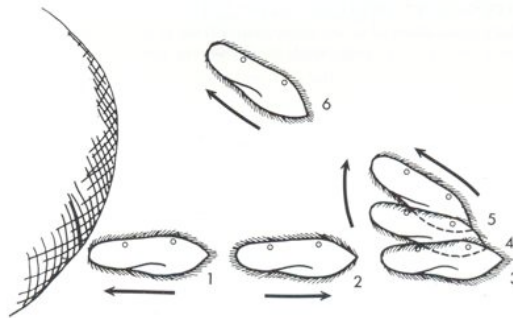
Figure 3.6: The avoiding reaction of *Paramecium* upon bumping into an obstacle. Notice the change in beating of the cilia. (Figure from *Behaviour of Lower Organisms* by H. S. Jennings, 1962).

It was proposed that the fibrillar network existing in the cortex propagates an electrical signal from one end of the cell to the other end and this potential difference creates a coordination in the beating pattern. However, experiments have shown that even after the destruction of the network, the metachrony persists [91]. Moreover, measurements of the membrane potential at both ends of *Paramecium* have shown that the electrical signal

spreads at a rate that is one hundred times faster than the metachronal wave propagation [30] and therefore the fibrilar network has no role in metachronal coordination.

Currently, the most probable explanation for the formation of metachronal pattern is hydrodynamic coupling between cilia [41, 62, 37]. Early experiments addressing this issue have shown that changing the viscosity of the medium in which paramecia swim affects the velocity and the direction of the metachronal waves. These observations suggest that hydrodynamics play a role in the metachronal coordination [71, 114] .

3.3.2 Membrane potential and ciliary beating

Extensive studies have revealed that the ciliary beating is directly controlled by the membrane potential, E_m. Two Ca^{++} and K^+ ion "batteries", denoted by E_{Ca} and E_K, respectively, provide the membrane potential of a *Paramecium* cell. In normal conditions, the concentration of Ca^{++} ions inside the cell is much lower than the outside with a ratio of $[Ca]_{out} / [Ca]_{in} = 10^4$. Whereas for K^+, the ratio is $[K]_{out} / [K]_{in} = 1/40$. At equilibrium, $E_m = -29$ mV, which means the inside of the cell is more negative that the outside. It can be expressed as [4]

$$E_m = \frac{g_K}{g_K + g_{Ca}} E_K + \frac{g_{Ca}}{g_K + g_{Ca}} E_{Ca} \tag{3.2}$$

where membrane conductance for Ca^{++} and K^+ ions, denoted by g_{Ca} and g_K, is related to the number of open channels for each of these ions. E_K and E_{Ca} are given by the Nernst equation

$$E_C = \frac{k_B T}{ze} \ln \frac{[C]_{out}}{[C]_{in}} \tag{3.3}$$

where $k_B T$ is the thermal energy, z is the valence, e is the charge of the electron, and $[C]_{in}$ and $[C]_{out}$ are the inside and outside ion concentrations. Given the concentrations of Ca^{++}

and K$^+$, $E_K = -81$ mV and $E_{Ca} = 116$ mV. From the measured value of $E_m = -29$ mV, $g_{\text{Ca}} = 0.4 \times g_{\text{K}}$ under natural conditions. If for any reason the membrane becomes more permeable to either one of these ions, the membrane potential will change and hence the ciliary beating will be modified.

A series of experiments performed by Naitoh and Eckert [90, 91, 30] have provided evidence that ciliary beating is directly controlled by the membrane potential. By using bioelectric measurements on a mechanically stabilized *Paramecium*, they found that when the anterior of the cell is stimulated by applying a controlled mechanical pulse using a piezoelectric transducer, the membrane becomes transiently depolarized. On the other hand, when the posterior of the cell is stimulated, the membrane becomes transiently hyperpolarized. The membrane potential was measured by micro-electrodes inserted in the cell and the degree of polarization was found to be different for each stimulation. Their data suggested that the posterior end is more sensitive to mechanical stimulation than the anterior end.

It was also established by by Naitoh and Eckert that the anterior stimulation increased the permeability of the membrane to Ca^{++} ions, through opening of mechanosensitive ion channels. This initial depolarization activates the voltage sensitive Ca^{++} ion channels, facilitating the influx of Ca^{++} ions. This influx further depolarizes the cell, shifting the direction of effective stroke counterclockwise and decreasing the beating frequency (measured by imaging the methachronal wave frequency, Fig.3.5(c and d). If the depolarization reaches a threshold value from -29 mV to 5 mV [73], it triggers ciliary reversal, which results in the backward swimming of the organism and increases the beating frequency. Similarly, posterior stimulation increases the permeability of the membrane to K$^+$ ions, causing an

out-flux of K^+ ions, which results in hyperpolarization of the membrane. Hyperpolarization increases the beat frequency and results in increased forward swimming. They did not observe any change in beating pattern when the middle section of the *Paramecium* cell was stimulated. From these essays they concluded that Ca^{++} ion channels are mostly located in the anterior section of the cell and K^+ ion channels are distributed in the posterior side with the middle section having evenly distributed channels.

Based on the above mentioned studies, the beating of the cilia is regulated by two separate but loosely connected mechanisms [93]: a change in the beating direction and a change in the beating frequency. In principle, these effects can be distinguished by studying the helical swimming trajectory of a specimen. Upon hyperpolarization a clockwise rotation of the beating direction, which makes the beating more parallel to the cell body, increases v_p and decreases ω_3. This effect results in a helical path with a longer pitch. Inversely, counterclockwise orientation of beating (depolarization), decreases v_p and therefore the pitch of the helical path is shortened. An increase in beating frequency does not affect the pitch of the helix, since it increases both v_p and ω_3. The reports on the effects of altered beating frequency on the amplitude of the helical path are inconsistent. In one study [89], it is described that an increase in the beating frequency, upon hyperpolarization, increases the amplitude of the helical path while in the other [78], the opposite is presented. It remains to be confirmed which of these responses is correct.

3.4 Mechanosensitive ion channels

So far we have introduced how in general a mechanical stimulus can induce a swimming response in *Paramecium*. The mechanical stimuli discussed so far clearly deform [90] the membrane of the cell and therefore activate mechanosensitive ion channels. One of the controversial questions that remains under investigation is at which lowest threshold a mechanosensitive, or stretch sensitive ions channel, is activated [45, 60]. In prokaryotic cells such as *Escherichia coli* bacteria, the Mechanosensitive channel Large (MscL) has been studied extensively. The function of these channels is to control the osmotic pressure inside the cell. The pressure range that activate MscL-s are on the order of kPa [45]. Considering the purpose of these channels, the sensitivity to such high pressures is explainable. However, studies have shown that for eukaryotic cells such as osteoblast cells [18], the membrane tension required to activate the mechanosensitive channels are two orders of magnitude lower than in prokaryotic cells. Even lower pressure thresholds (< 1 Pa) have been detected in endothelial cell and neurophils (see Refs.[60, 64, 45] for reviews). While the channels in prokaryotic and eukaryotic cells have very similar structures they have evolved to sense different ranges of forces because their functions differ.

Paramecium is known for sensing the force of gravity both by adjusting its orientation (gravitaxis) and also by adjusting its swimming speed (gravikinesis). It orients with its anterior end up and swims to the top of the container in search of food. Surprisingly, it does not possess any specific gravisensing organelles, such as amyloplasts, as do plant cells [5]. It has been suggested that the weight of the cell on the membrane acts as the gravisensing organelle [75]. A simple calculation shows that for *Paramecium*, the apparent

weight is:

$$w = \Delta\rho V g \approx 80 \text{ pN} \tag{3.4}$$

where $\Delta\rho = 40$ kg m^{-3}, given that the density of *Paramecium* is 1040 kg m^{-3} [65], and V is the volume. Throughout this thesis we approximate a *Paramecium* cell as a solid ellipsoid of revolution with minor axis $a = 20 \pm 5$ μm and $b = 100 \pm 10$ μm. Therefore $V = 4\pi a^2 b/3 = 1.7 \times 10^{-13}$ m^3. For a vertically swimming *Paramecium*, the pressure due to this force on the posterior (or anterior) part of the membrane considering a circular cross section with a radius of 20 μm, is only 60 mPa. This pressure is very small and the mechanisms by which the cell can sense these small forces is still unclear [27, 2].

Chapter 4

Experimental Setup

4.1   Introduction

The setups for experiments that require *in situ* visualization of objects inside a magnet have to overcome the challenges of developing an optical system that fits within the limited space provided inside a magnet bore. Moreover, the optical performance should not be compromised by the interaction of the strong magnetic fields with the optical components. A few microscope systems with these characteristics have been previously developed. Yanagiya *et al* [138] used an infinity corrected objective and a CCD camera to visualize crystal growth in intense magnetic fields. The system fit within a very small bore and had an optical axis parallel to the magnetic field direction. Valles and coworkers [128] designed a system with an optical axis that could be parallel or perpendicular to the magnetic field direction. The system was relatively large and made to fit within the 195 mm bore resistive magnet at the National High Magnetic Field Laboratory (NHMFL), in Tallahaassee Florida.

   In this chapter, a description of the experimental setups used for the *in situ* visualization

of swimming microorganisms inside two different magnet systems is detailed. The first magnet system is located at NHMFL. The second one, the AMI magnet, resides in the department of Physics of Brown University.

4.2 NHMFL magnet and setup [43]

The NHMFL system was designed specifically for the *in situ* visualization of swimming *Paramecium caudatum* in a 50 mm bore resistive magnet at the NHMFL facilities [11]. The maximum field available is 31 T and maximum BB' is about 5000 T^2 m^{-1}. The force homogeneity is 3% over a $(5mm)^3$ volume. Figure 4.1 shows the normalized B and BB' for this magnet. The main goal was to provide a side view visualization of a sample that was positioned parallel to the magnetic field. Figure 4.2 shows a photograph and a schematic of the magnet. Access to the magnetic field is provided from the top section, however one can adjust the vertical positioning of the setup from the bottom section. The other system requirements were a resolution of better than 40 μm, a field of view (FOV) of at least 4 mm in diameter, and temperature stability to better than a fraction of 1°C. Additionally, we needed to record the motion of the organisms in order to track them. The apparatus is composed of three main parts: I) the optics and illumination, II) the temperature control, and III) the support structure.

4.2.1 Optics and illumination

Figure 4.3 shows the various components of the experimental setup. A 6 mm diameter side view borescope (B) (Instrument Technology, Inc., Westfield, MA) served as the main optical component. It was chosen for the weak magnetization of its body and components,
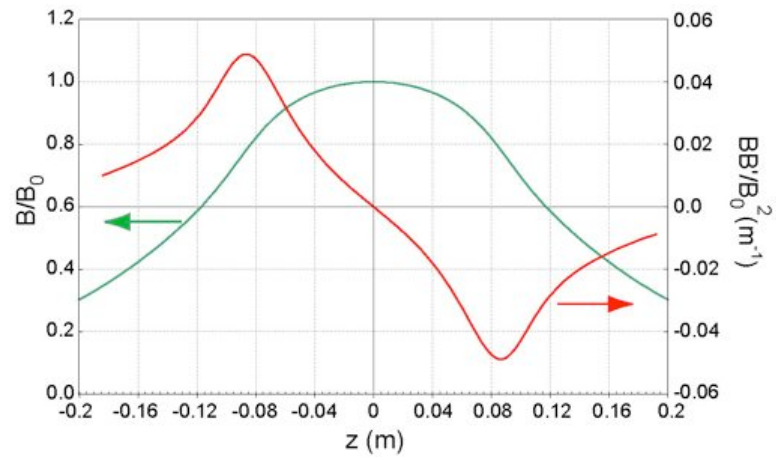
Figure 4.1: Profiles of B and BB' for the magnet NHMFL. The data are normalized to the central field value.
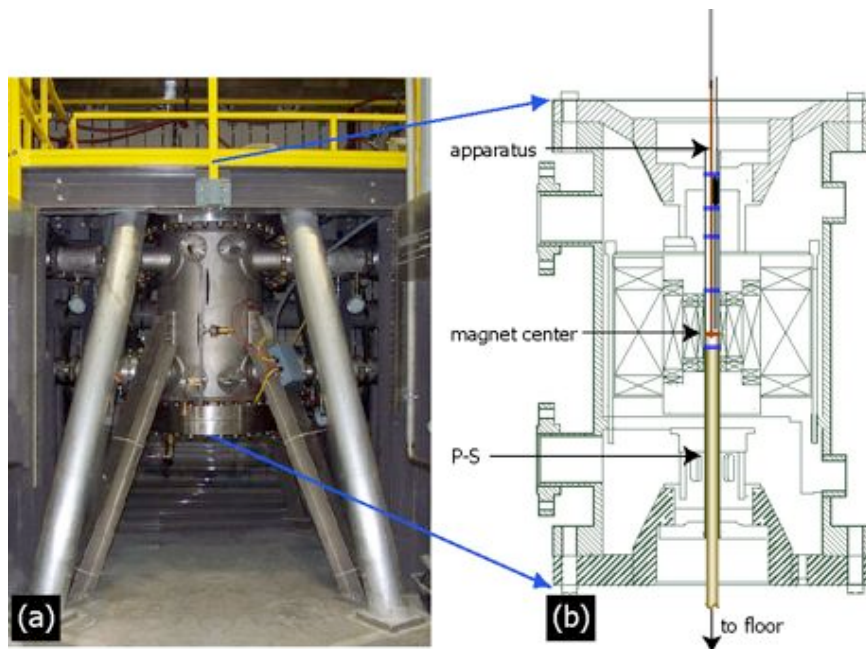
Figure 4.2: Magnet system at NHMFL. (a) A photograph of the magnet. (b) A cross sectional schematic of the magnet with the apparatus setup.

its small diameter and short working distance which make it suitable for the limited space available. The borescope has a 40° viewing angle which yields a minimum FOV of 2 mm in diameter at the minimum working distance of 3 mm from the axis of the borescope. A non-magnetic structure aligns and supports the borescope. The tip of the borescope rests on an adjustable screw that is used to fine tune its height (A-S) relative to the sample. The sample holder (S-H) is screwed to the copper plate and its position can be adjusted horizontally relative to the tip of the borescope. This adjustment allows for FOVs ranging from 4.7 mm to 11 mm in diameter. The motion of the microorganisms was recorded using a modified [128] analog CCD video camera (Sony XC-333) (C) with a $1/4''$ chip size. It was connected to the borescope through a C-mount adapter. The resolution of this camera was 20 μm for a 4.7 mm FOV. A frame grabber equipped with image analyzing software (EPIX®Inc., Buffalo Grove, IL) was used to digitize the movies.

Often the motion of microorganisms is altered by the spectrum and intensity of illumination. It is best for experiments to choose light of a specific wave length in order to minimize or maximize phototactic effects [68, 58]. The choice of monochromatic illumination in the visible spectrum also reduces heating, which can affect the tactic motion of organisms [72, 51]. For these reasons, Light Emitting Diodes (LED) were chosen as the light sources for this apparatus. *Paramecium caudatum* reacts the least to green light (565 nm) [15] and so we have used a high flux (120 lm) green LED (Luxeon®V star, Lumileds Lighting, LLC, San Jose, CA). Since these LEDs are magnetic, the LED was placed a few meters away from the magnet. A three meter long optical fiber, 3 mm in diameter (Edmund Optics) was used as the light guide. The light-guide was passed through openings in the PVC plates (discussed below) and was fixed at the top of the experimental chamber. For

more uniform illumination the tip of the fiber was tilted towards the experimental chamber. This setup creates dark field illumination. We note that we did not use the borescope's built in light guide as the illumination path. Its geometry produced glare on the front surfaces of the sample chambers that made imaging difficult.
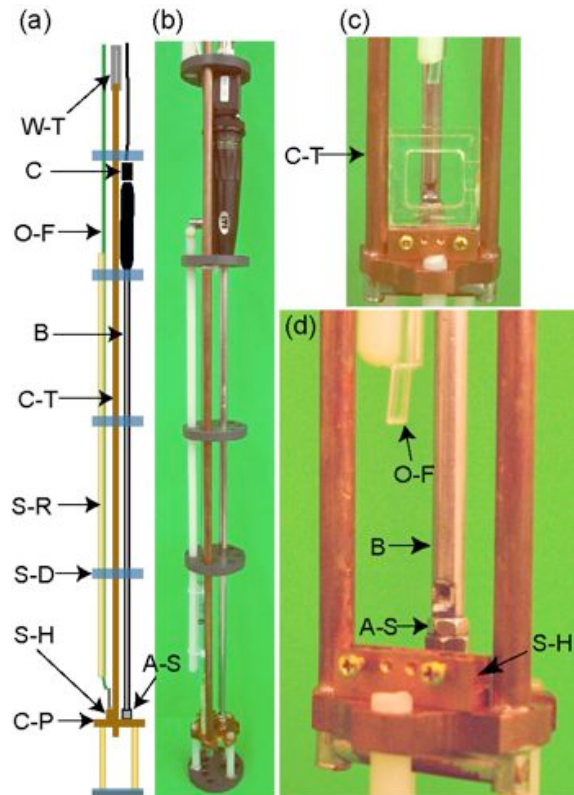
Figure 4.3: Schematic of the apparatus. (a) Various components of the apparatus are shown, C-P copper plate, S-H sample holder, A-S adjusting screw, S-D supporting disc, S-R supporting rod, C-T copper tubing, B borescope, O-F optical fiber, C camera, W-T water tubing. (b) Side view photograph of the apparatus. (c) Close up view of the front of the apparatus. The copper tubing runs through the copper plate. The sample holder is shown holding an experimental chamber. (d) Close up view of the various components of the apparatus.

4.2.2 Temperature control

The temperature inside the bore of the magnet changes considerably during magnetic field ramping. Since temperature variations alter the swimming behavior of paramecia we developed a water circulation system to keep the experimental chamber at room temperature. As seen in Fig. 4.3(c), the experimental chambers were mounted in a holder screwed to the copper plate. The plate was supported by two copper tubes that have been soldered to it. These tubes served as the input and the output of water that circulated through a copper chamber soldered to the copper plate. A water bath, placed about five meters from the magnet, provided temperature regulated water that was circulated through the copper tubes. Ten meter long Tygon tubes (W-T) connected the water bath to the upper ends of the copper tubes. The temperature of the sample holder was monitored with a thermocouple. The variation in temperature of the sample holder was less than 0.5°C.

4.2.3 Support structure

The support system consisted of a few 6 mm diameter solid nylon rods and two lengths of copper tubing that run through openings in five PVC discs and the copper plate (see Fig. 4.2). The disks also have openings for the borescope, the light guide and the thermocouple wires. The supporting discs are 5 mm thick and fit snugly into the bore of the magnet. The copper plate is slightly smaller in diameter than the PVC plates to reduce its contact with the bore tube wall. We covered the area shown in Fig. 4.3(d) with a rubber sheet to prevent condensation from contaminating the experimental chamber. This cover also served as an extra thermal insulator. The apparatus was placed inside the magnet from the top of the bore tube. It rests on a long 50 mm outer diameter PVC tubing (P-S) that

fits inside the bore and rests on the magnet cell floor (Fig. 4.2). Small adjustments to the vertical position of the apparatus were accomplished by inserting or removing short ($\approx$0.1 m) spacers between the PVC tube and the floor.

4.2.4 Tracking and analysis

With this setup, we were able to observe and record the effects of magnetic fields and magnetic forces on the swimming behavior of paramecia. Figure 4.5 (a) and (b) show frames of swimming paramecia in 0 T and 26 T respectively. These images were taken at the largest FOV position (11 mm away from the borescope axis), which corresponds to the lowest resolution. Nonetheless, this resolution is sufficient for detecting the paramecia, tracking them, and measuring their swimming velocities. Figures 4.5(c) and (d) show the tracking results obtained using XCAP$^{\text{TM}}$software (EPIX®Inc., Buffalo Grove, IL).

In general, the following steps are repeated for each set of data acquisition and analysis at various fields. We record the motion of paramecia for 3-4 minutes on a VCR tape. Then, using a frame grabber (EPIX®) and a computer the motion is digitized at a frame rate that is set to 5-7 frames per second (fps). Even though the frame grabber is capable of digitizing at as high as 30 fps, the digitizing speed is limited by the computer speed. Our computer allowed us to digitize up to 15 fps when needed. The spatial calibration for each experiment was performed either by placing a thin rod with known dimensions in the experimental chamber, or by measuring the visible dimension of the experimental chamber. The tracking of the particles is done using the XCAP$^{\text{TM}}$software. The general procedure for tracking using XCAP$^{\text{TM}}$is as the following. After importing all the frames to be analyzed into the software, they were averaged and the average frame was subtracted from each of

the frames separately. This will get rid of the background noise. Then the images were

properly thresholded to show the paramecia as white blobs on the black background. After

this point, "particle tracking" was performed in the "fuzzy" mode. To reduce computational

time, the output of the tracking should be limited to x and y. The parameters in the "fuzzy"

mode were adjusted to give the best tracks possible. This was done by first importing about

100 frames and adjusting the parameters. The correctness of tracks was then checked by

manually observing the position of each particle in each frame (by using the forward button).

After finding the optimum parameters, the tracking was performed on the whole frame set.

Note that it is crucial to chose "partial tracking". This allows tracking of the particles that

are present in only few of the frames. After the tracking is completed, the file is saved as a

".txt" file and later imported in MatLab for further analysis. The output of the software is

the horizontal and vertical positions of each particle in each frame. Further analysis of the

data was done using a custom code written in MatLab®. The code also filters out all the

trajectories that are the result of inaccurate tracking. Inaccurate tracking can be minimized
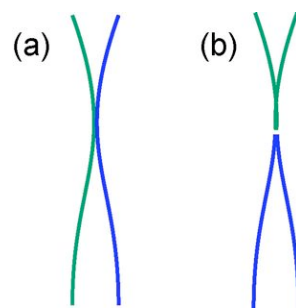
Figure 4.4: A sketch of an inaccurate tracking. (a) the correct track. (b) inaccurate tracking. The tracking software can not distinguish between these two cases.

by choosing optimized tracking parameters, though it can not be eliminated. It happens

due to the fact that when two particles come too close to each other, or their paths cross,

the program sometimes tracks them incorrectly at the intersection and therefore instead of two almost straight lines (Fig. 4.4 (a)), we obtain two lines that have very sharp curving angles (Fig. 4.4 (b)). Since the change in the direction of the track due to this effect is much sharper and faster than a curving due to natural effects (such as *Paramecium* bumping into an obstacle), it can be detected and subtracted from the other tracks. In later chapters, the specific methods used to calculate various parameters will be described in more detail.
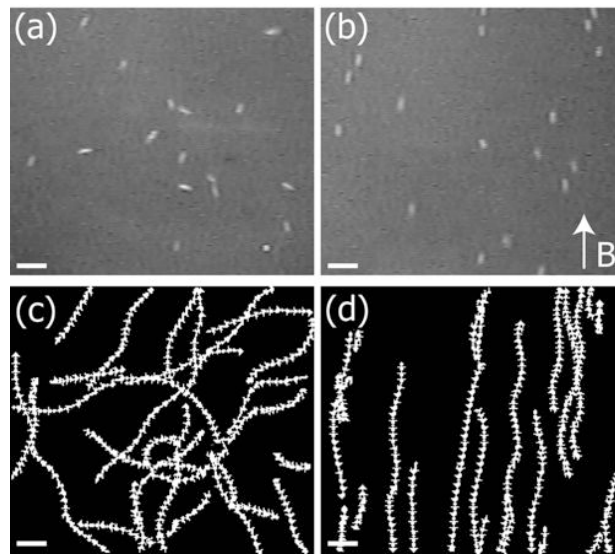
Figure 4.5: Images of swimming paramecia acquired by the borescope. (a) B=0 T. (b) B=26 T. (c) Swimming trajectories at B=0 T. (d) B=26 T. The bar is 0.5 mm

4.3   AMI magnet and setup

A superconducting solenoid with a maximum field of 9 T and $BB' = 1700$ T^2 m^{-1} was used for this setup. It has a room temperature bore of 11 mm and produces a magnetic field parallel to earth's gravity. Figures 2.1 shows the profiles for B and BB' produced by this magnet. The force homogeneity is 5% over (4 mm)^3. We accessed the magnet from the

lower end of the solenoid. As it is shown in Fig. 4.6, the experimental chamber was mounted on a copper or brass supporting rod that was attached to the same borescope with the help of 2-3 copper rings. The borescope is the same one that was introduced in Section 4.2.1. This setup provided a 90° optical axis.
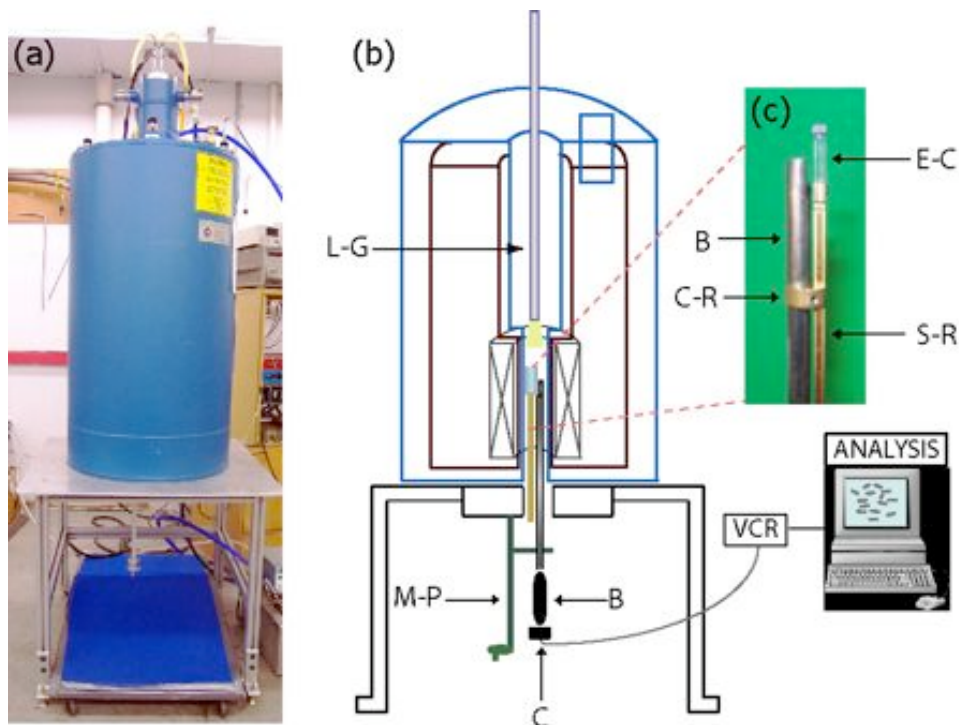
Figure 4.6: Experimental setup for the AMI magnet system. (a) The magnet. (b) Schematic of the experimental setup. Various components are the experimental chamber (E-C), supporting rod (S-R), copper ring (C-R), borescope (B), mechanical positioner (M-P) and light guide (L-G). (c)Photograph of the assembled borescope and the E-C.

The whole assembly was then mounted on a mechanical positioner which was fastened to the table. With the help of this positioner, the vertical location of the assembly was adjusted to within tens of a millimeter accuracy. The illumination was provided from the top section by using a light-guide attached to a halogen light source. Since we have used this setup exclusively for the studies on immobilized cells, the choice of light source was not important.

Due to the rather small bore size and the dimensions of the experimental chamber and the restriction of the distance from the borescope to the chamber (small FOV), this setup was not suitable for experiments on large swimming microorganisms such as *Paramecium*. Moreover, even though the magnet was designed to provide a room temperature bore, due to poor functioning, the temperature inside the bore would drop and produce frost because of condensation. To overcome this issue, room temperature air was blown through the bore from the top with a heat gun attached to a tube. Once the bore was at room temperature, the air blow was turned off and the experiment could begin. Generally, it would take about half an hour to one hour for the bore to get cold again, at which point, the experiment was stopped and the bore reheated.

In the following chapters we will present experiments that have been performed in both of these magnet systems.

Chapter 5

Aligning *Paramecium* with intense static magnetic fields

5.1 Introduction

Various external fields such as chemical gradients [29, 131, 9], light [44, 24, 57], gravity [77, 50, 97], and electric fields [73, 130, 80] alter the swimming of unicellular microorganisms. These effects may manifest themselves by orienting the cell in a specific direction, affecting the swimming speed, or modifying the rate at which they change directions. Most often, these chemotactic, phototactic, gravitactic and galvanotactic responses are active responses. They reflect a physiological sensitivity to these fields and depend on an underlying chemo-mechanical network that controls the reaction. An example of an active response is that displayed by a *Paramecium* in a DC electric field. It orients with the field and swims toward the cathode due to a change in its membrane potential. This phenomenon is not observed in non-swimming *Paramecium* [80]. Conversely, there also exist passive responses for which

a physical field, such as magnetic field, may directly orient an organism without eliciting a physiological change [94, 104, 33].

In this chapter we investigate the effects of magnetic fields greater than few Tesla (T) on the swimming trajectories of *Paramecium caudatum*. We have observed that their otherwise straight swimming trajectories curve in magnetic fields and eventually orient parallel or anti-parallel to the applied field direction. Neutrally buoyant immobilized paramecia also align with their long axis in the direction of the field. This magneto-orientation is modeled as a strictly passive response to a magnetic torque exerted on the diamagnetically anisotropic components of the paramecia and estimate the anisotropy of diamagnetic susceptibilities of a whole *Paramecium* cell. We also discuss results obtained by simulating the 3-dimensional motion of paramecia in magnetic fields.

5.2   Methods

5.2.1   *Paramecium* and the experimental chambers

P. caudatum was cultured on Hey medium and collected for experiments during their stationary phase of growth [135] (see Appendix A). They were collected using their gravitactic property and suspended in test solution comprised of 1 mM $CaCl_2$, 1 mM KCl, 0.1 mM $MgSO_4$, 1.5 mM MOPS, pH 7.2. The gravitactic collection was achieved by filling a small (25 ml) Erlenmeyer flask by *Paramecium* solution and covering it with a microscope slide. After 20-30 minutes the cells would gather in the neck of the flask, at which point we transfered them into a new flask that contained the test solution. The paramecia were left in the test solution to adapt for a period of 1-2 hours prior to experimentation. Two different
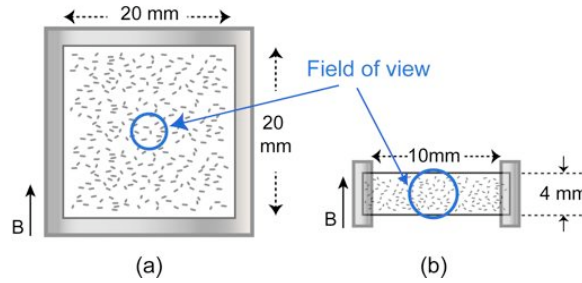
Figure 5.1: Sketches of the experimental chambers. (a) Square chamber. (b) Rectangular chamber. The circles show the field of view.

types of experimental chambers were employed. Both had a depth of 2 mm, which was much smaller than the width and length to provide a nearly two dimensional environment. The first type had square area to eliminate asymmetries arising in the swimming track distributions due to the geometry of the chamber [75]. It was made of an acrylic frame of 2 mm depth and 20 mm×20 mm area, (Fig. 5.1(a)). Both sides of the frame were covered with a microscope slide and sealed with 5 minute epoxy glue (Devcon). The chambers were flushed a few times with water and tested to be harmless to paramecia. Solution containing paramecia were injected with a syringe (PrecisionGlide needle, 25G5/8) through holes on one side of the frame. These holes were later sealed with VALAP (1:1:1 Vaseline, Lanolin and Paraffin) [96]. The second type of chamber had a rectangular geometry. These were made from a borosilicate rectangular tube (VitroCom, Inc., NJ) (2 mm×4 mm×10 mm) whose ends were sealed with acrylic caps (Fig. 5.1(b)).

Paramecium tetraurelia, kindly provided by Professor Judith Van Houten, were cultured on wheat grass inoculate with *Enterobacter aerogen* (Carolina Biological Inc.) and collected in their stationary phase of growth. We performed two sets of behavioral experiments on them using the above mentioned test solution and a test solution low in K^+ (1 mM $CaCl_2$, 0.5 mM $MgSO_4$, 2 mM Tris-HCl, pH 7.2 [92]).

Paramecia were immobilized by suspension in a 0.5 mM solution of $NiCl_2$ for 10-15 minutes [77]. The effect of $NiCl_2$ is to paralyze the cilia so that they can not beat but the cell is still alive. After immobilization, individual cells were transferred with a micropipette into the experimental chamber. Ficoll (Ficoll®400 Sigma-Aldrich, St. Louis, MO) solution with 11% w/v concentration, was used to provide a neutrally buoyant environment for the paramecia. The viscosity of Ficoll solution was estimated to be $(6.5 \pm 0.5) \times 10^{-3}$ Pa s at $(20 \pm 2)°C$ [19] (the temperature during the experiment).

5.2.2   Apparatus

The experiments were performed using the two magnet systems introduced in Chapter 4. A 50 mm bore, 25 T maximum field, resistive magnet at the National High Magnetic Field Laboratory (NHMFL)(this magnet was subsequently upgraded to 31 T in April 2005), and a superconducting solenoid (American Magnetics, Inc., Oak Ridge, TN) with an 11 mm room temperature bore and a maximum field of 9 T were used.

The imaging procedure for paramecia for the experiment involving swimming paramecia which was performed at NHMFL was explained in Sec. 4.2. The only difference here was that instead of one 3 mm thick optical fiber, in this experiment we used 3×1 mm optical fibers for illumination (the 3 mm optical fiber was not available at the time) and that we did not have temperature control mechanisms. The setup for experiments on immobilized paramecia is explained in Sec. 4.3. The movies were digitized at 5 frames per second (fps) over 3 minute intervals. Further analysis was performed using XCAP^{TM} software (EPIX®Inc., Buffalo Grove, IL) and custom Matlab codes.

The orientation of *Paramecium*'s swimming trajectory was defined to be the direction

of the axis of its helical motion [25, 26] shown in Fig.5.2(a). After a couple of helical periods, this orientation closely coincides with the orientation of the displacement vector of the total trajectory. Only trajectories that extended a couple of periods or more were analyzed. This condition generally corresponds to swimming for at least 2 seconds. The angles of individual trajectories, θ_i, were measured relative to the magnetic field direction. The tracking procedure utilized was as explained in Sec. 4.2.4. Since some paramecia reverse their direction or make abrupt turns due to avoiding reactions, a filtering procedure was used to eliminate those tracks (on average, about 15 % of the total tracks). The number of these tracks did not vary with field strength. The criterion for detecting these tracks was the difference in the moving direction between two consecutive frames (0.2 s) exceeding 90 degrees.
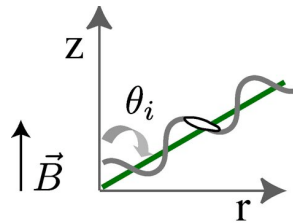
Figure 5.2: Orientation angle and the helical trajectory. The angle between the axis of the helix is considered as the orientation with respect to the magnetic field.

5.3   Orientation of swimming trajectories

The magnetic field induced alignment of motile paramecia is demonstrated in Fig. 5.3. In 0 T, the swimming tracks are randomly oriented and form straight helical trajectories. In 9 T, the tracks are also helical and straight but largely align parallel or anti-parallel to the magnetic field direction. The histograms of these orientations reinforce these observations

showing that the tracks in 0 T are oriented at all angles while the tracks in 9 T align to within 7.5 degrees of the magnetic field axis. The asymmetry in the number of upward and downward swimmers in the histograms can be attributed to the fact that the average downward swimming speed exceeds the average upward swimming speed due to sedimentation. In order for the downward flux of paramecia to equal the upward flux, the number of downward swimmers must be smaller that the number of upward swimmers. This argument neglects the effect of gravikinesis, which will be discussed in Chapter 7. Gravikinesis effect would decrease the number of upward swimmers and increase the number of downward swimmers by a small amount but the overall picture would not change.
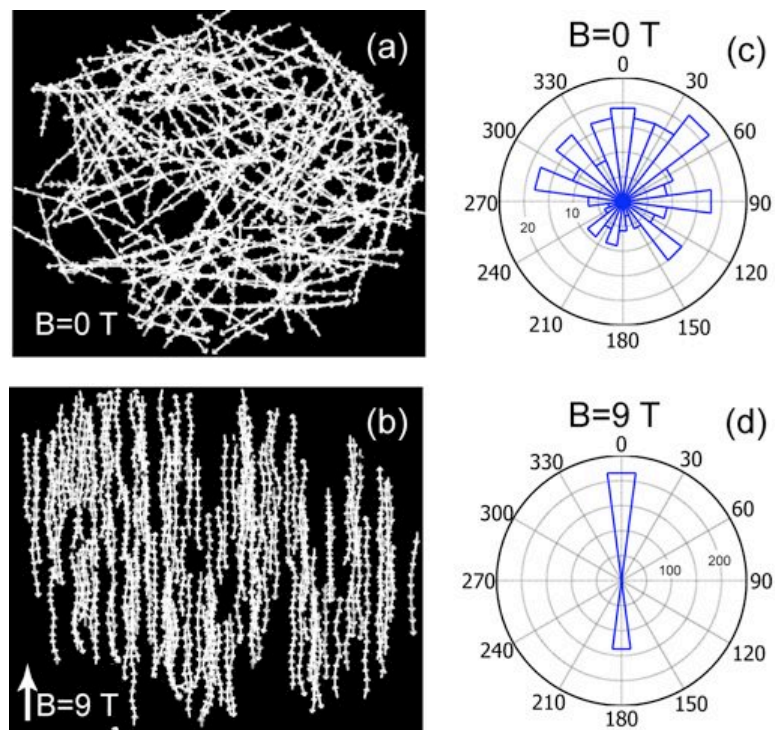
Figure 5.3: Orientation of swimming paramecia in a magnetic field. (a) and (b) are the swimming tracks at $B = 0$ T and $B = 9$ T respectively. Each track consists of a series of displacement vectors recorded at 5 fps. (c) and (d) are circular histograms of the track orientation for (a) and (b) respectively, the bin size is 15 degrees.
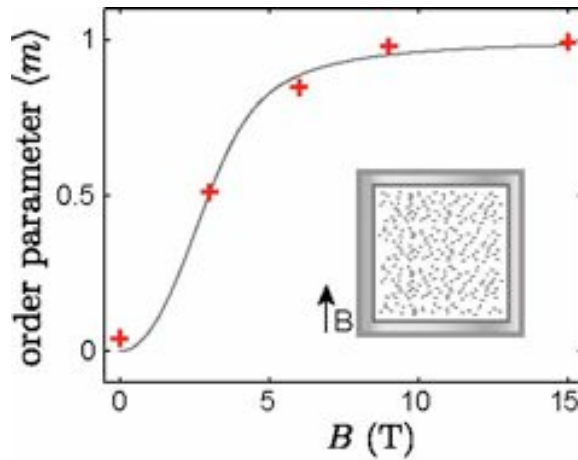
Figure 5.4: Order parameter $\langle m \rangle$ as a function of the magnetic field. $\langle m \rangle = 1$ indicates perfect alignment. The curve is to guide the eye.

The degree of alignment in different magnetic fields is characterized by using a two dimensional, uniaxial order parameter [99] defined as $\langle m \rangle = \langle 2\cos^2 \theta_i - 1 \rangle$. The angular brackets denote the average over the track distribution. For a set of tracks that are perfectly aligned parallel or anti-parallel with the field, $\langle m \rangle = 1$. Perpendicular and random alignments yield $\langle m \rangle = -1$, and $\langle m \rangle = 0$, respectively. It is important to emphasize that $\langle m \rangle$ describes orientation along a specific axis and thus, differs from the orientation coefficient employed in gravitaxis studies, which describes orientation along a specific direction [77]. The dependence of $\langle m \rangle$ on B in Fig. 5.4 shows that the tracks are substantially aligned near 4.5 T and completely aligned at 9 T.

5.4   Orientation of non-motile paramecia

To determine whether the magnetic field induced alignment is a passive (purely physical) or an active (physiological) response we investigated the effect of magnetic fields on immobilized *Paramecium*. Fig. 5.5 shows a time series of images of an immobilized, neutrally buoyant *Paramecium* in a Ficoll solution in 4 T magnetic field. Prior to being placed in the magnet, this cell was oriented horizontally (perpendicular to the magnetic field) by the use of a thin rod. Once in the magnet, it rotated to the vertical position over the course of about 4 minutes. This slow orientation is due to the viscosity of the Ficoll solution. The time dependence of this rotation and those observed at other magnetic field strengths for the same cell are shown in Fig. 5.7 (a). At higher fields the rotation occurs more rapidly and the rate of rotation is largest near 45 degrees. Thus, even non-motile *Paramecium* aligns with a magnetic field in tesla range in a manner that depends on field strength, suggesting that the response of motile *Paramecium* is passive.
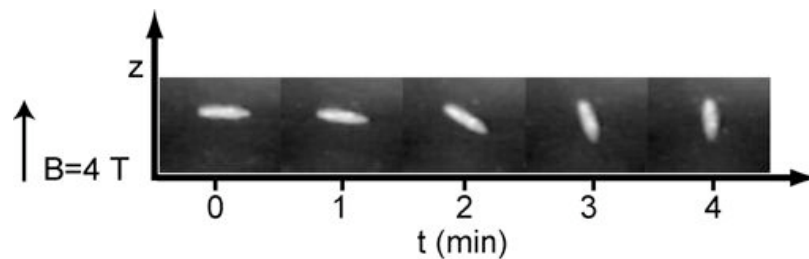
Figure 5.5: Orientation of non-motile *Paramecium* in magnetic field. Image sequence of a non-motile neutrally buoyant *Paramecium* in 4 T magnetic field in Ficoll solution.

5.4.1 Magnetic torque

Experiments on blood cells and other "non-magnetic" biomaterials indicate that the magnetic torque acting on the immobilized *Paramecium* could result from the interaction of the magnetic field with its diamagnetically anisotropic components [122, 83, 52]. Thus, we introduce the magnetic torque due to interaction of a uniform magnetic field with the diamagnetic anisotropy of the cell presuming it has a cylindrically symmetric geometry. For such a cell, shown schematically in Fig. 5.6, the magnetic energy is defined as [54]

$$U_B = \frac{-V}{2\mu_0} \vec{B} \cdot \overleftrightarrow{\chi} \cdot \vec{B}. \tag{5.1}$$

where μ_0 is the magnetic permeability of vacuum, $\mu_0 = 4\pi \times 10^{-7}$ H m^{-1}, B is the magnetic field, V is the volume of the cell and $\overleftrightarrow{\chi}$ is volume susceptibility tensor, that in the coordinate system of the cell, is given by:

$$\overleftrightarrow{\chi} = \begin{pmatrix} \chi_\perp & 0 & 0 \\ 0 & \chi_\perp & 0 \\ 0 & 0 & \chi_\| \end{pmatrix} \tag{5.2}$$

$\chi_\perp$ and $\chi_\|$ are the diamagnetic susceptibilities along the radial and axial direction respectively. Without loss of generality, we consider the magnetic field to be in the $x - z$ plane: $\vec{B} = B \sin\theta \hat{i} + B \cos\theta \hat{k}$, where θ is the angle between the long axis and object and the magnetic field. Therefore the energy simplifies to:

$$U_B = \frac{-VB^2}{2\mu_0} \left(\Delta\chi \cos^2\theta + \chi_\perp \right). \tag{5.3}$$

The magnetic torque is then obtained

$$\Gamma_B = -\frac{dU_B}{d\theta} = -\frac{\Delta\chi VB^2}{2\mu_0} \sin 2\theta. \tag{5.4}$$
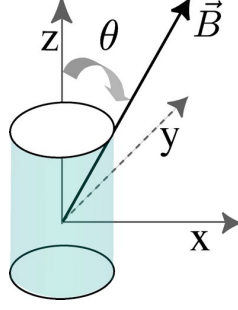
Figure 5.6: A cylindrically symmetric diamagnetic object in a static magnetic field B.

where $\Delta\chi = (\chi_\| - \chi_\perp)$ is the net anisotropy of the diamagnetic susceptibility of a *Paramecium* cell. Since the rotations occur at low Re numbers, the orientation rate is linearly proportional to the torque, that is

$$\Gamma_B = \beta\dot{\theta}. \tag{5.5}$$

where β is the drag coefficient for rotation about a minor axis. Integration yields:

$$\ln(\tan\theta) = \ln(\tan\theta_0) - \frac{\Delta\chi_p B^2}{\mu_0\beta}t \tag{5.6}$$

For simplicity define $\Delta\chi_p = \Delta\chi V$.

We compare our measurements of $\theta(t)$ to this prediction in Fig. 5.7 (b) by plotting $\ln(\tan\theta)$ versus a rescaled time axis where the scaled time is defined as $t_s = t(BB_0^{-1})^2$. For the set of experiments in Fig. 5.7, we chose $B_0 = 6.4$ T as the basis for scaling. With this scaling, the data collapse on a single line, suggesting that the model applies. The slope of the fitted line in Fig. 5.7(b) is used to estimate $\Delta\chi_p$. Using the solid ellipsoid of revolution approximation for a *Paramecium* (axes $a = 20$ μm and $b = 100$ μm, see Chap. 3), the rotational drag coefficient can be approximated from: $\beta = \frac{8\pi\eta}{3}b^3(\ln(\frac{2b}{a} - \frac{1}{2}))^{-1}$ [9]. For water $\eta = 10^{-3}$ Pa s, hence we obtained the following values for $\Delta\chi_p$ from three trials performed on three different paramecia: $(5.9 \pm 0.6) \times 10^{-23}$ m^3, $(7.1 \pm 1.4) \times 10^{-23}$ m^3 and

$(6.9 \pm 1.5) \times 10^{-23}$ m^3 respectively with the resulting mean value of $\langle \Delta\chi_p \rangle = (6.7 \pm 0.6) \times$ 10^{-23} m^3. This value of diamagnetic anisotropy yields a difference in magnetic potential energy as a function of B:

$$\Delta U_B = U_{B\perp} - U_{B\parallel} = \frac{\Delta\chi_p B^2}{2\mu_0}$$

$$= 0.3 \times 10^{-16} B^2. \tag{5.7}$$

In a 4 T magnetic field, $\Delta U_B = 4.8 \times 10^{-16}$ J or $10^5 \times k_B T$ indicating that the orientation is completely athermal.
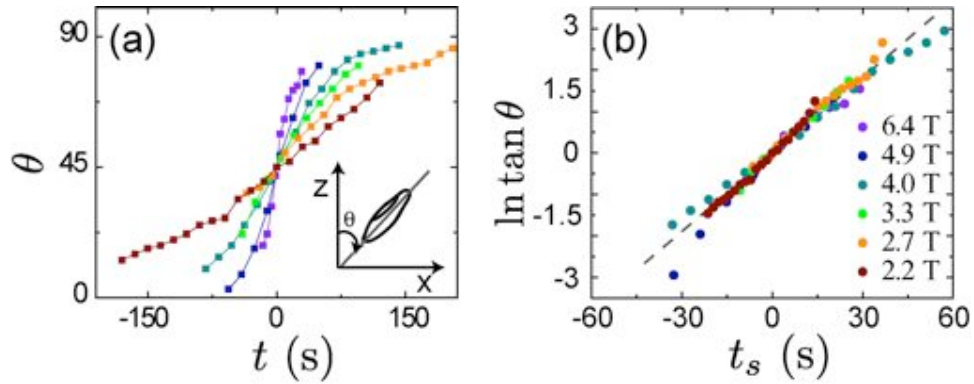
Figure 5.7: Orientation rate of immobilized *Paramecium* in various magnetic fields. (a) Orientation as a function of time. $t = 0$ is set for $\theta = 45°$, θ is defined by the inset. (b) $\ln\tan\theta$ vs. scaled time, $t_s = t(BB_0^{-1})^2$, where B_0=6.4 T. $\Delta\chi_p$ is measured from the slope of the fitted dashed line (see Eq. 5.6).

5.4.2 Magnetic orientation due to shape anisotropy

In principle, magnetic fields can exert torques on cells with a completely isotropic magnetic susceptibility, provided their shape is anisotropic. Since *Paramecium* has an ellipsoid shape, this effect might be of significance. Here we calculate this torque by using the analogy of this problem with the torque on ellipsoidal dielectric objects in external electric fields (see

[115] pages 232-233). For a *Paramecium* with diamagnetic susceptibility, χ_c (cell), placed in a solution with χ_s the torque due to the shape effect is:

$$\Gamma_{shape} = \frac{2}{3}\pi(\chi_c - \chi_s)a^2b\frac{B(B_{\parallel} - B_{\perp})}{\mu_0^2}\sin 2\theta \tag{5.8}$$

where θ is the angle between the magnetic field, B, and the major axis of the ellipsoid. $B_{\parallel}$ and $B_{\perp}$ are the fields induced in the ellipsoid when the external field is parallel and perpendicular to the major axis of the ellipsoid respectively. They are given by:

$$B_{\parallel} = \frac{-B}{\mu_0\{(\chi_c - \chi_s)\eta_0[(1 - \eta_0^2)\coth^{-1}\eta_0 + \eta_0] - (1 + \chi_c)\}} \tag{5.9}$$

$$B_{\perp} = \frac{2B}{\mu_0\{2(1 + \chi_s) + (\chi_c - \chi_s)\eta_0[(1 - \eta_0^2)\coth^{-1}\eta_0 + \eta_0]\}} \tag{5.10}$$

where $\eta_0 = b(b^2 - a^2)^{-1}$. Substituting $\chi_s = -9.05 \times 10^{-6}$ and $\chi_c = -9.11 \times 10^{-6}$ (Chapter 6, and using the previously introduced values for a and b for a *Paramecium*, we obtain

$$\Gamma_{shape} = 1.8 \times 10^{-27}\frac{B^2}{2\mu_0}\sin 2\theta. \tag{5.11}$$

Comparing Γ_{shape} to Eq. 5.4 and considering that $\Delta\chi_p$ is of the order of 10^{-23}, the correction to our measured value for $\Delta\chi_p$ is 10^5 times smaller in magnitude and therefore negligible. The shape effect is small because

5.4.3   Magnetic torque on motile paramecia

To investigate the origin of the alignment of motile paramecia we analyzed the trajectories of individuals upon their take off from the boundary of a chamber. Under natural conditions, paramecia take off at random angles. In magnetic fields, however, their trajectories curve toward the axis defined by the magnetic field. This phenomenon is shown in the inset of Fig. 5.8. Notice that the curvature appears for both upward and downward

swimmers. Qualitatively, this behavior is expected for a passive response to the magnetic

torque described above. The torque superimposes a rotation on the normal translation of

the *Paramecium*. This effect is tested below quantitatively.
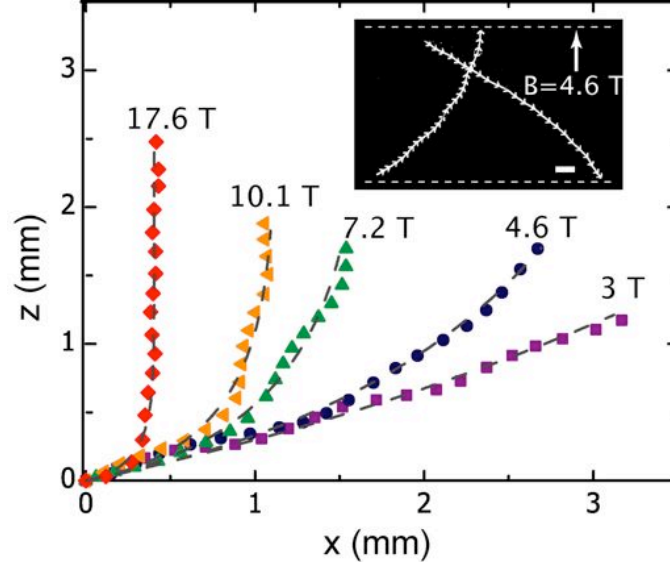
Figure 5.8: Swimming trajectories in various magnetic field strengths. A set of trajectories with the same initial angles in the magnetic fields indicated. The dashed lines are fits of Eq. 5.14 to the data. Inset: both downward and upward trajectories in a 4.6 T field, scale bar 500 μm, dashed line depicts the boundaries of the chamber

In our model, a motile *Paramecium* of density ρ_c, swimming with velocity v in a solution

with density, ρ_s, experiences a total force which is the superposition of the buoyant force,

propulsion force, $\vec{F}_P$, and the drag force, yielding:

$$\vec{F}_{tot} = \Delta \rho V g \hat{z} + \vec{F}_P - \xi \vec{v} \tag{5.12}$$

where $\Delta \rho = \rho_c - \rho_s$, g is the acceleration due to gravity and V is the volume of the cell.

The linear drag coefficient, $\xi = 6\pi\eta(4a + b)/5$ [47], is given for an ellipsoid of revolution.

We presume that F_p is directed along the long axis of the *Paramecium*. This approximation

neglects the torques and resulting angular velocities [25, 89] that give rise to the helical

motion that is superimposed on their normal, relatively straight trajectories. This approximation reduces the number of fitting parameters and is justified by the quality of the fits. Since the motion is governed by low Re numbers hydrodynamics, $F_{tot} = 0$, the equation of motion reduces to:

$$\xi \dot{x} = F_p \sin \theta \tag{5.13}$$

$$\xi \dot{y} = F_p \cos \theta - \Delta \rho V g$$

$$\beta \dot{\theta} = \Gamma_B$$

Integration yields:

$$x = v_P \tau \ln \left(\frac{\tan(\frac{\pi}{4} + \frac{\theta}{2})}{\tan(\frac{\pi}{4} + \frac{\theta_0}{2})} \right) \tag{5.14a}$$

$$y = v_P \tau \ln \left(\frac{\tan(\frac{\theta}{2})}{\tan(\frac{\theta_0}{2})} \right) - \frac{\Delta \rho V g \tau}{\xi} \left(\frac{\tan \theta}{\tan \theta_0} \right)$$

$$\theta = \tan^{-1} \left(\tan \theta_0 \exp \left(\frac{t}{\tau} \right) \right) \tag{5.14b}$$

where $v_P = F_P / \xi$ is the propulsion speed [35], $\tau = -\beta \mu_0 / \Delta \chi_p B^2$ and θ_0 is the initial angle. Figure 5.8 shows examples of a set of tracks with similar take off angles (symbols) and their respective fits (dashed lines) using the three free parameters, v_p, θ_0 and $\Delta \chi_p$. Figure 5.9 shows the values obtained for $\Delta \chi_p$ for a number of tracks as a function of magnetic field. The results of averaged values of $\Delta \chi_p$ and v_p are summarized in Table 5.2. Notice that the average value of $\Delta \chi_p$ varies little as the field increases from 3 T to 10 T (a 10 fold increase in torque). At 17.6 T however, $\Delta \chi_p$ is significantly lower. This field turns paramecia in less than a helical period, which may render our simplified equations of motion invalid. Excluding the result for 17.6 T, the average $\Delta \chi_p$ for motile paramecia

is $(8.3 \pm 0.9) \times 10^{-23}$ m^3, which is comparable to the values obtained for the immobilized

paramecia.
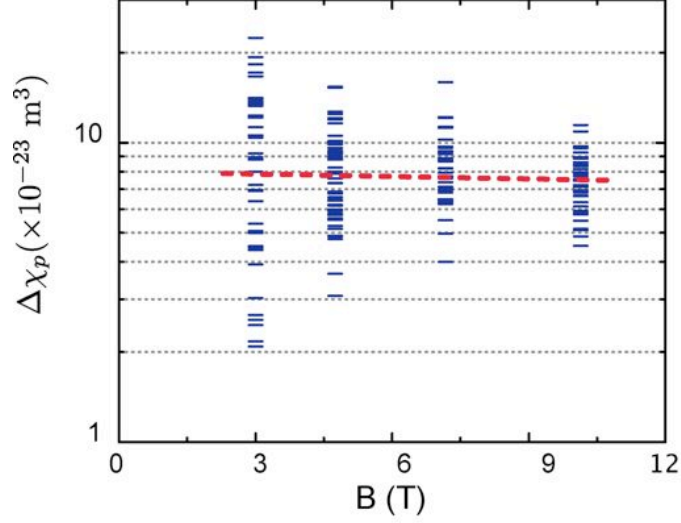
Figure 5.9: Measured $\Delta\chi_p$ as a function of magnetic field. Values are obtained from fits of Eqs. 5.14 to swimming trajectories; the dashed line is a linear fit to $\Delta\chi_p$ vs. B.

5.5   3D Simulation

The proceeding analysis presented in this chapter is based on the assumption that the

motion of paramecia is two dimensional. However in reality, depending on the orientation

of the *Paramecium*, the swimming trajectories vary from one another and will result in

different projections in the x-z plane. To investigate how much this 3D motion might affect

our measured values of $\Delta\chi_p$, we simulated the motion of paramecia in a static magnetic

field. The simulations are based on the methodology presented by Crenshaw [25] for the

helical motion of microorganisms. The helical motion of *Paramecium* decomposes into

its one degree of translational freedom in the anterio-posterior (A-P) direction with linear

velocity v_p and three degrees of rotation freedom with angular velocities ω_1 around left-right

(L-R), ω_2 around dorso-ventral (D-V) axis and ω_3 around around A-P axis (see Fig. 5.10).

In the absence of magnetic field, the motion of *Paramecium* is formulated as:

$$\vec{v} = v_p \hat{k} - v_s \hat{K}, \tag{5.15}$$

$$\vec{\omega} = \omega_1 \hat{i} + \omega_2 \hat{j} + \omega_3 \hat{k},$$

$$= \omega_\rho \hat{\rho} + \omega_3 \hat{k}. \tag{5.16}$$

Note that $\overrightarrow{ijk}$ is the reference frame attached to the *Paramecium* as shown in Fig. 5.10(a)

and $\overrightarrow{IJK}$ is the lab coordinate. v_s is the sedimentation speed. Adding the magnetic field,
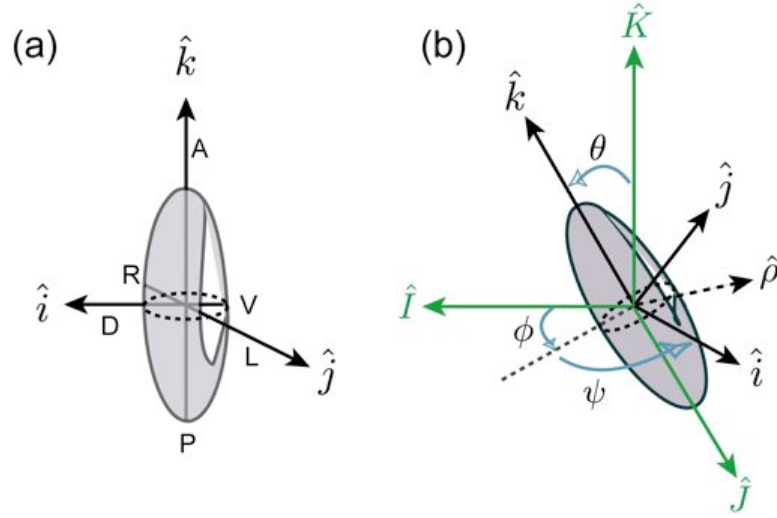
Figure 5.10: *Paramecium* in body and lab reference frames. (a) The body axis of *Paramecium*, $\hat{i}$: D-V, $\hat{j}$: L-R and $\hat{k}$: A-P. The angular velocities around each of these axes are ω_1, ω_2 and ω_3 respectively. (b) Orientation of *Paramecium* with respect to the lab frame

changes the in plane angular velocity, ω_ρ, are noted according to the following:

$$\vec{\Gamma}_B = \frac{\Delta\chi_p B^2}{2} \sin 2\theta \frac{\hat{k} \times \vec{B}}{|\hat{k} \times \vec{B}|} = \beta\omega_\rho \hat{\theta}. \tag{5.17}$$

Therefore, the angular velocity is modified as $\omega'_\rho = \omega_\rho + \Delta\omega_\rho$. By substituting ω'_ρ in Eq. 5.16, we obtain the trajectories of paramecia in magnetic fields. To simulate the motion, we need to chose the initial orientation angles of *Paramecium*. This is defined using the Euler angles [118], ϕ, θ and ψ shown in Fig. 5.10(b). The dependence of the 2D projection of the trajectories on the initial angles is shown in Fig. 5.11(a). These simulations were performed for $B = 7$ T, with $\phi = 0$, $\theta = -60$ and variable ψ in $45°$ intervals. Other parameters used for the simulation are summarized in Table 5.1. For details of the procedure refer to the review article by Crenshaw [25]. $\Delta\chi_p$ of each of the trajectories was obtained by fitting Eqs. 5.14 to these helical trajectories. From the fittings, we obtained $\Delta\chi_p$ and v_p as a function of initial angle, ψ. The results shown in Fig. 5.11 (b) and (c) suggest that the error attributed to the 2D projection is smaller than the error due to population effects. The variation in v_p is only 1% and the error in $\Delta\chi_p$ is 6%, well below the uncertainties obtained from immobilized paramecia.

Table 5.1: Simulation parameters

parameter	value	parameter	value
total time	10 s	helix angle (θ_h)	$10°$
v_p	1000 μm s^{-1}	ω_1	0
v_s	100 μm s^{-1}	ω_2	$\omega_3 \tan\theta_h$
$\Delta\chi_p$	7.5×10^{-23} m^3	ω_3	2 rad s^{-1}

5.5.1 Orientation of swimming distributions

Finally, this passive model suggests how the orientation distributions presented in Fig. 5.3 arise. Without a magnetic field, the tracks have all possible orientations, implying that there are collisions that randomize their swimming directions. At the low *Paramecium*
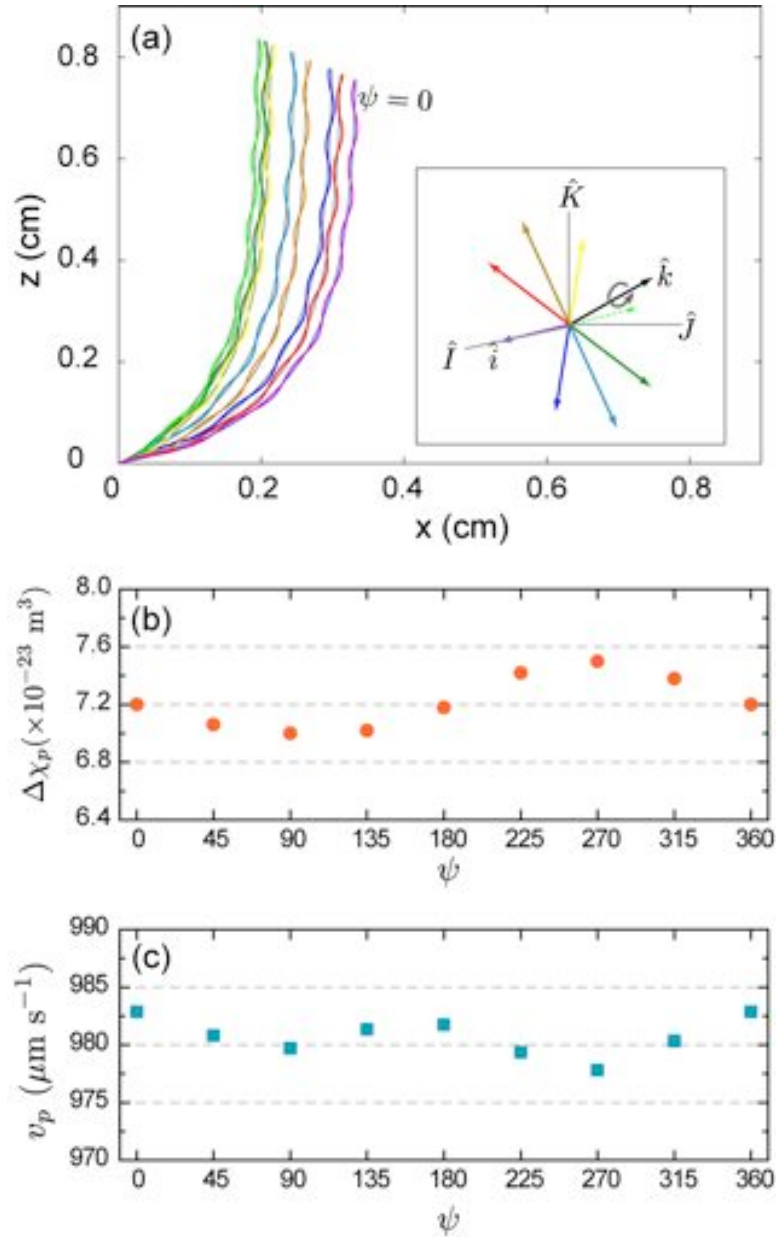
Figure 5.11: Simulation of helical trajectories of *Paramecium*. (a) Depending on the initial orientation of *Paramecium*, the 2D projection will vary. The fits using Eqs. 5.14 is shown as grey curves. Inset shows the color coded initial orientation of $\hat{i}$. Variations in $\Delta\chi_p$ (b) and v_p (c) obtained from the fits, to trajectories in (a).

densities used in these experiments, these collisions most likely occur with the walls rather than with other paramecia. In a magnetic field, these randomly oriented trajectories turn to align with the magnetic field as they swim toward the field of view. The longer they swim or the stronger the field, the more aligned they become. Using this idea, we have simulated the evolution of the distribution in magnetic field. We start with a random distribution of orientations and let each orientation change with time according to Eq. 5.6. By iteration, we obtain a characteristic time τ_c, at which the calculated and measured values of $\langle m \rangle$ are comparable. For the data shown in Fig. 5.4, $\tau_c \simeq 10$ s. This characteristic time corresponds to a characteristic length, l_c, traveled by the organism and estimated by $l_c = \tau_c \times v_p \simeq 10 \times 900 \times 10^{-6} = 9$ mm, where v_p is the approximate speed of *Paramecium* (900 μm s^{-1}). This length is nearly identical to the distance that a *Paramecium* swims to reach the field of view (center of the chamber) coming from the wall.
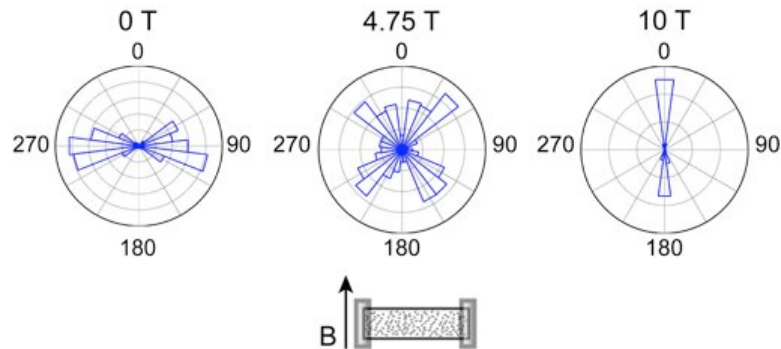
Figure 5.12: Orientation histograms of trajectories in a rectangular chamber.

We have performed a similar analysis on data obtained using a rectangular shaped container shown in Fig. 5.1(b). The associated orientation histograms at different magnetic fields are shown in Fig. 5.12. Notice that at 0 T the distribution is no longer random but oriented along the long dimension of the chamber. Such geometrical effects have been

observed previously but their origin is not well understood [75]. Figure 5.13 shows measured and simulated values of $\langle m \rangle$ for the rectangular chamber. In the simulation we employed the 0 T orientation distributions as the initial distribution and evolved it in time using Eq. 5.6. Two characteristic times were necessary for fitting the data. We found that for $\langle m \rangle \leq 0$ ($B \leq 4.75$ T), which corresponds to more horizontal than vertical swimmers, $\tau_c \simeq 6$ s provided a good fit (open triangles in Fig. 5.13). On the other hand, for $\langle m \rangle > 0$, which corresponds to more vertical than horizontal swimmers, $\tau_c \simeq 2$ s provided a good fit (open diamonds in Fig. 5.13). Accordingly, the characteristic length over which the horizontal swimmers can turn in B is $l_h = 5.4$ mm, which is substantially longer than the length over which vertical swimmers can turn $l_v = 1.8$ mm. These two lengths correspond to the half width and half height of the experimental chamber. This simple approach provides an explanation for the orientation of a distribution based on magnetic torque model and reinforces that the swimming trajectories are oriented through a passive mechanism.
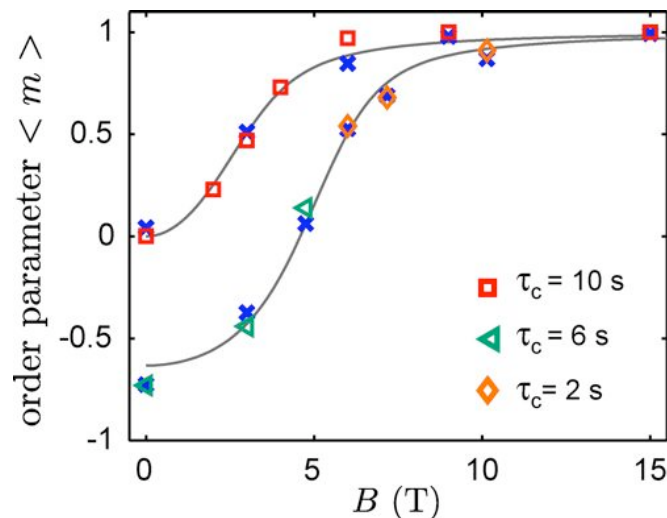
Figure 5.13: Order parameter of the square and the rectangular chambers. The crosses are the measured values of $\langle m \rangle$ and the open symbols are from the simulation described in the text.

Table 5.2: The average $\Delta\chi_p$, and v_p for each field. σ is the standard deviation of $\Delta\chi$. The uncertainty in each measurement is the S.E ($\sqrt{\sigma}/N$)

B (T)	Number of tracks (N)	$\langle\Delta\chi_p\rangle(\times 10^{-23}$ m$^3)$	$\sigma \times (10^{-23}$ m$^3)$	$\langle v_p\rangle (\mu$m s$^{-1})$
3	39	9.4 ± 0.9	5.3	908 ± 17
4.8	55	8.0 ± 0.3	2.7	920 ± 15
7.2	43	8.5 ± 0.3	2.2	920 ± 13
10.1	43	7.5 ± 0.2	1.5	940 ± 15
17.6	15	5.4 ± 0.6	2.2	874 ± 12

5.6   Discussion

We have shown that the swimming trajectories of *Paramecium caudatum* align with intense static magnetic fields exceeding 3 T. Since immobilized paramecia also align and the time dependence of their alignment is comparable to that of motile paramecia, the alignment of motile paramecia appears to be a passive response to the magnetic torque. That is, the torque acts on the whole *Paramecium* and not on some sensing organelle that dictates changes in swimming. The details of the time dependence of the rotation is consistent with a magnetic torque that is proportional to $B^2 \sin 2\theta$, where θ is the angle between the long axis of the *Paramecium* and the magnetic field. This dependence intimates that the torque originates in an interaction between the magnetic field and a net anisotropy of the diamagnetic susceptibilities of the constituents of the paramecia.

The result that paramecia respond passively to magnetic fields of the intensity used in our experiments was not predictable. It was at odds with the suggestions made by Rosen and Rosen based on their experiments on *Paramecium bursaria* in moderate static magnetic fields (0.13 T) [107]. They observed the magnetic field to induce changes in swimming speed

and thus, to exert a physiological influence. They speculated that the magnetic fields change the cilia beating pattern by affecting the ion fluxes across the membrane. This alteration could occur if the magnetic field were to distort the membrane shape [105, 106]. Speed changes might also result from magnetic torques exerted directly upon the beating cilia. We saw no clear evidence of speed changes in our substantially larger data set (Table 5.2) or of altered swimming mechanics and thus, concluded that such physiological effects, if any, are negligible.

5.6.1 Induced electromotive forces due to magnetic fields

We should address the issue of induced voltages in the membrane of a *Paramecium* due to its swimming in the magnetic field. For simplicity we approximate the *Paramecium* as a rectangular loop with short and long axes equal to $2a$ and $2b$ respectively. Since the flux of magnetic field changes in the loop due to rotational motion of *Paramecium* along its short axis, the induced EMF is

$$\mathscr{E} = -\frac{d}{dt} \oint_A B \cdot d\vec{a} = -\frac{d}{dt}(BA\cos\omega t) \tag{5.18}$$

$$= BA\omega \sin\omega t$$

where $\phi = \omega t$ is the angle of the loop with the field and A is the area of the loop. The angular velocity of *Paramecium* around its the short axis is equal to $\omega = 1.8$ rad s^{-1} [86]. Taking $a = 20$ μm and $b = 100$ μm, the induced EMF in 1 s is $\mathscr{E} \approx 1.4 \times 10^{-8}B$ V. At 10 T, for example, the EMF is about 10^{-7} V a very small value compared to the resting membrane potential of *Paramecium*, which is about -29 V. Also, the power dissipated in the membrane is then given as: $W_{diss} = \mathscr{E}^2/R$, where R is the resistance of the membrane.

The approximate value for R_A is 0.2 Ω m^2 [102], which considering the cross sectional area of the paramecium ($A = 8 \times 10^{-9}$ m^2) yields $R = 2.5 \times 10^{11}$ Ω. Thus the dissipated power is $W_{diss} \simeq 10^{-27}B^2$, a very small value compared to the rotational energy.

5.6.2 Comparison with magnetotactic bacteria

The passive alignment of motile paramecia with magnetic fields differs from that exhibited by magnetotactic bacteria [33]. The bacteria swim parallel to much weaker magnetic fields that are of order 10^{-4} T or less. The magnetic torque acts directly on internal chains of permanently magnetic magnetite particles or magnetosomes that are rigidly fixed to the bacterium. Also, they only swim toward a specific magnetic pole because the torque on a permanent magnetic dipole has a $\sin\theta$ dependence. By contrast, the induced magnetic moment in paramecia orient them toward both poles because their torque has a $\sin 2\theta$ dependence.

5.6.3 The effects of gravitational and hydrodynamic torques

In our model of the magnetic reorientation of motile *Paramecium* we have been able to neglect the influence of gravitational and hydrodynamic torques. Hydrodynamic torques can arise because of shape asymmetry [103] and the gravitational torques arise due to internal density inhomogeneities. Both of these tend to orient the *Paramecium* parallel with the gravity vector. In our experiments, the gravity vector and magnetic field vector are parallel. The gravitational and hydrodynamic torques combined can be expressed in the general form: $\Gamma_g = \gamma \sin\theta$ [87]. Mogami et al. [87] experimentally determined Γ_g=0.09 rad s^{-1} for *P. caudatum*, but point out that this value depends on the age of the cells, which affects their

shape and internal density variation. This value for γ would give rise to a considerable alignment (order parameter $\langle m \rangle = 0.7$) at 0 T for the characteristic time $\tau_c = 10$ s of our experiments. However our data show a close to random distribution at B=0 T (5.4). We conclude that for our paramecia, $\gamma \ll 0.09$ rad s^{-1} and thus, ignoring gravitational torques is justified.

5.6.4 Association of $\Delta\chi_p$ to the cortex

Given that the alignment appears to be a passive diamagnetic response, we consider whether the measured anisotropy in the diamagnetic susceptibility, $\Delta\chi_p$, is reasonable. We start by identifying the structures that are most likely to couple to the magnetic field. Such structures must be rigidly connected to the *Paramecium*. Their superposition must possess an axis of symmetry coincident with the long axis of the *Paramecium*.
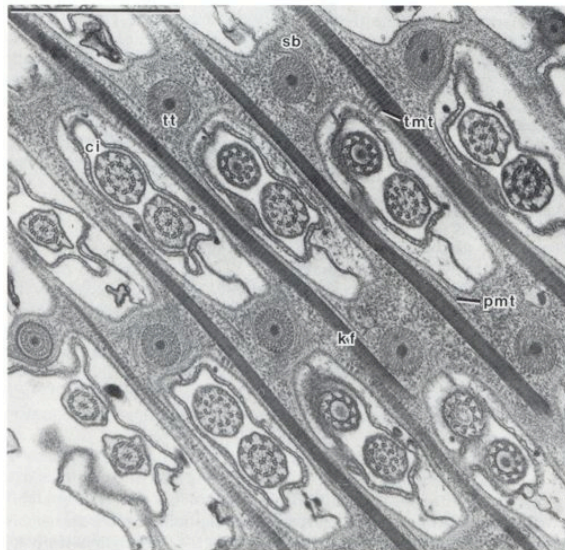
Figure 5.14: Electron micrograph of the cortex. The cross section shows a mosaic pattern with each unit about 1 μ m^2 area. Scale bar is 1 μm. The photograph from R. Wichterman *The Biology of Paramecium* [135].

The structures in the cytoplasm, including the nuclei and food vacuoles, do not exhibit much symmetry or rigidity and, seem unlikely targets. The most obvious candidates are structures associated with the cortex of the *Paramecium*. The cortex, which envelops the cell, is 4 μm thick, constitutes 40% of the total cell volume and is responsible for its rigidity [135]. The overall structure of the cortex is quite uniform except in the region near the oral groove. Thus, it has the required overall symmetry. Electron micrographs (Fig. 5.14) have revealed that the cortex is composed of nearly identical units approximately 1 μm^2 in area that are connected to each other in a mosaic pattern in plane with the surface of the *Paramecium*. Each "cortical unit" includes cilia, trychocysts, plasma membrane, cortical microtubules and fibrils [3], all of which have anisotropies in their diamagnetic susceptibilities. It is therefore plausible that a cortical unit has a net anisotropy in its diamagnetic susceptibility, $\Delta\chi_{cu}$ assuming the units are cylindrically symmetric. To have the paramecia align with the magnetic field, the majority of the cortical units should align in such a way that their long axis is perpendicular to the magnetic field as demonstrated in Fig. 5.15; this leads to $\Delta\chi_{cu} < 0$.

How large is $\Delta\chi_{cu}$ and is its value reasonable? To address this question, we model the cortex of a *Paramecium* as a cylindrical shell with inner and outer radii $r_1 = 16$ μm and $r_2 = 20$ μm respectively. The cylindrical shell has a length of $l = 200$ μm and hemispherical endcaps as depicted in Fig. 5.15. The total magnetic energy associated with the endcaps does not vary with angle by symmetry. The energy of the shell depends on its orientation

in the field. For parallel and perpendicular alignments we have

$$U_\perp = \frac{\Delta\chi_{cu} N_{cu}}{V_{cu}} \frac{B^2}{2\mu_0} l \int_0^{2\pi} \int_{r_1}^{r_2} \cos^2\theta r \, dr \, d\theta,$$

$$= \frac{\Delta\chi_{cu} N_{cu}}{V_{cu}} \frac{V}{2} \frac{B^2}{2\mu_0}, \tag{5.19}$$

$$U_\parallel = 0, \tag{5.20}$$

where N_{cu} is the number of cortical units in the cylindrical shell, V_{cu} is the volume of one cortical unit, θ is the angle of each cortical unit with the magnetic field and $V = \pi(r_2^2 - r_1^2)l$ is the volume of the shell. The energy difference is

$$\Delta U = U_\parallel - U_\perp = -\frac{1}{2}\left(\Delta\chi_{cu} N_{cu} \frac{B^2}{2\mu_0}\right). \tag{5.21}$$

Estimating $N_{cu} = 25,000$ and equating Eq. 5.21 to $\Delta\chi_p B^2/2\mu_0$ yields $\Delta\chi_{cu} = -5.4 \times 10^{-27}$ m^3. In this calculation we have used $\Delta\chi_p = 6.7 \times 10^{-23}$ m^3. To determine whether this value is realistic, we compare it to the anisotropy of the diamagnetic susceptibility of microtubules. The total anisotropy of the diamagnetic susceptibility of perfectly aligned microtubules filling a volume equivalent to the volume of a cortical unit is $N_\mu \Delta\chi_\mu = (1.6 \times 10^3) \times (2.6 \times 10^{-29}) = 4 \times 10^{-26}$ m^3, where N_μ is number of microtubules filling a cortical unit and $\Delta\chi_\mu$ is the anisotropy of the diamagnetic susceptibility of a 5 μm long microtubule [12]. This result suggests that if all the material in the cortical unit has approximately the same degree of anisotropy of the diamagnetic susceptibility as a microtubule then 14% of the total material would have to be aligned to give rise to the observed $\Delta\chi_{cu}$. Consequently, we conclude that the measured $\Delta\chi_p$ is reasonable.
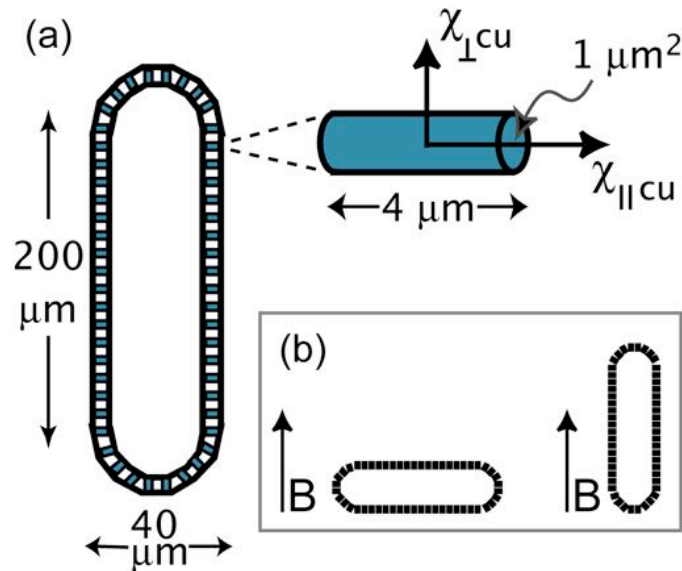
Figure 5.15: Schematic of simplified cortex and a cortical unit. (a) The outer radius is 20 μm and the inner one is 16 μm. A cortical unit with its long axis perpendicular to the cell surface. (b) Orientation energy of the cell is the difference between the two depicted orientations.

5.6.5 Prediction for the alignment of other microorganism

One might expect many other swimming, elongated, unicellular organisms to orient in a static magnetic field on the basis of the analysis above and measurements on other cell types [52, 53]. Indeed, we have observed that the swimming trajectories of *P. multimicronucleatum* and *P. tetraurelia* align along magnetic field lines at similar field strengths. Others [92] reported that *P. tetraurelia* align perpendicular to weak magnetic fields (0.68 T) in test solutions low in K^+, but we could not reproduce that result. In our model, the cell walls of the organisms only need to be homogeneous and composed of diamagnetically anisotropic material. A simple scaling argument based on Eq. 5.6 suggests that even very small organisms could be observed to align. The characteristic time for alignment scales as

the rotational drag over the magnetic torque. Since the magnetic torque scales with the cell volume, then this characteristic time depends linearly on the ratio of the long axis to the short axis of a cell (i.e. b/a). Within this picture, only random thermal fluctuations would prevent the smallest cells from aligning. Cells as short as 4 μm with a 0.8 μm diameter have a magnetic energy equivalent to the thermal randomizing energy, $k_B T$, at 5 T. Interestingly, there is evidence that the bacteria, *Escherichia coli*, (length = 1 μm and diameter = 0.5 μm) align completely within tens of seconds in fields of about 12 T [123].

5.7   Summary and future applications

We have shown that using an intense static magnetic field we can manipulate the motion of motile paramecia without affecting their swimming speed. Similar to *Paramecium*, many other microorganisms can be manipulated with magnetic fields. The direction of their orientation (parallel or perpendicular) and also the polarity of the orientation (monopolar or bipolar) can yield useful information about the average arrangement of molecular structures in the body or the existence of magnetic particles in the cell. Moreover, one can use the magneto-alignemnt of the swimming population of microorganisms as a tool to direct them towards a external stimulus (such as chemicals) and measure their tactic or kinetic responses. In less rigid cells such as neutrophils [124], we suspect that the magnetic fields can alter the cell shape and hence alter the motion. The cell deformation in magnetic fields can be an alternative to the current micropipette method [69] or the electromagnetic needle [84] used in the investigations of cell mechanics.

Chapter 6

Varying the effective buoyancy of cells using magnetic forces

6.1 Introduction

The body force of gravity influences myriad phenomena including the development of biological systems [76, 116, 13] , biopolymerization reactions [119], the crystallization of materials [133], and colloidal systems [20, 111] as well as others. Gravity couples to many of these systems through the relative buoyancy of their constituents. For example the single cell protist, *Paramecium*, has been known to orient with the gravity vector, and tends to swim against gravity, a phenomenon known as negative gravitaxis [77]. When swimming in a medium matched to its density, these responses cease [97]. The mechanisms behind these particular responses and other cellular responses to changes in gravity have been under investigation (for review see Refs.[75] and [48]). Present experimental methods employed include centrifugation (hypergravity), drop tower, space shuttle and parabolic flights (microgravity)

75

and/or methods to vary the density of the medium [56].

In this chapter we describe Magnetic Force Buoyancy Variation (MFBV), a technique for continuously tuning and even inverting the effective buoyancy of diamagnetic objects, such as cells, using an inhomogeneous magnetic field. We demonstrate MFBV on immobilized (i.e. non-swimming) paramecia, and describe its potential for simulating a microgravity environment for cell cultures.

6.2   The principle

As we have already mentioned in Sec. 2.4, when a diamagnetic object such as a cell in solution is placed in an inhomogeneous magnetic field, $B(z)$, its buoyancy changes due to the forces that the magnetic field applies to both the cell and the solution. The net force is then given by:

$$\vec{F}_{net} = \vec{F}_{mag} + \vec{F}_{drag} + \vec{F}_{buoy} \tag{6.1}$$

In Eq. 6.1, $\vec{F}_{mag}$ is the magnetic force acting on the cell and the solution, $\vec{F}_{drag}$, is the linear drag and $\vec{F}_{buoy}$ is the buoyancy. Since the axial forces are much larger than the radial force caused by the radial component of the field, we only consider the axial motion in the $\hat{z}$ direction. In this case,

$$\vec{F}_{mag} = \frac{(\chi_{cell} - \chi_{sol})V}{\mu_0} B(z) B'(z) \hat{z}. \tag{6.2}$$

Note that χ_{cell} is the volume average of the magnetic susceptibilities of the constituents of the cell, $B'(z) = dB(z)/dz$, V is the volume of the cell and μ_0 is the permeability of free space ($\mu_0 = 4\pi \times 10^{-7} \mathrm{H\ m^{-1}}$). The drag force, F_{drag}, is a linear function of a cell's speed and is given by: $F_{drag} = -\xi v_z \hat{z}$, where ξ is the linear drag coefficient and v_z is the

vertical component of the velocity. The buoyant force, $F_{buoy} = -(\rho_{cell} - \rho_{sol})V g \hat{z}$, where g is gravitational acceleration. In the low Reynolds number regime, $F_{net} = 0$ and Eq. 6.1 can be rearranged as:

$$b_{eff} = (\rho_{cell} - \rho_{sol})g - \frac{(\chi_{cell} - \chi_{sol})}{\mu_0}B(z)B'(z) = -kv_z, \tag{6.3}$$

where b_{eff} is the "effective buoyancy" and $k = \xi/V$.

To see more clearly how the magnetic force modifies the buoyancy of the cells, we normalize b_{eff}, to its value in the absence of the magnetic field ($b_0 = (\rho_{cell} - \rho_{sol})g = \Delta\rho g$). Therefore,

$$\frac{b_{eff}}{b_0} = 1 - \frac{1}{g\mu_0}\frac{(\chi_{cell} - \chi_{sol})}{(\rho_{cell} - \rho_{sol})}B(z)B'(z). \tag{6.4}$$

It is now apparent how b_{eff} can be adjusted to act in tandem with or opposite to the normal buoyant force by varying χ_{sol}, ρ_{sol} and/or $B(z)B'(z)$. Note that b_{eff} is similar to the quantity defined in centrifugation for which $g_{eff}/g = 1 + \omega^2 r/g$ where ω and r are the angular frequency and radius parameters for the centrifuge. The MFBV method is more versatile, however, as it enables decreased ($b_{eff}/b_0 < 1$) and even inverted ($b_{eff}/b_0 < 0$) buoyancy. This capability suggests novel methods for investigating the influence of gravity on the swimming behavior of microorganisms and for simulating variable gravity on cells in culture, for example.

6.3   Materials and methods

We have performed the proof of principle by using the AMI superconducting solenoid based magnet system and *Paramecium caudatum* cells. Samples of immobilized *Paramecium* in solution were reproducibly positioned along the axis of the bore to within 0.2 mm. A 6 mm

side view borescope (made by ITI) and a Sony XC-333 video camera were used for *in situ* sample imaging. A more detailed description of the setup is given in Sec.4.3

The paramecia were cultured in wheat solution using standard techniques (Appendix A). At their stationary phase of growth, they were immobilized with 0.5 mM $NiCl_2$ solution for about 10 minutes [67]. This time was limited to less than 20 minutes to prevent any shape change that would affect their hydrodynamic properties. Solution of immobilized paramecia were then collected with a micropipette and placed in a $5 \times 5 \times 30$ mm^3 cuvette (Beckman Instruments, Inc. CA). The magnetic susceptibility and the density of the solution were adjusted to produce a large potential variation in b_{eff}. This was achieved by adding a polymer of sucrose (Ficoll 400, Sigma-Aldrich) to the experimental solution (1 mM $CaCl_2$, 1 mM KCl, 5 mM Tris-HCl, pH 7.2). The effects of the magnetic properties of the Ficoll solution on the effective buoyancy of the *Paramecium* described here are similar to those used to magnetically levitated water immersed in a paramagnetic gas [56], i.e. it enhances the susceptibility difference $(\chi_{cell} - \chi_{sol})$. The addition of Ficoll also increased the viscosity of the medium, which facilitated the cell velocity measurements by slowing the cell motions and damping convective currents. The physical properties of these solutions are given in Table 6.1. The concentrations of Ficoll were 9% and 10% in different trials. The densities, ρ_{sol} are estimated using the material data sheet provided by the manufacturer (Amersham Biosciences) and the viscosities, η_{sol}, are published values [19]. We determined the susceptibility of the experimental solutions, χ_{sol} by the method described in Sec. 2.3.

Table 6.1: The physical properties of Ficoll solution.

Trial	Ficoll (w/v)	ρ_{sol} kg m^{-3}	χ_{sol} (SI) $(\times - 10^{-5})$	$\eta_{sol}(21 \pm 1°)$ mPa s
1 & 2	9%	1034 ± 1	0.921 ± 0.004	5 ± 1
3	10%	1037 ± 1	0.922 ± 0.004	6 ± 1

6.4 Experiments and results

Figure 6.1 demonstrates how the effective buoyancy of *Paramecium* is varied using magnetic forces.The interesting point in Fig. 6.1(a) is that the levitation ($b_{eff} = 0$) occurs below the center of the magnet. This is opposite to the case described in Sec. 2.2, where the water was levitated above the center of the magnet. In the case of *Paramecium* in Ficoll, $\chi_{sol} < \chi_{cell}$, making $\Delta\chi = \chi_{cell} - \chi_{sol} > 0$. Hence the solution is pushed away harder than the cell and the result is that the cell acts as a *paramagnetic* object: it appears that the cell feels a net force toward the center of the magnet as a paramagnetic object would in vacuum.

The direction of the net force on paramecia in Fig. 6.1 varies with its position in the solenoid. Paramecia sediment when placed in the yellow regions where $b_{eff}/b > 0$ and rise when placed in the orange region where $b_{eff}/b > 0$. At the center of the solenoid, where the magnetic field is homogeneous and thus the magnetic force is zero, the paramecia sediment only in response to gravity, as they do outside of the solenoid. The "normalized" sedimentation velocities of a single *Paramecium* at 21°C, in different positions in the solenoid are shown in Fig. 6.2 (circles). These were obtained by measuring the time for a *Paramecium* to move one body length. The velocities are normalized to the sedimentation speed at the center of the solenoid denoted by v_0.

As qualitatively described by Fig. 6.1, the *Paramecium* sediments down, then rises up,
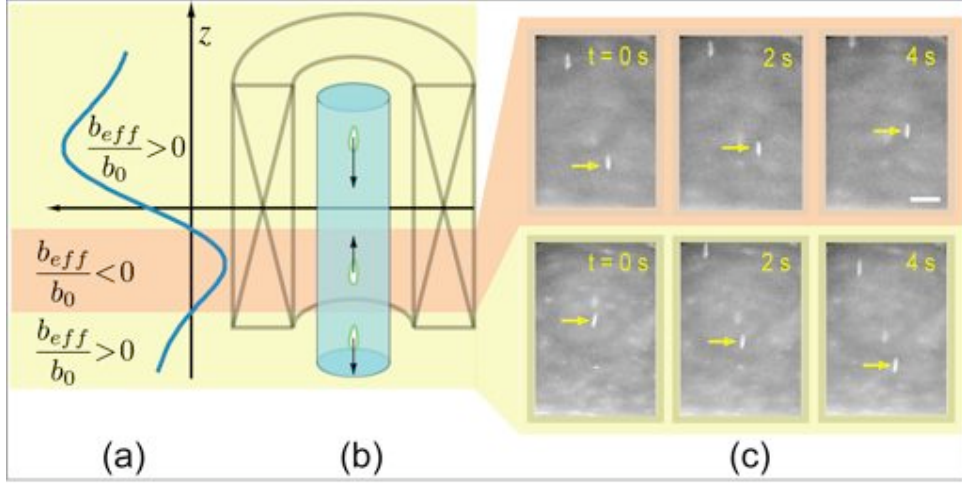
Figure 6.1: Varying the buoyancy of immobilized *Paramecium*. (a) Schematic of the effective buoyancy as a function of position in the solenoid. (b) Schematic of the solenoid with paramecia at different heights in a fluid column. (c) Images of immobilized paramecia in 9% Ficoll solution at the times, t, indicated. The upward moving *Paramecium* (see arrow in upper panels) is located where the effective buoyancy is negative. The downward moving *Paramecium* (see arrow in lower panels) is located where the effective buoyancy is positive (scale bar: 500 mm).

and then sediments down again as it is moved from $-z$ to $+z$. We have determined χ_{cell} for a *Paramecium* by fitting the normalized sedimentation/rising velocity measurements to Eq. 6.4. Using Eq. 6.3 and Eq. 6.4, we normalize the force to its absolute value at the center, $\Delta\rho g = |kv_0|$. This is related to the normalized velocity via:

$$\frac{b_{eff}}{b_0} = -\frac{kv_z}{\Delta\rho g} = -\frac{v_z}{v_0}. \tag{6.5}$$

The curve in Fig. 6.2 is a fit of $b_{eff}(z)/b_0$ to the peak region of the velocity data, obtained by adjusting $\zeta = (\chi_{cell} - \chi_{sol})/(\rho_{cell} - \rho_{sol})$. Using the values given in Table 6.1 for χ_{sol} and ρ_{sol} and the published value of $\rho_{cell} = 1040$ kg m^{-3} [121] the fit yields χ_{cell}. Results from three trials with different paramecia are summarized in Table 6.2. They yield an average value of $\langle\chi_{cell}\rangle = -(0.911 \pm 0.004) \times 10^{-5}$ in SI units. We emphasize that this

is the volume average magnetic susceptibility over all the constituents of the cell. Earlier

work [127] suggests that the magnetic susceptibilities of the constituents are similar to this

average. As a check of the density difference, we calculated the density of *Paramecium*

using the sedimentation data at the center of the magnet where the magnetic force is

zero. In this region, $(\rho_{cell} - \rho_{sol})Vg = \xi v_0$. V and ξ are calculated using the ellipsoid

approximation for *Paramecium* with semi-minor and semi-major axis of a and b ($V =$

$4\pi a^2 b/3$ and $\xi = 6\pi\eta(4a + b)/5$ [47]). Measurements on tens of paramecia in our lab have

yielded: $a = 23 \pm 2 \times 10^{-6}$ m and $b = 90 \pm 10 \times 10^{-6}$ m. The values for ρ_{cell} estimated

with this approach are presented in Table 6.2. The average ρ_{cell}, $\langle\rho_{cell}\rangle = 1042 \pm 2$ kg m^{-3},

is very close to the published value of $\rho_{cell} = 1040$ kg m^{-3} which is measured by a density

matched solution[121].

Table 6.2: Susceptibility and density measurements of *Paramecium*.

Trial	ρ_{sol} kg m^{-3}	χ_{cell} (SI) $(\times - 10^{-5})$	ρ_{cell} (estimated) kg m^{-3}
1	1034 ± 1	0.909 ± 0.004	1041 ± 3
2	1034 ± 1	0.909 ± 0.004	1042 ± 3
3	1037 ± 1	0.914 ± 0.003	1043 ± 2

6.5 Discussion and Applications

MFBV has multiple potential applications. As mentioned earlier, it can be used as a method

to investigate the mechanisms behind gravisensitivity of swimming protists. This aspect of

it will be addressed in Chapter 7. MFBV can also be used as an alternative to centrifugation

for collecting cells. Finally MFBV can be applied to address the challenge of adequately
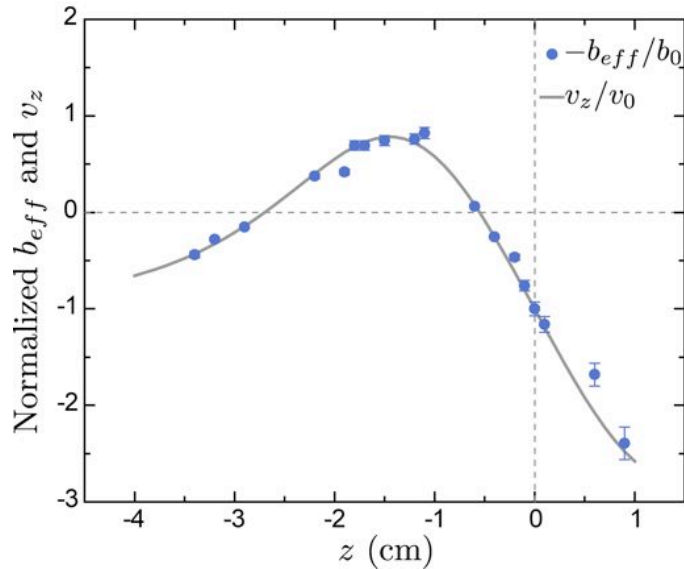
Figure 6.2: Sedimentation velocities of non-swimming *Paramecium* in variable buoyancy. Normalized velocities (circles) of non-swimming *Paramecium* in 9% Ficoll solutions as a function of position along the magnets axis. The zero in position corresponds to the center of the solenoid. The solid line is the fit of Eq. 6.4 to the data. Error bars are calculated from uncertainties in V and ξ due to uncertainties in a and b.

feeding suspended cell cultures in microgravity or simulated microgravity.

On Earth, gravity driven convection provides the necessary mixing and replacement of nutrient deficient volumes that develop near growing cells. Without convection, cells starve as diffusion rates are too slow. The rotating wall vessel bioreactor, developed at NASA, provides one method for overcoming this obstacle and a method for suspending cultured cells indefinitely on Earth [34]. Cells are placed in a culture medium that is rotated about a horizontal axis at a rate set to cancel the cell sedimentation rate. In it, cells sediment indefinitely in the culture medium and thus, constantly encounter new fresh medium. Similarly, magnetic forces can be used to "drag" cells through fresh medium as depicted in Fig. 6.3. Placing the solution in the region between the upper yellow region and the orange region, causes the cells to move and settle at the boundary of the two regions,
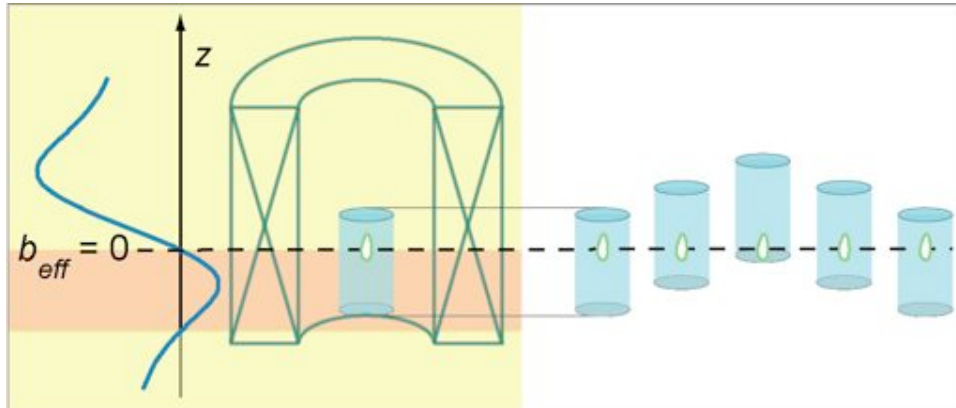
Figure 6.3: A schematic showing how MFBV can be used to suspend a cell and move the solution around it.

where the net force on them is zero. This position is vertically stable. Thus, cells can rest at that position indefinitely as though they were in a density matched solution. What is truly novel, however, is that the solution can be moved relative to the cells simply by moving the container up and down. The cells are at equilibrium in a position relative to the magnet and not the solution. Thus, it is possible to constantly refresh the solution around the cells, simply by oscillating the container. In the absence of gravity, magnetic forces could be used to replace gravity to drive the necessary convection.

In applying MFBV to simulate "variable gravity" it is important to control for potential magnetic field induced side effects. Diamagnetic structures in cells can experience magnetic torques due to their anisotropic magnetic properties. In some cases these torques can produce substantial changes [28]. By comparing specimens subjected to a magnetic force as in MFBV with specimens subjected to a uniform magnetic field, changes due to "magnetic field side effects" can be evaluated and accounted for.

Chapter 7

Paramecium's swimming response to magnetically varied buoyancy

7.1 Introduction

Swimming unicellular microorganisms such as bacteria and protozoa exhibit a variety of kinetic responses to external fields. *Kinesis* refers to a change in an organism's swimming speed or direction when exposed to external stimuli such as a chemical gradient [132], temperature gradient [22] and light [95]. Of interest here is the gravikinesis exhibited by protozoa such as *Paramecium*, *Didinium* and *Loxodes* [97, 14, 75]. They actively alter their swimming speed as their orientation changes relative to Earth's gravity vector. This response enables them to fight sedimentation as they seek more favorable habitats [61]. It is remarkable since it requires the ability to sense forces on the order of their apparent weight, which for *Paramecium* is only on the order of 100 pN. The details of how cells sense these small forces are not yet established[60, 18].

84

Increasing the effective gravitational force accentuates graviresponses that are sometimes screened by other factors at normal gravity and thus difficult to detect [79, 32]. Therefore, centrifugation simulations of increased gravity are attractive for studies of gravisensitivies of swimming organisms [97, 14, 32], plant gravitropism [98], and cell culture systems (12). Here we show that magnetic forces can be employed to simulate variable gravity environments for paramecia. This work builds on previous studies including the application of magnetic levitation [7, 36, 127] to simulate zero gravity for protein crystallization [70, 139] and fluid dynamics experiments [82]. Also, magnetic forces have been applied to alter gravitropism in plants [66]. In Chapter 6, we introduced magnetic force buoyancy variation (MFBV), a method used to vary the apparent weight of immobile cells with magnetic forces. Here we apply MFBV, with some modifications, to swimming paramecia to investigate their gravikinetic response.

The advantage of MFBV as a gravity simulation technique is that it can simulate enhanced, reduced and inverted gravities. Apart from centrifugation experiments in space, it is the only available method that can simulate both hyper- and hypogravities in a single experimental setup. This quality permits subjecting the same sample of cells to both conditions and therefore facilitates comparative studies of these conditions. Our experiments show that paramecia exhibit a similar "negative" response to a magnetically simulated gravity environment as they do in centrifugation experiments. Their self-propulsion is greater when swimming against the simulated gravity force than when swimming with it. The gravikinetic response is linear from -5 g to 5 g and becomes nonlinear at higher simulated gravities. The gravikinetic factor obtained for the linear regime agrees with previous centrifugation results [97, 14]. When the simulated gravity approaches 10 g, most paramecia

orient anti-parallel to the force direction and on average propel without advancing, i.e. they stall. This behavior suggests a maximum propulsive force for *Paramecium* of around 0.7 nN.

7.2 Materials and Methods

7.2.1 *Paramecium* and Gd-DTPA solution

Paramecium caudatum (Carolina Biological Supply) was cultured on Hey medium inoculated by *Enterobacter aerogenes* (Appendix A). At their stationary phase of growth, they were collected using low speed centrifugation and suspended in test solution containing 1 mM $CaCl_2$, 1 mM KCl, 0.1 mM $MgSO_4$, 1.5 mM MOPS at pH 7.2. The paramecia were left in this solution for up to two hours to adapt prior to experimentation.

To enhance the magnetic properties of the aqueous solution Gadolinium-diethylene-triamine-pentaacetate (Gd-DTPA, Sigma-Aldrich), a paramagnetic MRI contrast enhancing agent [136, 134] was added to the test solution in 2 mM and 4 mM concentrations. Unlike $GdCl_3$ salt, Gd-DTPA is a stable compound that does not introduce Gd^{+3} ions in the solution and therefore it is non-toxic. The pH of the solution was adjusted to 7.2 by using NaOH and HCl. At these low concentrations, paramecia showed no behavioral changes such as a change in swimming pattern and could survive for a few days. We did observe, however, that the swimming speed of paramecia dropped uniformly in these Gd-DTPA solutions. No direct relationship between the amount of Gd-DTPA and the speed change could be deduced due to large variation in speeds.

To immobilize the paramecia, they were exposed to 0.5 mM $NiCl_2$ for 10 minutes. The

$NiCl_2$ solution was made such that the final solution had the desired concentration of Gd-DTPA (2 mM or 4 mM). This was done by diluting high concentration of $NiCl_2$ with solution containing *Paramecium* and high concentration of Gd-DTPA. After the paramecia were immobilized, they were collected with a micropipette and transferred into the experimental chamber containing the same concentration of Gd-DTPA (2 mM or 4 mM) as the immobilizing solution. This protocol was followed to insure that the immobilized paramecia were subjected to the same amount of Gd-DTPA as the swimming ones.

The experiments were performed in two types of chambers similar to the ones introduced in Chapter 5. Both had a depth much smaller than the width and length to provide a nearly two-dimensional environment. The only difference was that due to limited space in this experiments, the size of the square chambers was smaller (2 mm×15 mm×15 mm). During the experiments, we encountered some problems, such as currents in the square chambers, therefore the use of rectangular tubes or larger square chambers is recommended. The specifics of the experiments are summarized in Table 7.1.

Table 7.1: Specifics of the three trials

Trial	chamber shape	[Gd-DTPA]
1	Rectangular	4 mM
2	Rectangular	4 mM
3	Square	2 mM

7.2.2 Apparatus

The experiments were carried out using a resistive magnet at the National High Magnetic Field Laboratory (Tallahassee, FL). The magnet has a 50 mm bore and produces a 31 T

maximum field and 4754 ± 170 T^2 m^{-1} maximum BB'. The temperature of the chambers containing paramecia was kept at $22\pm0.2°$ C using a water-circulating bath. Details are explained in Chapter 4, Sec. 4.2.

Reduced and inverted simulated gravity experiments were performed by placing the experimental chamber above the center of the magnet and the external field was varied to achieve various force strengths. Vice versa, the chamber was placed below the center of the magnet for increased simulated gravity experiments. The control experiments at 1 g with $BB = 0$ was carried out at the center of the magnet.

The velocity of a *Paramecium* was calculated as the displacement vector of the total trajectory divided by total time. Only trajectories that extended a couple of spatial periods or more and which had an inclination angle of a maximum of 10 degrees from the vertical were analyzed. The latter constraint insured that only vertical trajectories were analyzed. To minimize the influence of hydrodynamic interactions with the walls, only tracks that were at least a few body lengths away from the walls were analyzed. Since some paramecia reverse their swimming direction or make abrupt turns due to avoiding reactions such as bumping into other paramecia or particles in water, a filtering procedure was used to eliminate those tracks from final analysis (Chapter 4).

7.2.3   Sedimentation measurements

We measured v_S, the sedimentation rate in 1 g, by first levitating immobilized cells in a 3.6 mM Gd-DTPA solution and then releasing them to sediment by turning off the magnetic field. Figure 7.1 shows the sedimentation speed histograms for two trials. Measurements on about 130 cells yielded $v_S = 96.6 \pm 1.9$ μm s^{-1} (mean$\pm$S.E., $\sigma_S = 21.7$ μm s^{-1}), similar
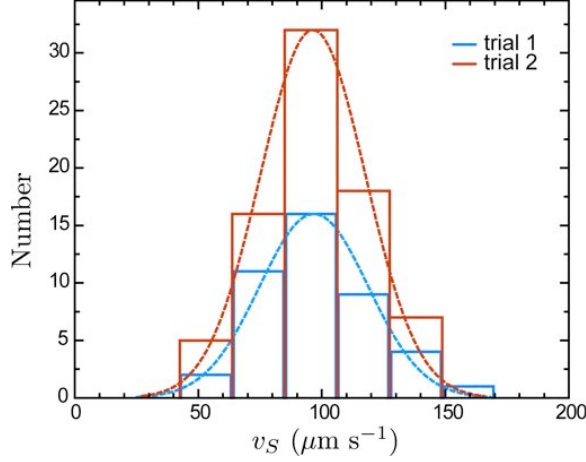
Figure 7.1: Sedimentation measurements for two trials presented in Table 7.2. The dashed lines are the gaussian fit to the data.

to previous results [75]. The width of the distribution of the sedimentation speeds can be attributed to the variation in size and density of the *Paramecium* which will affect their hydrodynamics. The details of our measurements are presented in Table 7.2.

Table 7.2: Sedimentation values at 1 g

Trial	Number	v_S (μm s^{-1})	σ_S (μm s^{-1})
1	47	96.8	22.0
2	82	96.4	21.3

We can compare our measured sedimentation speeds with the ones expected by balancing the forces of gravity and buoyancy on a sedimenting body in the low Re number regime:

$$\Delta\rho V g = \xi v_S. \tag{7.1}$$

where $\Delta\rho = 40$ kg m^{-3} is the difference in the densities of *Paramecium* and water, V is the volume, ξ is the linear drag coefficient and v_S is the sedimentation speed. As before, $\xi = 6\pi\eta(4a + b)/5$ [47], where $\eta = \eta_{water} = 10^{-3}$ Pa s. Within this approximation, $v_S \approx 98$ μm, which is very close to our measured value and it suggests that cilia do not

increase the drag considerably.

7.3 Experimental procedure

The gravity simulation method is based on the magneto-Archimedes principle, which has been employed to "float" gold and other relatively dense diamagnetic materials [56, 17] and cells [42, 136] in solutions of lesser density. When a cell in solution is placed in an inhomogeneous magnetic field, $B(z)$, the magnetic force changes the buoyancy or the apparent weight per volume from $w = \Delta\rho g$ to

$$w = \Delta\rho g - \frac{\Delta\chi}{\mu_0}BB'. \tag{7.2}$$

where B' is the derivative of $B(z)$ with respect to the vertical direction z, $\Delta\rho = \rho_{cell} - \rho_{sol}$ and $\Delta\chi = \chi_{cell} - \chi_{sol}$ represent the differences between the cell and solution densities and magnetic susceptibilities respectively, and $\mu_0 = 4\pi \times 10^{-7}$ H m^{-1} is the permeability of free space. It is important to note that in this approach we consider the cell as homogenous and thus χ_{cell} and ρ_{cell} are the average values for the whole cell. For simplicity, we define the net force per mass, f_{gm},

$$f_{gm} = g - \frac{\Delta\chi}{\mu_0\Delta\rho}BB'. \tag{7.3}$$

Similar to a centrifuge, f_{gm} can be increased continuously. Moreover, simulated zero gravity, where $f_{gm} = 0$, or inverted gravity, where $f_{gm} < 0$, also can be attained.

According to Eq. 7.3, the magnitude and the direction of f_{gm} can be tuned by changing either or all of $\Delta\chi$, $\Delta\rho$ and BB'. In our experiments, $\Delta\rho$ was held fixed at its natural value, which is $\Delta\rho = 40$ kg m^{-3}. We produced a large range of f_{gm} by doping the solution with a fixed concentration of the paramagnetic compound, Gd-DTPA (see Materials and

Methods), to enhance $|\Delta\chi|$ and by varying BB'. The following section is a description of the method used to calibrate f_{gm}.

7.3.1 Calibration of f_{gm}

For *Paramecium* in water, $\chi_{sol} = -0.904 \times 10^{-5}$ and $\chi_{cell} = -0.911 \times 10^{-5}$ (Chapter 6 so that $\Delta\chi = -0.007 \times 10^{-5}$ (SI). This value affords a maximum adjustment of f_{gm} of only about 50%, with the available BB'. Adding 4 mM and 2 mM Gd-DTPA modifies $\chi_{sol}(4\text{ mM}) = -0.764 \times 10^{-5}$ and $\chi_{sol}(2\text{ mM}) = -0.834 \times 10^{-5}$ (SI), respectively. This estimations were done using $\chi_{Gd-DTPA} = 0.028$ cm^3 mol^{-1} [136] (Sec. 2.4). The addition of Gd-DTPA also increases χ_{cell} since paramecia exchange solution constantly. However χ_{cell} changes by a smaller amount, leading to a net increase in $\Delta\chi$. To determine $\Delta\chi$, we measured $(BB')_0$ at which immobilized paramecia were neutrally buoyant (i.e. $f_{gm} = 0$). At 4 mM Gd-DTPA, $(BB')_0 = -510 \pm 10$ T^2 m^{-1}, implying $\Delta\chi = -(0.097 \pm 0.002) \times 10^{-5}$ (SI) and at 2 mM Gd-DTPA, $(BB')_0 = -1020 \pm 20$ T^2 m^{-1} implying $\Delta\chi = -(0.048 \pm 0.002) \times 10^{-5}$ (SI). In a given trial, we vary BB' at fixed Gd-DTPA concentration. Accordingly it is convenient to rewrite Eq. 7.3 in the form:

$$f_{gm} = g \left(1 - \frac{BB'}{(BB')_0} \right),$$
$$(7.4)$$

Thus, varying BB' yield the ranges $-8\,g \leq f_{gm} \leq 10\,g$ and $-3\,g \leq f_{gm} \leq 5\,g$ for the 4 mM and the 2 mM Gd-DTPA concentrations, respectively.

7.3.2 The effect of Gd-DTPA on $\Delta\chi$

We estimated the amount of exchanged solution by considering that the volume of a *Paramecium* consists of 70% water and 30% protein and lipids and other components. Therefore

$$\chi_{cell} = 0.3\chi_{p-l} + 0.7\chi_{water} \tag{7.5}$$

$$\chi_{cell} = \beta + 0.7\chi_{water}$$

Using $\chi_{cell} = -0.911 \times 10^{-5}$ we obtain $\beta = 0.278 \times 10^{-5}$. Now, if after transferring the cell into the Gd-DTPA solution, some fraction, n, of the water inside the cell is replaced by the solution, the susceptibility of the cell will be modified as:

$$\chi'_{cell} = \beta + n\chi_{sol} + (0.7 - n)\chi_{water} \tag{7.6}$$

Or

$$n = \frac{\chi'_{cell} - \beta - 0.7\chi_{water}}{\chi_{sol} - \chi_{water}} \tag{7.7}$$

On the other hand, the levitation measurements at each concentration of Gd-DTPA yields $\chi'_{cell} = \Delta\chi + \chi_{sol}$. Therefore n is given by:

$$n = \frac{\Delta\chi + \chi_{sol} - \beta - 0.7\chi_{water}}{\chi_{sol} - \chi_{water}} \tag{7.8}$$

Using our measured values for Δ_χ for 4 mM and 2 mM Gd-DTPA concentrations, $n = 33\%$ and $n = 41\%$, respectively. As can be seen, not all the water in the cell is replaced by Gd-DTPA solution. We do not know wether the solution enters the cell via membrane, or food vacuoles or both. We speculate since not all the water is replaced by the external solution, probably the solution is entering true food vacuoles. It might be worthwhile to estimate the volume fraction of food vacuoles in a cell to verify this possibility. Moreover,

using larger compounds of Gd- salt, might be more efficient in the sense that the exchange by the membrane will be suppressed.

7.4 Results and Discussion

Samples of swimming tracks of paramecia in $f_{gm} = 4\ g$, $0\ g$ and $-4\ g$ are shown in Fig. 7.2. These and virtually all of the tracks can be labeled as either upward (green) or downward (red) due to a helpful artifact of this gravity simulation method. Magnetic fields align the trajectories of swimming paramecia parallel to the field lines as we showed in Chapter 5 without influencing their swimming speed. In our setup, where the magnetic field is parallel to the simulated gravity vector, the fraction of vertical swimmers within $10°$ of vertical approaches 100% for $B > 10$ T, as we already have shown in Chapter 5. This artifact ameliorates the quality of the statistical analysis.

Inspection of the swimming tracks reveals that paramecia swim faster downward (red) than upward (green) in $f_{gm} = 4\ g$ and vice versa in $f_{gm} = -4\ g$. At $f_{gm} = 0\ g$ the upward and downward rates are comparable. The histograms in Fig. 7.2 show the corresponding velocity distributions (the bin size is chosen to be one standard deviation). 80% of all the distributions were normal to a 95% confidence level as determined by the Lilliefors test (using *Origin* software). Moreover, for all distributions, the maximum variation between the mean and the median of the velocities was 3%, which justifies the use of the mean rather than the median velocity in our analysis. Evaluation of a few hundred tracks at each f_{gm} shows that the mean speeds of vertical upward, V_U, and downward, V_D, swimmers decrease and increase, respectively, nearly linearly with f_{gm} from $-5\ g$ to $5\ g$ as shown

in Fig. 7.3. Note that "up" and "down" are relative to Earth's gravity and therefore for $f_{gm} > 0$ "up" signifies against the force and for $f_{gm} < 0$ "up" signifies with the force. To assess whether the variation of $V_U(f_{gm})$ and $V_D(f_{gm})$ involves an active kinetic response to this magnetically generated force, it is necessary to first account for their passive tendency to sediment. Sedimentation is expected to lead to a linear dependence of $V_U(f_{gm})$ and $V_D(f_{gm})$ on f_{gm} as given by:

$$V_U(f_{gm}) = V_0 - v_S f_{gm}/g = V_0 - V_S(f_{gm}), \tag{7.9}$$

$$V_D(f_{gm}) = V_0 + v_S f_{gm}/g = V_0 + V_S(f_{gm}). \tag{7.10}$$

where V_0 denotes the average swimming speed at $f_{gm} = 0$ and v_S is the sedimentation rate at 1 g. $v_S = 96.6 \pm 1.9$ μm s^{-1} (mean$\pm$S.E., $\sigma_S = 21.7$ μm s^{-1}) as discussed in the Sec. 7.2.3. We have assumed that the sedimentation rate grows linearly with f_{gm} [97].

The two solid lines in Fig. 7.3 are the representation of this passive model embodied in Eq. 7.9. The error in the sedimentation speeds is indicated by the thickness of each line in Fig. 7.3. V_0 was estimated from the weighted average of intercepts of the linear fits to the data (Fig. 7.3) at $f_{gm} = 0$ g. The tendency to sediment without active regulation leads to a difference between downward and upward swimming rates given by:

$$V_D(f_{gm}) - V_U(f_{gm}) = 2V_S(f_{gm}). \tag{7.11}$$

which corresponds to the vertical separation of the solid lines in Fig. 7.3. The measured $V_U(f_{gm})$ and $V_D(f_{gm})$, however, fall within the envelope defined by these lines indicating that paramecia exhibit a negative kinetic response to f_{gm}. To analyze this response, we use
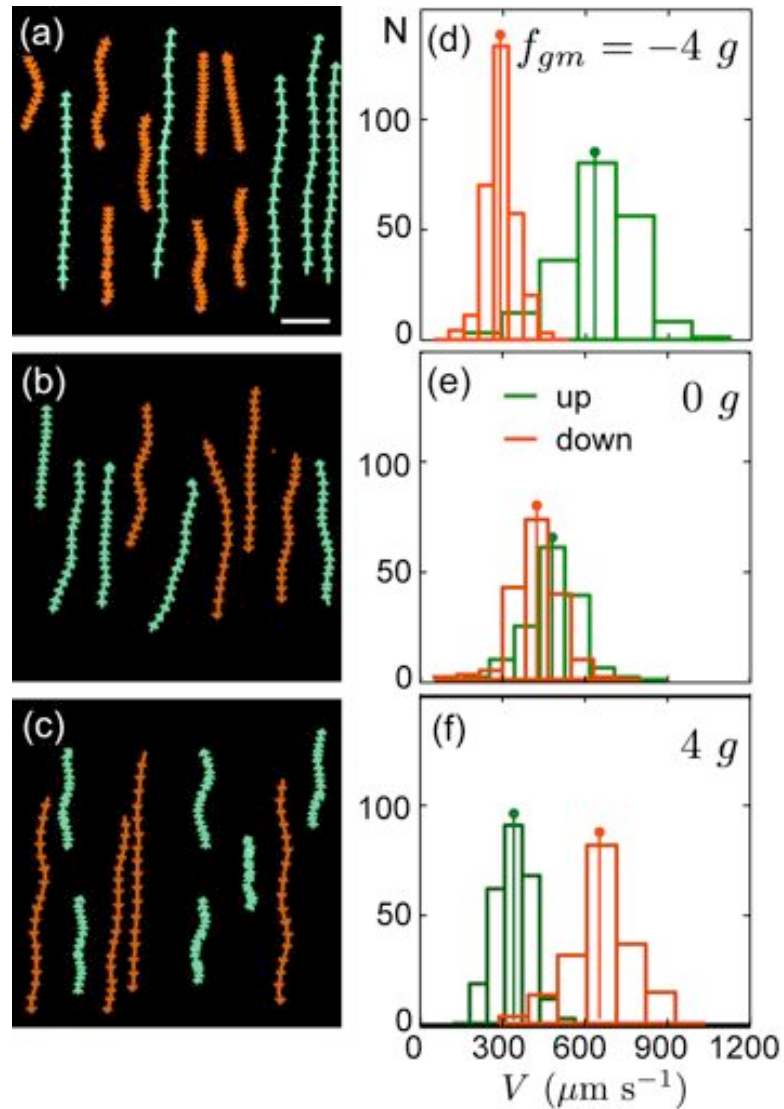
Figure 7.2: The swimming trajectories and speed distributions of paramecia in variable simulated gravity. From (a) to (c) f_{gm} is $-4\ g$, $0\ g$ and $4\ g$, respectively. Upward (green) and downward (red) swimming trajectories were each tracked for 3 seconds in simulated gravity (scale bar = 500 μm). (d) to (f) give the upward and downward swimming speed distributions at each field, respectively. The bulleted line shows the mean velocity. The bin size is the standard deviation of speed distribution in each direction. Notice that virtually all of the tracks are upward or downward due to magnetic field alignment (see text)
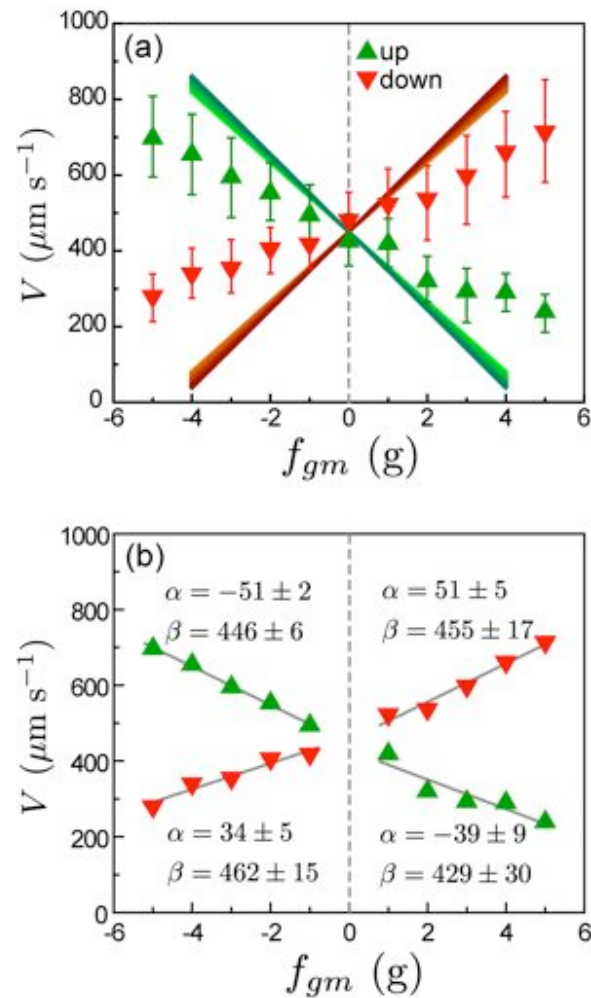
Figure 7.3: Swimming speed of *Paramecium* in simulated gravity. (a) Mean upward (green triangles) and downward (red triangles) swimming speeds as a function of simulated gravity for trial 1. The bars indicate the widths of the speed distributions. The upper bar represents the first 68% of swimmers above the mean and the lower bar indicates the first 68% of the swimmers below the mean. The solid lines denote the predicted change in the swimming speed in the absence of any kinetic effects. Their widths indicate the uncertainty in the mean sedimentation rate. (b) Linear fits to up and down swimming speeds. α and β are the fitting parameter to the line $V = \alpha \times f_{gm} + \beta$. Data at $f_{gm} = 0$ are eliminated to reduce fitting error. Inverting the simulated gravity inverts the effect.

the terminology of Machemer *et al.* [75]; decomposing the speed in each direction as:

$$V_U(f_{gm}) = V_0 - V_S(f_{gm}) - \Delta_U(f_{gm}), \qquad (7.12)$$

$$V_D(f_{gm}) = V_0 + V_S(f_{gm}) + \Delta_D(f_{gm}).$$

Here, $\Delta_U(f_{gm})$ and $\Delta_D(f_{gm})$ are the gravikinetic factors for up or down swimmers. The average gravikinetic factor,

$$\Delta(f_{gm}) = \frac{\Delta_D(f_{gm}) + \Delta_U(f_{gm})}{2}, \qquad (7.13)$$

can be rewritten as the following using Eq. 7.12

$$2\Delta(f_{gm}) = V_D(f_{gm}) - V_U(f_{gm}) - 2V_S. \qquad (7.14)$$

The measured Δ values as a function of f_{gm} for three different trials are plotted in Fig. 7.4. They all show a linear dependence described as $\Delta(f_{gm}) = \delta \times f_{gm} + \Delta_0$ for the $-5\ g \leq f_{gm} \leq 5\ g$ regime with similar slopes, δ. The specifics of each trial are summarized in Table 7.3. The average value of δ from the three trials, $\langle \delta \rangle = -50 \pm 1\ \mu\text{m s}^{-1}$, agrees with that measured for paramecia in the hypergravity of centrifuges [97, 14, 75, 77]. Δ_0 exhibits a small variation of unknown origin from experiment to experiment. We cannot discern whether it is zero.

Table 7.3: Gravikinetic factors Δ, Δ_-, and Δ_+ measured in the range of $-5\ g \leq f_{gm} \leq 5\ g$ from three trials.

Trial	$\Delta = \delta \times f_{gm} + \Delta_0$ (μm s^{-1})		V_0 (μm s^{-1})	$\Delta_- = \delta_- \times f_{gm} + \Delta_{-0}$ (μm s^{-1})		$\Delta_+ = \delta_+ \times f_{gm} + \Delta_{+0}$ (μm s^{-1})	
	δ	Δ_0		δ_-	Δ_{-0}	δ_+	Δ_{+0}
1	-53 ± 1	15 ± 2	450 ± 25	-63 ± 5	12 ± 15	-46 ± 2	4 ± 6
2	-57 ± 1	3 ± 4	400 ± 30	-66 ± 2	3 ± 7	-48 ± 1	2 ± 3
3	-49 ± 1	17 ± 3	510 ± 25	-65 ± 1	17 ± 3	-32 ± 2	19 ± 5

The slopes of fitted lines to up and down swimming speeds in Fig. 7.3(b) differ, suggesting that the regulation depends on whether the paramecia are swimming with or against the force. To quantify these phenomena, we define $\Delta_+(f_{gm})$ and $\Delta_-(f_{gm})$ to be the kinetic factors for swimming with or opposed to the applied force, respectively.

$$
\begin{aligned}
\Delta_+(f_{gm}) &= \Delta_D(f_{gm}) = V_D(f_{gm}) - V_0 - V_S(f_{gm}), \\
\Delta_-(f_{gm}) &= \Delta_U(f_{gm}) = V_U(f_{gm}) - V_0 + V_S(f_{gm}).
\end{aligned} \qquad f_{gm} > 0 \qquad (7.15)
$$

$$
\begin{aligned}
\Delta_+(f_{gm}) &= \Delta_U(f_{gm}) = V_U(f_{gm}) - V_0 + V_S(f_{gm}), \\
\Delta_-(f_{gm}) &= \Delta_D(f_{gm}) = V_D(f_{gm}) - V_0 - V_S(f_{gm}).
\end{aligned} \qquad f_{gm} < 0 \qquad (7.16)
$$

Our measured values for $\Delta_+(f_{gm})$ and $\Delta_-(f_{gm})$ for the three trials are summarized in Table 7.3.

Even though an exact measurement of $\Delta_+(f_{gm})$ and $\Delta_-(f_{gm})$ is difficult due to uncertainties in estimating $V_S(f_{gm})$ and V_0, there are common trends in all trials; while the regulation for both up and down swimmers increases by increasing f_{gm}, in all cases $|\delta_-| > |\delta_+|$, which means paramecia swimming against the force adjust more than those swimming with the force. This finding agrees with previous experiments based on centrifugation [97, 14, 77].

At high f_{gm}, nonlinearities in the response become evident, as shown in Fig. 7.5(a). $V_U(f_{gm})$ appears to saturate at a minimum speed of ≈ 220 μm s^{-1} for 5 g < f_{gm} < 10 g. $V_D(f_{gm})$ also saturates in this regime but less prominently. In both cases these behaviors are consistent with an enhanced negative gravikinetic response in the high f_{gm} regime. It is possible to extract the average propulsion force exerted by the paramecia and measure directly their active fight against sedimentation. Their propulsion force, $F_P(f_{gm})$,
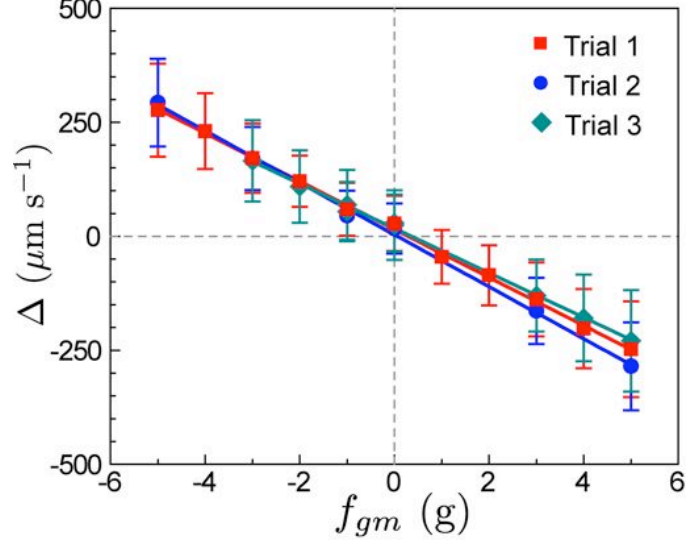
Figure 7.4: Gravikinetic factor measured for the three trials introduced in Table 7.1 for $-5\ g \leq f_{gm} \leq 5\ g$. The lines are the least square fits to the data. The negative slope implies negative gravikinesis. The fit parameters are given in Table 7.3. The uncertainty bars are ± 1 standard deviation.

is balanced by the sum of their apparent weight and the drag force exerted on them by the solution.

$$F_{P\uparrow}(f_{gm}) = \xi V_U(f_{gm}) + \Delta\rho V f_{gm}, \quad \text{Upward swimmers} \tag{7.17}$$

$$F_{P\downarrow}(f_{gm}) = \xi V_D(f_{gm}) - \Delta\rho V f_{gm}. \quad \text{Downward swimmers.} \tag{7.18}$$

As described in Sec. 7.2.3, ξ is the linear drag coefficient and η is the viscosity of the medium. As before, by modeling the paramecia as solid ellipsoids we calculate $F_{P\uparrow}$ and $F_{P\downarrow}$ as plotted in Fig. 7.5(b). Up to 5 g, they both appear linear in f_{gm}. Above $f_{gm} = 5\ g$, $F_{P\uparrow}$ rises more rapidly than $F_{P\downarrow}$ decreases, consistent with the nonlinearity in Fig. 7.5(a). At the highest f_{gm}, both the downward and upward swimmers reach their capacity for adjusting their forward propulsion force. Near $f_{gm} = 8\ g$, $F_{P\downarrow} \rightarrow 0$ suggesting the paramecia stop swimming. It is not clear whether they cease to beat their cilia entirely or adjust the angle of

their ciliary beating so that they exert no forward propulsion force. Detailed investigations of individual swimmers may discern which possibility is correct. Whichever the case, their behavior is consistent with free sedimentation. The upward swimmers, on the other hand, approach their maximum propulsion force, 0.7 nN at $f_{gm} = 8$ g.

Above $f_{gm} = 8$ g, a number of downward swimmers were observed to flip mid-trajectory to orient anterior end up and swim against the force. At $f_{gm} \approx 10$ g, the upward oriented cells do not advance much with time (i.e. $V_U \simeq 0$) as shown by the plot of the vertical position as a function of time for a number of paramecia, (Fig. 7.6). To get a more accurate measurements, the movies for this experiment were digitized at 10 fps. They occasionally move slowly forward or backward a couple of body lengths before stalling in a new position for a few seconds. Many move slowly upward for a few seconds and then drop abruptly. These falling events are indicated by the arrows. Analysis of 30 tracks shows that these drops occur at a rate 1044 ± 225 μm s^{-1} (mean$\pm$ S.D.), which is close to the estimated passive sedimentation speed at $f_{gm} = 10$ g. Our measured stalling force, $F_{P\mathrm{max}} = \Delta \rho V f_{gm} = 0.7$ nN, is about 10 times smaller than that reported by Kuroda and Kamiya [65] using density graded solutions and a high speed centrifuge.

7.4.1 Dependence of σ on f_{gm}

The distribution widths in Fig. 7.2 show an interesting trend with f_{gm}. At $f_{gm} = 0$ g, the width defines as σ of both upward and downward swimming speed distributions are almost equal. Moving to nonzero f_{gm}, the distributions narrow (broaden) for the swimmers moving against (with) the force. The plot of σ as a function of f_{gm} is shown in Fig. 7.7. The dashed lines are fit to the data described below.
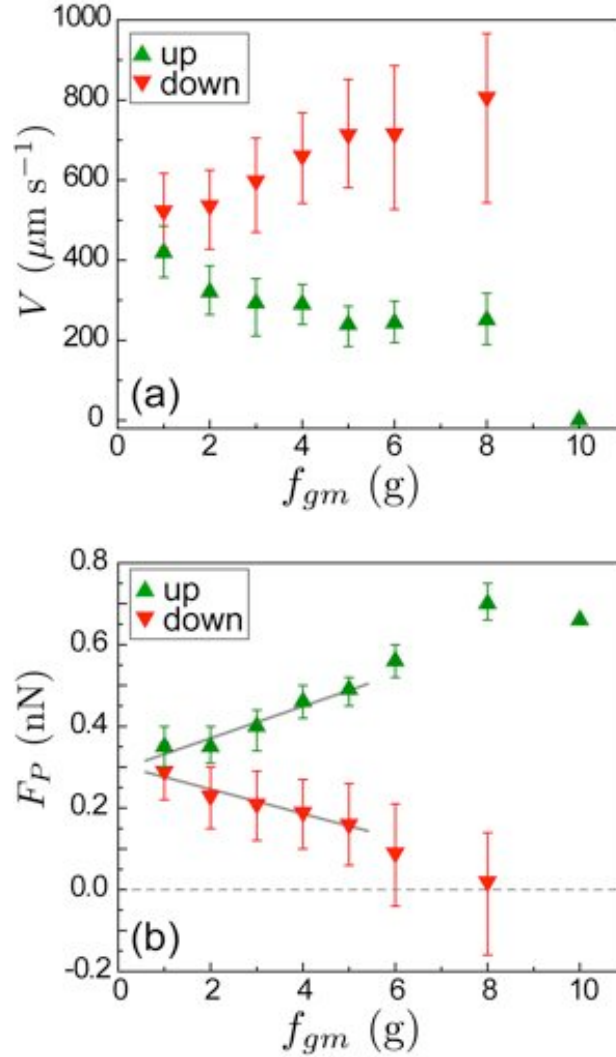
Figure 7.5: Gravikinesis in the high f_{gm} regime. (a) The swimming speed response becomes nonlinear for $f_{gm} > 5$ g. At 10 g, upward swimming paramecia stop advancing. No downward swimmers were observed. (b) Mean propulsion force, F_P, for up and down swimmers given by: $F_{P\uparrow}(f_{gm}) = \xi V_U(f_{gm}) + \Delta\rho V f_{gm}$, and $F_{P\downarrow}(f_{gm}) = \xi V_D(f_{gm}) - \Delta\rho V f_{gm}$, respectively. At $f_{gm} = 10$ g, $F_{P\uparrow}$ is estimated from stalled paramecia. The bars indicate the range of propulsion forces exhibited by the 68% of the swimmers nearest the mean.
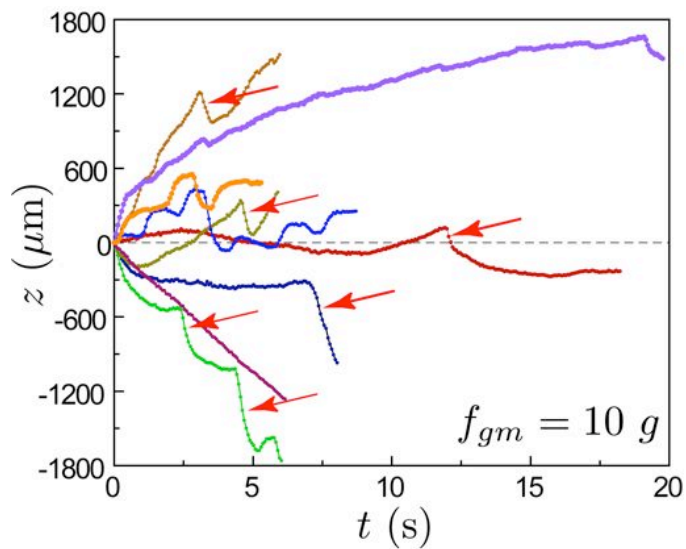
Figure 7.6: Vertical position of upward oriented paramecia at $f_{gm} = 10\ g$ as a function of time. Arrows show points where paramecia stop propelling and drop at a rate consistent with free sedimentation at $f_{gm} = 10\ g$.
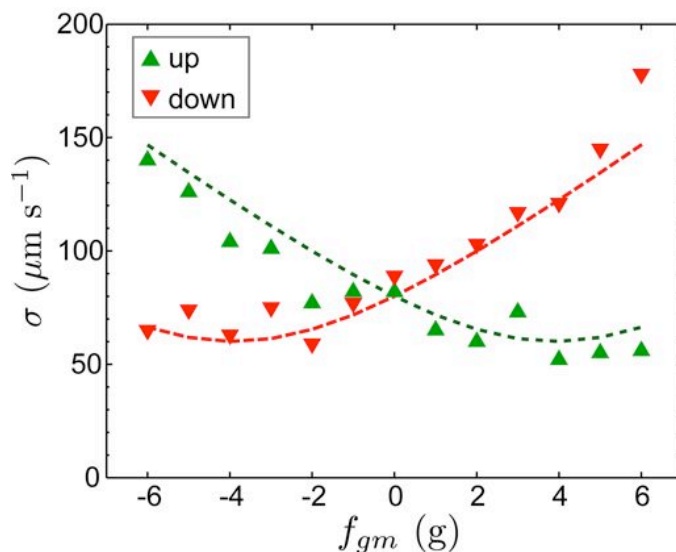
Figure 7.7: The dependence of the width of the velocity distribution, σ, on f_{gm}. The dashed lines are simultaneous fits to both sets of data considering two fitting parameters (see text for detail).

We can explain this behavior by considering the factors that contribute to σ and depend on f_{gm}. According to Eq. 7.12 the swimming speed of a paramecia at a given f_{gm} is the sum of its zero gravity propulsion, V_0, sedimentation, $V_S(f_{gm})$, and gravikinetic response, Δ_i (where i denotes up or down). These parameters each have a corresponding distribution width of $\sigma_{\Delta i}$, σ_S and σ_0, respectively. Generally, the total width, σ_i of the speed distribution can be written as:

$$\sigma_i^2 = \left(\frac{\partial V_i}{\partial V_0}\right)^2 \sigma_0^2 + \left(\frac{\partial V_i}{\partial V_S}\right)^2 \sigma_S^2 + \left(\frac{\partial V_i}{\partial \Delta_i}\right)^2 \sigma_{\Delta i}^2 +$$
$$+ 2\frac{\partial V_i}{\partial V_0}\frac{\partial V_i}{\partial V_S}\sigma_{0,S} + 2\frac{\partial V_i}{\partial V_0}\frac{\partial V_i}{\partial \Delta_i}\sigma_{0,\Delta i} + 2\frac{\partial V_i}{\partial V_S}\frac{\partial V_i}{\partial \Delta_i}\sigma_{S,\Delta i}. \tag{7.19}$$

where the cross terms are given by [100]:

$$\sigma_{0,S} = \frac{1}{N}\sum_{j=1}^{N}(V_{0j} - \bar{V}_0)(V_{Sj} - \bar{V}_S), \tag{7.20}$$

$$\sigma_{0,\Delta_i} = \frac{1}{N}\sum_{j=1}^{N}(V_{0j} - \bar{V}_0)(\Delta_{ij} - \bar{\Delta}_i),$$

$$\sigma_{S,\Delta_i} = \frac{1}{N}\sum_{j=1}^{N}(V_{Sj} - \bar{V}_S)(\Delta_{ij} - \bar{\Delta}_i).$$

The subscript j denotes the value for each individual, and N is the total number of paramecia. $\bar{V}_S$, $\bar{V}_0$, and $\bar{\Delta}_i$ represent the mean values of the distributions.

In the absence of correlations, the cross terms in Eq. 7.19 are zero and hence we expect σ_i to increase with $|f_{gm}|$. This is because $V_S(f_{gm})$ and $\Delta_i(f_{gm})$ are proportional to $|f_{gm}|$ and therefore σ_S and $\sigma_{\Delta i}$ are also linear functions of $|f_{gm}|$. Note that σ_0 does not depend on $|f_{gm}|$. To account for the near independence of σ_i on $|f_{gm}|$ for *Paramecium* swimming against the force, we need to consider the correlation terms. These can be negative, which will tend to reduce the total width. As a plausible example, consider that both propulsion and sedimentation depend on the drag coefficient. Paramecia that propel faster are likely to

sediment faster as well. Consequently, this correlation leads to $\sigma_{0,S} > 0$. For swimmers with the force, $\frac{\partial V_i}{\partial V_0} \frac{\partial V_i}{\partial V_S} > 0$, since the sedimentation and propulsion velocities point in the same direction. Therefore σ_i increases with f_{gm}. Conversely, σ_i decreases for swimmers against the force because the sedimentation and propulsion velocities point in opposite directions, resulting in $\frac{\partial V_i}{\partial V_0} \frac{\partial V_i}{\partial V_S} < 0$. That is, sedimentation pulls the faster swimmers back into the pack.

Considering a linear dependence of σ_S and $\sigma_{\Delta i}$ on f_{gm}, we rewrite Eq. 7.19, using Eq. 7.12

$$\sigma_U^2(f_{gm}) = \sigma_0^2 + \sigma_S^2 f_{gm}^2 + \sigma_{\Delta U}^2 f_{gm}^2 - 2\sigma_{0,S} f_{gm} - 2\sigma_{0,\Delta U} f_{gm} + 2\sigma_{S,\Delta U} f_{gm}^2, \tag{7.21}$$

$$\sigma_D^2(f_{gm}) = \sigma_0^2 + \sigma_S^2 f_{gm}^2 + \sigma_{\Delta D}^2 f_{gm}^2 + 2\sigma_{0,S} f_{gm} + 2\sigma_{0,\Delta D} f_{gm} + 2\sigma_{S,\Delta D} f_{gm}^2.$$

for the widths of the up and down distrtibutions. These have general parabolic form

$$\sigma_U^2(f_{gm}) = A - 2B f_{gm} + C f_{gm}^2, \tag{7.22}$$

$$\sigma_D^2(f_{gm}) = A + 2B f_{gm} + C f_{gm}^2.$$

where $A = \sigma_0^2$, $B = \sigma_{0,S} + \sigma_{0,\Delta}$, and $C = \sigma_S^2 + \sigma_\Delta^2 + 2\sigma_{S,\Delta}$. For simplicity we have assumed $\sigma_{S,\Delta U} = \sigma_{S,\Delta D} = \sigma_{S,\Delta}$.

A is known from the speed distribution at $f_{gm} = 0$ g, $\sigma_0 \simeq 85$ μm s^{-1}. Also from the sedimentation speed distribution, $\sigma_S \simeq 20$ μm s^{-1}. We tentatively assumed $\sigma_\Delta \simeq 10$ μm s^{-1} (about 20% of total Δ). The data in Table 7.4 includes the correlation parameters obtained from least square fitting of Eq. 7.21 to the data using two free parameters B and C. From C we can deduce $\sigma_{S,\Delta}$, but B only gives the sum of $\sigma_{0,\Delta} + \sigma_{0,S}$. Note that there is an upper bound to the fitting parameters given by Schwarz inequality: $|\sigma_{0,S}| \leq \sigma_0 \sigma_S$, $|\sigma_{0,\Delta}| \leq \sigma_0 \sigma_\Delta$, and $|\sigma_{S,\Delta}| \leq \sigma_S \sigma_\Delta$ [100].

Table 7.4: Correlation parameters from fits to Figure 7.7

Known parameter	Value (μm s^{-1})	Correlation coefficient	Value (μm s^{-1})	Upper threshold	Value μm s^{-1}
σ_0	85	$\sigma_{S,\Delta}$	-164	$\sigma_S \sigma_\Delta$	200
σ_S	20	$\sigma_{0,S} + \sigma_{0,\Delta}$	747	$\sigma_0 \sigma_S \times \sigma_0 \sigma_\Delta$	2250
σ_Δ	10				

Useful information can be obtained from these correlation parameters. For example, if a *Paramecium* sediments faster than average ($V_{Sj} > \bar{V}_S$), then in order for $\sigma_{S,\Delta} < 0$, we should have $\Delta_j < \bar{\Delta}$ (Eq. 7.20), meaning that a faster sedimenting *Paramecium* regulates more (Δ is a negative value). Since both $\sigma_{0,\Delta}$ and $\sigma_{0,S}$ are linearly proportional to f_{gm}, we can not comment on the nature of the correlation.

7.5 Helical trajectories in variable f_{gm}

Analyzing the helical motion of paramecia in various force fields can give useful information about their swimming mechanics. As we mentioned in Chapter 3, the amplitude and the pitch of these helical trajectories depend on the beating direction of the cilia. In turn, the beating direction and frequency of cilia are controlled by the membrane potential. Therefore, stimulations, such as an electric field or a mechanical obstacle that changes the membrane potential, changes the characteristics of the swimming trajectories. The question here is whether simulated gravity forces also affect the membrane potential to produce a kinetic response.

We attempted to measure the helix parameters for populations of paramecia when the simulated gravity was increased up to 5 g. From the swimming trajectories we were able
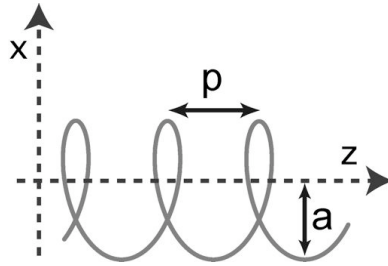
Figure 7.8: A schematic of a helix showing the amplitude (a) and the pitch (p). ω is related to the time between the two peaks.

to measure the pitch (p) which is the z distance between two consecutive peaks, the amplitude (a), which was determined by half the distance in the x direction between two peaks (Fig. 7.8), and also the time (t) of travel between two peaks. The latter is related to the angular velocity $\omega = 2\pi/t$. Figure 7.9 shows these three parameters. The dashed lines are linear fits to the data. The first approximation of the force simply seems to extend or compress the helix without altering a or ω. The data are very scattered which makes it quite hard to derive firmer conclusions. Perhaps measuring these parameters for an individual *Paramecium* in various gravity regions will yield more reliable results and would help clarify how the beating direction and the frequency of cilia are affected by variations in simulated gravity.

7.6   Summary

Paramecium exhibits a linear response to magnetically simulated hyper-gravity up to $f_{gm} = 5$ g, modifying its swimming as it would in the hyper-gravity of a centrifuge. Moreover, experiments from $f_{gm} = 0$ g to $f_{gm} = -5$ g showed that the response is symmetric, implying that the regulation of the swimming speed is primarily related to the buoyancy of the cell. The response becomes non-linear for simulated gravities higher than $f_{gm} = 5$ g. At
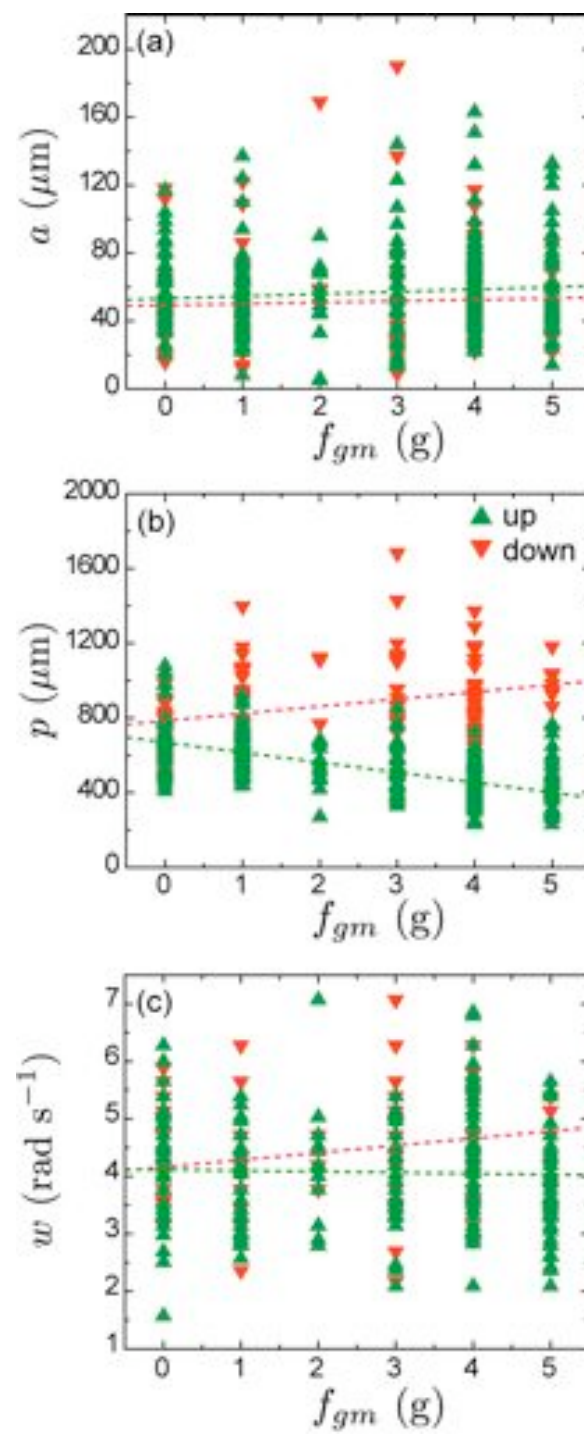
Figure 7.9: Helix parameters as a function of f_{gm}. (a) The amplitude. (b) The pitch. (c) the angular velocity.

$f_{gm} = 10 \, g$, many paramecia "stall" (i.e. swim in place against the force) exerting a maximum propulsion force estimated to be 0.7 nN.

Magnetic forces can vary the buoyancy of the cells in solutions similar to density variation methods. Moreover, one can invert the direction of total buoyancy as shown in Fig. 7.3. This quality can be helpful for determining whether paramecia employ a gravisensing mechanism similar to *Loxodes* [31]. *Loxodes* have organelles, called Müller bodies, containing $BaSO_4$ grains that are attached to the cell membrane by filaments. In a gravitational field, the displacement of this dense body with respect to the cell acts as the gravisensor [31]. *Paramecium* and others [63, 117], lack a specific gravisensing unit and it has been proposed that the whole cell acts as the statocyte [77]. These two mechanisms can be distinguished by changing the buoyancy of the cells. Increasing the density of the medium decreases the graviresponses of *Paramecium* [97, 121, 50] whereas it does not affect that of *Loxodes*. The symmetry of the graviresponse in Fig. 7.3 (i.e. inverting the buoyant force inverts their graviresponse). reinforces the claim that paramecia do not have an internal gravisensing organelles similar to $BaSO_4$ in *Loxodes*. If a gravisensing organelle were present then its buoyancy within the cytoplasm would have to vary in the same way as the buoyancy of the cell in solution. That is

$$\frac{\rho_{cell} - \rho_{sol}}{\chi_{cell} - \chi_{sol}} = \frac{\rho_{org} - \rho_{cyt}}{\chi_{org} - \chi_{cyt}} \tag{7.23}$$

would be necessary. The density and the diamagnetic susceptibility of the organelle and the cytoplasm is denoted by subscripts "org" and "cyt", respectively. For $BaSO_4$, $\rho_{org} = 4500$ kg m^{-3} and $\chi_{org} = -1.8 \times 10^{-5}$ (SI). If we approximately consider that $\chi_{cell} = \chi_{cyt} = \chi'_{cell}$ and $\rho_{cell} = \rho_{cyt}$ then the left-hand side of Eq. 7.23 will be about 10 times smaller than the right-hand side, which excludes the possibility of internal organelles or any other dense

particles responsible for gravisensitivity. Moreover, if there were any organelles, which satisfied Eq. 7.23, given the fact that we obtained very similar responses with two different Gd-DTPA concentrations, it seems highly unlikely that Eq. 7.23 would be satisfied for both concentrations. Therefor the presence of any internal organelle or external particle digested by the cell, which could act as a gravisensing body is highly unlikely. Considering that the forces exerted by the cytoplasm to the membrane are extremely small, the details by which such cells senses the gravitational field remains to be determind.

Chapter 8

Conclusion

Using intense magnetic fields and forces, it was shown that we can manipulate single cell organisms such as *Paramecium caudatum*. For example, the swimming trajectories of paramecia were affected by the presence of intense magnetic fields in such a way that they aligned parallel to the field. The orientation of motile paramecia by magnetic field was modeled successfully as a passive reaction to a magnetic torque exerted on diamagnetically anisotropic, structurally rigid components of the cells. The quality of the fits to this model indicates that the influence of other possible orienting mechanisms is negligible.

The orientation of immobilized *Paramecium* in the field supports the conclusion that the orientation is a passive response and thus, no physiological networks are required for this reaction. We have attributed the required net anisotropy of the diamagnetic anisotropy, to structures rigidly fixed within the cell cortex. The shape asymmetry of the cortex and the sign of the anisotropy of each of the cortical units combine so that paramecia experience a net torque aligning their long axis with a magnetic field.

The capability to exert a calibrated, non-invasive torque on a population of swimming

organisms has potential as a tool to aid investigations of their responses to other fields or perturbations. For instance, the galvanotactic response of paramecia involves a reorientation, whenever the applied electric field changes direction. This reorientation necessarily requires paramecia to exert a turning torque. The strength of this turning torque can be measured directly by balancing it with a magnetic torque. Thus, an active response can be measured using the passive response to a magnetic torque.

Moreover, magneto-orientation can be used to direct a population of swimming paramecia. This can be extremely helpful in studying the "kinetic" responses of paramecia to other fields such as gravity or chemical gradients, since it can yield a large population of directed swimmers. For example, *P. caudatum* exhibits a small negative gravikinesis. Upward swimmers propel themselves forward harder than downward swimmers [77, 49, 88, 97]. This behavior has received a great deal of attention as it is an example of gravisensitivity at the single cell level [74, 50, 16]. It can be difficult to measure, however, because it requires statistical vector analysis of a large number of swimming tracks that are oriented in random directions. To simplify matters, Machemer came up with the elegant idea of applying a second physical field to align the swimming paramecia along the gravity vector [77]. He exploited the galvanotactic response of the paramecia to create populations of either upward or downward swimmers. Unfortunately, the active response to the electric fields, which includes speed changes, complicates the analysis of the active gravitational response. By using magneto-orientation in gravikinesis experiments one can enjoy the benefits of Machemer's approach without the complications introduced by the superposition of two active responses.

We envision using this non-invasive physical field in conjunction with other fields such

as chemical gradients or electric fields to aidl in the studies of the sensitivity of *Paramecium* to these stimuli.

It was shown that magnetic forces can create variable buoyancy environments for living cells. As an application, neutrally buoyant immobilized *Paramecium* was subjected to simulated increased and inverted gravities and its magnetic susceptibility was measured from its moving rate in these simulated gravities. Also, this technique was applied to swimming populations of paramecia. With proper manipulation of the magnetic properties of the medium in which the paramecia swim, we were able to achieve a large range of simulated gravities between -8 g to 10 g. This experiment revealed that paramecia respond to simulated gravities by regulating their swimming speed in such a way that they always swim harder against the force than with the force (negative gravikinesis [77]).

These findings are promising in that they show that using magentically simulated gravities one can obtain true biological response which require sensing forces of about few pN. It can be used as an alternative to current "microgravity" simulation such as the rotating wall vessel suspension technique. For example, it can be used for the investigations of reduced shear stress on 3D tissue engineering [39, 112], changes in osteoblast growth [55], gene expression [46], and skeletal muscle adaptation [1], and cell signaling [23] that are induced by microgravity. More generally, this non-invasive technique can be used to apply forces to the whole bodies of populations of cells, and thus, can serve as an alternative to "point-like" methods like AFM [6] and magnetic tweezers [134] that apply local stresses to single cells.

Appendix A

Paramecium Culture

A.1 General information

Paramecium caudatum was purchased from Carolina Biological company. The culture usually contains some type of much smaller size flagellate. Before performing any experiments it is advisable to clean the culture of these flagellates. To do so, we need to start a new culture from a single *Paramecium*. This is done by first preparing the culture medium (below). Prepare about 6-8 small petri-dishes filled with test solution (1 mM $CaCl_2$, 1 mM KCl, 0.1 mM $MgSO_4$, 1.5 mM MOPS at pH 7.2). Take a small amount of *Paramecium* culture and dilute it in in a petri-dish with test solution. Using a glass pipette, take one *Paramecium* and place it in one of the petri-dishes. In this step probably more than one paramecium is caught. Now, from this second dish, track one *Paramecium* and transfer it to a clean dish. Repeat this few times until you make sure there is none of the other flagellate in the final dish. Then catch the *Paramecium* and place it in a small test tube filled with culture medium. Hopefully it will survive and multiply. For higher chance of

success. Prepare several test tube cultures. The tip of the glass pipette can be modified to become thinner by pulling it with a tweezer on a flame.

I would suggest that for future experiments, paramecia be obtained from a known lab. This will eliminate the problem of mixed cultures and also the strain of the *Paramecium* will be known. The latter is important for comparing results from various research groups. Carolina Biological Inc., does not have information about the strain of their paramecia.

A.2   Culturing procedure

They feed on bacteria that grows on decaying grains like rice and wheat or decaying timothy hey. The supply from the company comes in small containers of about 50 mL. To grow the culture, a culture medium which is based on one or a combination of the above mentioned grains is made. Then either one can leave the medium to sit for a day or so before inoculating it with *Paramecium* culture, or one can first inoculate the medium with a known Aerobactor and then inoculate it with *Paramecium* the next day. The latter is more accurate and more controllable method and thus recommended. Several culturing techniques can be found in literature [135].

A.2.1   culturing medium

The following is the wheat grass medium *. Wheat grass can also be substituted by timothy hey.

---

*Protocol provided by Megan S. Valentine from Prof. J. VanHouten's lab

Wheat grass was purchased from Pines International. It can be purchased in forms of pellets or animal grade powder.

Make sure to have:

- Stigmasterol (Sigma). Make 5 mg/mL in 100% Ethanol. The Stigmasterol should be kept in the freezer when not used. Before starting to make the medium, take it out of the freezer and place it on the stir plate.

- $Na_2HPO_4 \cdot 7H2O$.

- 2-3 one-liter Erlenmeyer Flasks

- 4 half liter or 8 quarter liter flasks

The following gives about 1 L of culture medium.

Wheat grass medium

1. Add 2.5 g wheat grass to 400 mL of distilled water 1 L and bring to boil.

2. Once the mixture comes to boil, reduce heat and simmer for 20 minutes.

3. After 20 min. take the flask off the heat and set aside on the counter

4. Pour 1 g of $Na_2HPO_4 \cdot 7H2O$ in a second empty 1 L flask. You can use distilled water to rinse the measuring boat.

5. Filter the medium into the second flask by using wrapped Kim Wipes with cheese cloth.

6. Once all the medium has been filtered into the second flask, use a Buchner funnel with Whatman #42 ashless filters to further filter the medium. Wet the filter with

distilled water before placing it in the funnel and be sure to only handle the filter by its edges. This process is slow and you might need to change the filter once or twice.

7. After all the fluid is filtered, add 0.6 mL of Stigmasterol into the fluid and bring the entire solution to

8. Mix the fluid by swirling it.

9. Divide the fluid in flask size of your choice. The flask should be filled by half.

10. Cover the top of the flask with aluminum foil and autoclave in a plastic bin for 50 minutes on "liquid".

A.3 Inoculation

After the culture medium has been autoclaved and cooled down to room temperature, we inoculate it with some type of Aerobactor that we have cultured on agar gel and we keep in the fridge.

1. Take out one plate of bacteria from the fridge

2. Use an inoculating loop that is sterilized by being held on a flame until it gets red. Wait few seconds.

3. Take a small dot of bacteria using the loop and insert it in the medium. Repeat this for each flask.

4. Cover the flasks, label the date and the type of culture (e.g. wheat medium inoculated by *aerobactor aeoregene*) and place it in an incubator at 32° over night.

5. After 24 h, the bacteria have grown in the medium (this is clear from the hazy medium) and it is time to inoculate the medium with paramecia from an old culture.

6. Add about 1/4 of the medium with the *Paramecium* culture. For example, if there is 200 mL of medium in the flask, I add 50 mL of *Paramecium.* If one has very dense stock then much smaller amout (about few mL will be enough).

7. Close the flask with Parafilm and replace it in auroclave in 22-25° for 3-4 days. After few days, the medium will clear up and the culture will be grown. If after 7-10 days the culture has not cleared up, this means that the medium is infected and the bacteria have taken over. At this point, one need to start a new culture.The way to avoid this from happening is to make sure all the equipment has been sterilized before using and also not to put too much bacteria from the agar culture. For experiments, the culture should be at least 5-7 days old to be in its logaritmic phase of growth.

A.4   Bacterial culture

To start for the first time, buy bacteria grown on agar from a supplier (e.g. *aerobactor aerogenes* from Carolina Biological Supply) and use it as described in section A.3 to have a medium with bacterial culture in it. From then on, keep some agar plates with bacteria always available in the fridge.

Bacteria are cultured on agar plates. To prepare the agar plates, first pour 4.6 g nutrient agar (purchased from any biological supplier) in 200 mL distilled water and boil for about 1 minute while stirring. Let cool down until temperature of medium is about 45-50°. Prepare 10 disposable sterile petri- dishes (keep the lids on until ready to pour the medium) and

pour the agar medium in them. Cover quickly with the lead and wait to cool down to room temperature. They will set like a stiff gelatine. These plates can be kept in the fridge for few months. Stack them upside down to prevent the condensation to contaminate the gel.

To start the bacterial culture, take few of the plate out of the fridge and let warm up to room temperature. Sterilize the inoculation loop as before and after few second dip into an inoculated medium from step 5, Sec.A.3. Then run the loop smoothly in a zig-zag pattern on the agar. Close the lid. Repeat this for all the plates. Remember to sterilize the loop each time. Store the plates upside down in the incubator at 32°. After 1-2 days the zig-zag pattern will be thick and small dotted areas of bacteria will be apparent. Store them upside down in the fridge.

A.5   Maintaining the *Paramecium* culture

The *Paramecium* culture need to be disinfected from time to time to stay healthy. Get a high density solution by low speed centrifugation and place them in 10 mL of room temperature Dryl's solution with 100 μL of gentimicin (gentimicin sulfate, Sigma). Let them stay in this solution for one hour to kill the bacteria as well as allow any food vacuoles to pass through the paramecia. After one hour, the tubes are spun down and the pelleted paramecia are removed and placed in the new culture.

Appendix B

AMI magnet cool-down procedure

B.1   24 hours before transferring He

- Blow N_2 gas for 15 minutes in the inside compartment. Pressure about 40 kPa.

- Connect Ohm meter to the leads

- Open side flange.

- Connect two rubber tubings to leads but let ends open.

- Transfer liquid N_2 to the inside partition. Starting resistance of the leads is about 1.5 Ohms (with the stabilizing resistance attached, without this resistance the resistance across the leads is about 5 ohms). Note, since the N_2 transfer tube is not long enough, first put the long-end inside the magnet dewar and then connect the other end to the storage tank.

- Takes about 1 hour to transfer.

- After liquid N_2 starts to come out of the side flange, stop the transfer.

- Close all openings.

B.2 The day of He transfer

- Close the leads by connecting the rubber tubing from one to the other.

- Transfer liquid N_2 into the outside jacket by connecting He gas (or N_2) to the side flange. Pressure approximately 30 kPa.

- Usually after 15 minutes liquid N_2 starts collecting in the jacket.

- Takes about 45 minutes for the inner compartment to become empty of liquid N_2. This can be seen by softening of the rubber transfer tube.

- Blow He gas inside the inner compartment for 30 minutes Note: let gas blow from each lead separately to be sure there is no liquid N_2 trapped in between.

- Wait one hour before transferring He.

B.3 During He transfer

- Check lead resistance (normally around 1.5 Ohms with the stabilizing resistor).

- Put the transfer line first in the He storage dewar, entering very slowly so that the tube gets cold. Someone should hold the other end of the tube and be ready to insert it inside the magnet inner dewar as soon as liquid starts to come out. Make sure the side flange is open.

- Connect He gas to storage dewar. Pressurize slightly (between first and second black lines about 20-30kPa).

- The resistance drops to 0.3 Ohms after about 45-50 minutes

- Check the plume situation. A sharp plume indicates that the He storage dewar is empty.

- A typical transfer takes about 1 hour.

- Remember to mark down the total transferred and lost helium.

B.4   After transfer

- Connect the nozzle to the side flange and attach the rubber tube on it.

- Pull out leads. Leave the 2 pieces of the rubber tubing hanging from the leads.

- Set the He sensor to sample mode (30 min or 1 h).

- Use RS 232 cable + hyperterminal on windows to record sensor values. Save every once in a while as txt file. Later, this file can be imported into a speadsheet and be used to determine the He loss rate.

Bibliography

[1] G. R. Adams, V. J. Caiozzo, and K. M. Baldwin. Skeletal muscle unweighting: Space-flight and ground-based models. *Journal of Applied Physiology*, 95(6):2185–2201, 2003.

[2] G. Albrecht-Buehler. Possible mechanisms of indirect gravity sensing by cells. *ASGSB Bull*, 4(2):25–34, 1991.

[3] R. D. Allen. Fine structure of the memranous and microfibrillar sysytem in the cortex of paramecium caudatum. *J. Cell. Biol.*, 49:1–20, 1973.

[4] S. A. Baba, Y. Mogami, and T. Otsu. Evaluation of gravity-dependent membrane potential shift in paramecium. *Life Sciences: Microgravity Research I*, 23:2065–2073, 1999.

[5] P. W. Barlow. Gravity perception in plants - a multiplicity of systems derived by evolution. *Plant Cell and Environment*, 18(9):951–962, 1995.

[6] A. R. Bausch, F. Ziemann, A. A. Boulbitch, K. Jacobson, and E. Sackmann. Local measurements of viscoelastic parameters of adherent cell surfaces by magnetic bead microrheometry. *Biophysical Journal*, 75(4):2038–2049, 1998.

[7] E. Beaugnon and R. Tournier. Levitation of organic materials. *Nature*, 349(6309):470–470, 1991.

[8] E. Beaugnon and R. Tournier. Levitation of water and organic-substances in high static magnetic-fields. *Journal De Physique Iii*, 1(8):1423–1428, 1991.

[9] Howard C Berg. *Random Walks in Biology*. Princeton University Press, 1993.

[10] A K Geim Berry M V. Of flying frogs and levitrons. *European Journal of Physics*, 18:307–313, 1997.

[11] A. D. Bird, I. R. Dixon, and J. Toth. Design of the next generation of florida-bitter magnets at the nhmfl. *Ieee Transactions on Applied Superconductivity*, 14(2):1253–1256, 2004.

[12] W. Bras, G. P. Diakun, J. F. Diaz, G. Maret, H. Kramer, J. Bordas, and F. J. Medrano. The susceptibility of pure tubulin to high magnetic fields: A magnetic birefringence and x-ray fiber diffraction study. *Biophysical Journal*, 74(3):1509–1521, 1998.

[13] J. S. Brooks, J. A. Reavis, R. A. Medwood, T. F. Stalcup, M. W. Meisel, E. Steinberg, L. Arnowitz, C. C. Stover, and Jaaj Perenboom. New opportunities in science, materials, and biological systems in the low-gravity (magnetic levitation) environment (invited). *Journal Of Applied Physics*, 87(9):6194–6199, 2000.

[14] R. Brucker, S. Machemer Rohnisch, and H. Machemer. Graviresponses in paramecium-caudatum and didinium-nasutum examined under varied hypergravity conditions. *Journal Of Experimental Biology*, 197:271–294, 1994.

[15] R. Brucker, A. Murakami, K. Ikegaya, K. Yoshimura, K. Takahashi, S. Machemer-Rohnisch, and H. Machemer. Relaxation and activation of graviresponses in paramecium caudatum. *Journal Of Experimental Biology*, 201(14):2103–2113, 1998.

[16] Richard; Brucker, Augusto; Cogoli, and Ruth Hemmersbach. Graviperception and graviresponse at the cellular level. In Gerda Horneck and Christa Baumstark-Khan, editors, *Astrobiology: The Quest for the Conditions of Life.*, pages 287 – 296. Springer, Berlin, 2002.

[17] A. T. Catherall, L. Eaves, P. J. King, and S. R. Booth. Floating gold in cryogenic oxygen. *Nature*, 422(6932):579–579, 2003.

[18] G. T. Charras, B. A. Williams, S. M. Sims, and M. A. Horton. Estimating the sensitivity of mechanosensitive ion channels to membrane strain and tension. *Biophysical Journal*, 87(4):2870–2884, 2004.

[19] X. B. Chen and H. C. Berg. Torque-speed relationship of the flagellar rotary motor of escherichia coli. *Biophysical Journal*, 78(2):1036–1041, 2000.

[20] Z. D. Cheng, P. M. Chaikin, J. X. Zhu, W. B. Russel, and W. V. Meyer. Crystallization kinetics of hard spheres in microgravity in the coexistence regime: Interactions between growing crystallites. *Physical Review Letters*, 88(1), 2002.

[21] Stephen Childress. *Mechanics of Swimming and Flying.* Cambridge University Press, 1981.

[22] M. R. Clegg, S. C. Maberly, and R. I. Jones. Behavioural responses of freshwater phytoplanktonic flagellates to a temperature gradient. *European Journal of Phycology*, 38(3):195–203, 2003.

[23] A. Cogoli, A. Tschopp, and P. Fuchsbislin. Cell sensitivity to gravity. *Science*, 225(4658):228–230, 1984.

[24] G. Colombetti and F. Lenci. Photoreception and photomovements in microorganisms. *Symposia of the Society for Experimental Biology*, 36:399–422, 1983.

[25] H. C. Crenshaw. Orientation by helical motion .3. microorganisms can orient to stimuli by changing the direction of their rotational velocity. *Bulletin Of Mathematical Biology*, 55(1):231–255, 1993.

[26] H. C. Crenshaw and L. Edelsteinkeshet. Orientation by helical motion .2. changing the direction of the axis of motion. *Bulletin Of Mathematical Biology*, 55(1):213–230, 1993.

[27] R. Hemmersbach D. P. Hader and M. Lebert. *Gravity and the Behavior of Unicellular Organisms.* Cambrodge University Press, 2005.

[28] J. M. Denegre, J. M. Valles, K. Lin, W. B. Jordan, and K. L. Mowry. Cleavage planes in frog eggs are altered by strong magnetic fields. *Proceedings of the National Academy of Sciences of the United States of America*, 95(25):14729–14732, 1998.

[29] S. Dryl. Chemotaxis in paramecium caudatum as adaptive response of organism to its environment. *Acta Biol Exp (Warsz)*, 21:75–83, 1961.

[30] R. Naitoh Y. Eckert. Passive electrical properties of paramecium and problems of ciliary coordination. *J Gen Physiol*, 55(4):467–83, 1970.

[31] T. Fenchel and B. J. Finlay. Geotaxis in the ciliated protozoan loxodes. *Journal of Experimental Biology*, 110(MAY):17–33, 1984.

[32] K. J. Fitzelle and J. Z. Kiss. Restoration of gravitropic sensitivity in starch-deficient mutants of arabidopsis by hypergravity. *Journal of Experimental Botany*, 52(355):265–275, 2001.

[33] R. B. Frankel and R. P. Blakemore. Navigational compass in magnetic bacteria. *Journal Of Magnetism And Magnetic Materials*, 15-8(JAN-):1562–1564, 1980.

[34] L. E. Freed, R. Langer, I. Martin, N. R. Pellis, and G. VunjakNovakovic. Tissue engineering of cartilage in space. *Proceedings of the National Academy of Sciences of the United States of America*, 94(25):13885–13890, 1997.

[35] K. Fukui and H. Asai. Negative geotactic behavior of paramecium-caudatum is completely described by the mechanism of buoyancy-oriented upward swimming. *Biophysical Journal*, 47(4):479–482, 1985.

[36] A. K. Geim, M. D. Simon, M. I. Boamfa, and L. O. Heflinger. Magnet levitation at your fingertips. *Nature*, 400(6742):323–324, 1999.

[37] L. Gheber, A. Korngreen, and Z. Priel. Effect of viscosity on metachrony in mucus propelling cilia. *Cell Motility and the Cytoskeleton*, 39(1):9–20, 1998.

[38] I. R. Gibbons. Cilia and flagella of eukaryotes. *Journal of Cell Biology*, 91(3):S107–S124, 1981.

[39] T. J. Goodwin, T. L. Prewett, D. A. Wolf, and G. F. Spaulding. Reduced shear-stress - a major component in the ability of mammalian-tissues to form 3-dimensional assemblies in simulated microgravity. *Journal of Cellular Biochemistry*, 51(3):301–311, 1993.

[40] S. Gueron and K. Levit-Gurevich. Energetic considerations of ciliary beating and the advantage of metachronal coordination. *Proceedings of the National Academy of Sciences of the United States of America*, 96(22):12240–12245, 1999.

[41] S. Gueron, K. LevitGurevich, N. Liron, and J. J. Blum. Cilia internal mechanism and metachronal coordination as the result of hydrodynamical coupling. *Proceedings of the National Academy of Sciences of the United States of America*, 94(12):6001–6006, 1997.

[42] K. Guevorkian and J. M. Valles. Varying the effective buoyancy of cells using magnetic force. *Applied Physics Letters*, 84(24):4863–4865, 2004.

[43] Karine Guevorkian and James M Valles. In situ imaging of micro-organisms in intense magnetic fields. *Review of Scientific Instruments*, 76:103706–8, 2005.

[44] D. P. Hader. Polarotaxis, gravitaxis and vertical phototaxis in the green flagellate, euglena-gracilis. *Archives Of Microbiology*, 147(2):179–183, 1987.

[45] O. P. Hamill and B. Martinac. Molecular basis of mechanotransduction in living cells. *Physiological Reviews*, 81(2):685–740, 2001.

[46] T. G. Hammond, F. C. Lewis, T. J. Goodwin, R. M. Linnehan, D. A. Wolf, K. P. Hire, W. C. Campbell, E. Benes, K. C. O'Reilly, R. K. Globus, and J. H. Kaysen. Gene expression in space. *Nature Medicine*, 5(4):359–359, 1999.

[47] J. Happel and H. Brenner. *Low Reynolds Number Hydrodynamics, with Special Applications to Particulate Media*. Leyden, Noordhoff International Publishing, 2d rev. ed edition, 1973.

[48] R. Hemmersbach and D. P. Hader. Graviresponses of certain ciliates and flagellates. *Faseb Journal*, 13:S69–S75, 1999.

[49] R. Hemmersbach, R. Voormanns, W. Briegleb, N. Rieder, and D. P. Hader. Influence of accelerations on the spatial orientation of loxodes and paramecium. *Journal Of Biotechnology*, 47(2-3):271–278, 1996.

[50] R. Hemmersbach, R. Voormanns, B. Bromeis, N. Schmidt, H. Rabien, and K. Ivanova. Comparative studies of the graviresponses of paramecium and loxodes. *Life Sciences: Microgravity Research*, 21(8-9):1285–1289, 1998.

[51] T. Hennessey and D. L. Nelson. Thermosensory behavior in paramecium-tetraurelia - quantitative assay and some factors that influence thermal avoidance. *Journal Of General Microbiology*, 112(JUN):337–347, 1979.

[52] T. Higashi, S. Sagawa, N. Kawaguchi, and A. Yamagishi. Effects of a strong static magnetic-field on blood-platelets. *Platelets*, 4(6):341–342, 1993.

[53] T. Higashi, A. Yamagishi, T. Takeuchi, N. Kawaguchi, S. Sagawa, S. Onishi, and M. Date. Orientation of erythrocytes in a strong static magnetic-field. *Blood*, 82(4):1328–1334, 1993.

[54] F. T. Hong. Magnetic-field effects on biomolecules, cells, and living organisms. *Biosystems*, 36(3):187–229, 1995.

[55] M. HughesFulford and M. L. Lewis. Effects of microgravity on osteoblast growth activation. *Experimental Cell Research*, 224(1):103–109, 1996.

[56] Y. Ikezoe, N. Hirota, J. Nakagawa, and K. Kitazawa. Making water levitate. *Nature*, 393(6687):749–750, 1998.

[57] K. Iwatsuki and Y. Naitoh. Photoresponses in colorless paramecium. *Experientia*, 38(12):1453–1454, 1982.

[58] K. Iwatsuki and Y. Naitoh. Behavioral-responses in paramecium-multimicronucleatum to visible-light. *Photochemistry And Photobiology*, 37(4):415–419, 1983.

[59] Van Wagtendonk W. J., editor. *Paramecium a Current Survey*. Elsevier Scientific Publishing Company, 1974.

[60] P. A. Janmey and D. A. Weitz. Dealing with mechanics: Mechanisms of force transduction in cells. *Trends in Biochemical Sciences*, 29(7):364–370, 2004.

[61] H. S. Jennings. *Behavior of Lower Organisms*. Indiana University Press, Bloomington, 1962.

[62] M. Kim and T. R. Powers. Hydrodynamic interactions between rotating helices. *Physical Review E*, 69(6), 2004.

[63] J. Z. Kiss. Mechanisms of the early phases of plant gravitropism. *Critical Reviews in Plant Sciences*, 19(6):551–573, 2000.

[64] C. Kung. A possible unifying principle for mechanosensation. *Nature*, 436(7051):647–654, 2005.

[65] K. Kuroda and N. Kamiya. Propulsive force of paramecium as revealed by the video centrifuge microscope. *Experimental Cell Research*, 184(1):268–272, 1989.

[66] O. A. Kuznetsov and K. H. Hasenstein. Intracellular magnetophoresis of amyloplasts and induction of root curvature. *Planta*, 198(1):87–94, 1996.

[67] J. Larsen, K. Barkalow, T. Hamasaki, and P. Satir. Structural and functional-characterization of paramecium dynein - initial studies. *Journal of Protozoology*, 38(1):55–61, 1991.

[68] F. Lenci and G. Colombetti. Photo-behavior of microorganisms - biophysical approach. *Annual Review Of Biophysics And Bioengineering*, 7:341–361, 1978.

[69] C. T. Lim, E. H. Zhou, and S. T. Quek. Mechanical models for living cells - a review. *Journal of Biomechanics*, 39(2):195–216, 2006.

[70] S. X. Lin, M. Zhou, A. Azzi, G. J. Xu, N. I. Wakayama, and M. Ataka. Magnet used for protein crystallization: Novel attempts to improve the crystal quality. *Biochemical and Biophysical Research Communications*, 275(2):274–278, 2000.

[71] H. Machemer. Ciliary activity and origin of metachromy in paramecium - effects of increased viscosity. *Journal of Experimental Biology*, 57:239, 1972.

[72] H. Machemer. Temperature influences on ciliary beat and metacronal coordination in paramecium. *Journal of mechanochemical cell motility*, 1:57–66, 1972.

[73] H. Machemer. Frequency and directional responses of cilia to membrane potential chnages in paramecium. *J. comp. Physiol.*, 92:293–316, 1974.

[74] H. Machemer. Mechanisms of graviperception and response in unicellular systems. *Life Sciences: Microgravity Research*, 21:1243–1251, 1998.

[75] H. Machemer and R. Braucker. Gravireception and graviresponses in ciliates. *Acta Protozoologica*, 31(4):185–214, 1992.

[76] H. Machemer, S. Machemerrohnisch, and R. Braucker. Velocity and graviresponses in paramecium during adaptation and varied oxygen concentrations. *Archiv Fur Protistenkunde*, 143(4):285–296, 1993.

[77] H. Machemer, S. Machemerrohnisch, R. Braucker, and K. Takahashi. Gravikinesis in paramecium - theory and isolation of a physiological-response to the natural gravity vector. *Journal Of Comparative Physiology A-Sensory Neural And Behavioral Physiology*, 168(1):1–12, 1991.

[78] H. Machemer and K. Sugino. Electrophysiological control of ciliary beating - a basis of motile behavior in ciliated protozoa. *Comparative Biochemistry And Physiology A-Physiology*, 94(2):365–374, 1989.

[79] S. Machemer Rohnisch, R. Braucker, and H. Machemer. Neutral gravitaxis of gliding loxodes exposed to normal and raised gravity. *Journal of Comparative Physiology a-Sensory Neural and Behavioral Physiology*, 171(6):779–790, 1993.

[80] S. Machemer Rohnisch, H. Machemer, and R. Braucker. Electric-field effects on gravikinesis in paramecium. *Journal Of Comparative Physiology A-Sensory Neural And Behavioral Physiology*, 179(2):213–226, 1996.

[81] M. P. Mahajan, P. L. Taylor, and C. Rosenblatt. Magnetic levitation of liquid crystals. *Liquid Crystals*, 23(4):547–550, 1997.

[82] M. P. Mahajan, M. Tsige, S. Y. Zhang, J. I. D. Alexander, P. L. Taylor, and C. Rosenblatt. Collapse dynamics of liquid bridges investigated by time-varying magnetic levitation. *Physical Review Letters*, 84(2):338–341, 2000.

[83] G. Maret. Recent biophysical studies in high magnetic-fields. *Physica B*, 164(1-2):205–212, 1990.

[84] B. D. Matthews, D. A. LaVan, D. R. Overby, J. Karavitis, and D. E. Ingber. Electromagnetic needles with submicron pole tip radii for nanomanipulation of biomolecules and living cells. *Applied Physics Letters*, 85(14):2968–2970, 2004.

[85] J. Miyakoshi. Effects of static magnetic fields at the cellular level. *Progress In Biophysics and Molecular Biology*, 87(2-3):213–223, 2005.

[86] Y. Mogami and S. A. Baba. Super-helix model: A physiological model for gravitaxis of paramecium. *Life Sciences: Microgravity Research*, 21:1291–1300, 1998.

[87] Y. Mogami, J. Ishii, and S. A. Baba. Theoretical and experimental dissection of gravity-dependent mechanical orientation in gravitactic microorganisms. *Biological Bulletin*, 201(1):26–33, 2001.

[88] U. Nagel and H. Machemer. Physical and physiological components of the graviresponses of wild-type and mutant paramecium tetraurelia. *Journal Of Experimental Biology*, 203(6):1059–1070, 2000.

[89] Y. Naitoh and K. Sugino. Ciliary movement and its control in paramecium. *Journal of Protozoology*, 31(1):31–40, 1984.

[90] Y. Eckert R. Naitoh. Ciliary orientation: Controlled by cell membrane or by intracellular fibrils? *Science*, 166(913):1633–5, 1969.

[91] Y. Eckert R. Naitoh. Ionic mechanisms controlling behavioral responses of paramecium to mechanical stimulation. *Science*, 164(882):963–5, 1969.

[92] Y. Nakaoka, R. Takeda, and K. Shimizu. Orientation of paramecium swimming in a dc magnetic field. *Bioelectromagnetics*, 23(8):607–613, 2002.

[93] Y. Nakaoka, H. Tanaka, and F. Oosawa. Ca-2(+)-dependent regulation of beat frequency of cilia in paramecium. *Journal of Cell Science*, 65(JAN):223–231, 1984.

[94] D. C. Neugebauer, S. Machemer-Rohnisch, U. Nagel, R. Braucker, and H. Machemer. Evidence of central and peripheral gravireception in the ciliate loxodes striatus. *Journal Of Comparative Physiology A-Sensory Neural And Behavioral Physiology*, 183(3):303–311, 1998.

[95] W. Nultsch and D. P. Hader. Photomovement in motile microorganisms .2. *Photochemistry and Photobiology*, 47(6):837–869, 1988.

[96] Tim Oliver, Micah Dembo, and Ken Jacobson. Separation of propulsive and adhesive traction stresses in locomoting keratocytes. *J. Cell Biol.*, 145(3):589–604, 1999.

[97] M. Ooya, Y. Mogami, A. Izumikurotani, and S. A. Baba. Gravity-induced changes in propulsion of paramecium-caudatum - a possible role of gravireception in protozoan behavior. *Journal Of Experimental Biology*, 163:153–167, 1992.

[98] G. Perbal and D. Driss-Ecole. Mechanotransduction in gravisensing cells. *Trends in Plant Science*, 8(10):498–504, 2003.

[99] T.C. Lubensky P.M. Chaikin. *Principles of Condensed Matter Physics.* Cambridge University Press, 1995.

[100] Taylor J. R. *An Introduction to Error Analysis.* University Science Books, Sausalito, 2nd edition, 1997.

[101] R. R. Raylman, A. C. Clavo, and R. L. Wahl. Exposure to strong static magnetic field slows the growth of human cancer cells in vitro. *Bioelectromagnetics*, 17(5):358–363, 1996.

[102] A. M. Roberts. Motion of paramecium in static electric and magnetic fields. *Journal of Theoretical Biology*, 27:97–106, 1969.

[103] A. M. Roberts. Motion of paramecium in static electric and magnetic fields. *Journal of Theoretical Biology*, 27(1):97–106, 1970.

[104] A. M. Roberts and F. M. Deacon. Gravitaxis in motile micro-organisms: The role of fore-aft body asymmetry. *Journal Of Fluid Mechanics*, 452:405–423, 2002.

[105] A. D. Rosen. A proposed mechanism for the action of strong static magnetic fields on biomembranes. *International Journal of Neuroscience*, 73((1-2)):115–9, 1993.

[106] A. D. Rosen. Mechanism of action of moderate-intensity static magnetic fields on biological systems. *Cell Biochemistry And Biophysics*, 39(2):163–173, 2003.

[107] M. S. Rosen and A. D. Rosen. Magnetic-field influence on paramecium motility. *Life Sciences*, 46(21):1509–1515, 1990.

[108] P. Satir, J. Waissteider, S. Lebduska, A. Nasr, and J. Avolio. The mechanochemical cycle of the dynein arm. *Cell Motility and the Cytoskeleton*, 1(3):303–327, 1981.

[109] J. F. Schenck. Safety of strong, static magnetic fields. *Journal of Magnetic Resonance Imaging*, 12(1):2–19, 2000.

[110] I. B. Schiffer, W. G. Schreiber, R. Graf, E. M. Schreiber, D. Jung, D. M. Rose, M. Hehn, S. Gebhard, J. Sagemuller, H. W. Spiess, F. Oesch, M. Thelen, and J. G. Hengstler. No influence of magnetic fields on cell cycle progression using conditions relevant for patients during mri. *Bioelectromagnetics*, 24(4):241–250, 2003.

[111] P. N. Segre, F. Liu, P. Umbanhowar, and D. A. Weitz. An effective gravitational temperature for sedimentation. *Nature*, 409(6820):594–597, 2001.

[112] V. I. Sikavitsas, G. N. Bancroft, and A. G. Mikos. Formation of three-dimensional cell/polymer constructs for bone tissue engineering in a spinner flask and a rotating wall vessel bioreactor. *Journal of Biomedical Materials Research*, 62(1):136–148, 2002.

[113] M. D. Simon and A. K. Geim. Diamagnetic levitation: Flying frogs and floating magnets (invited). *Journal of Applied Physics*, 87(9):6200–6204, 2000.

[114] M. A. Sleigh. Ciliart coordination in protozoa. *Progress in Protozoology*, pages 110–111, 1965.

[115] William R. Smythe. *Static and Dynamic Electricity*. McGraw-Hill Book Company, 3rd edition, 1968.

[116] K. A. Souza, S. D. Black, and R. J. Wassersug. Amphibian development in the virtual absence of gravity. *Proceedings of the National Academy of Sciences of the United States of America*, 92(6):1975–1978, 1995.

[117] M. P. Staves. Cytoplasmic streaming and gravity sensing in chara internodal cells. *Planta*, 203:S79–S84, 1997.

[118] Keith R. Symon. *Mechanics*. Addison-Wesley Publishin Company, 1971.

[119] J. Tabony. Morphological bifurcations involving reaction-diffusion processes during microtubule formation. *Science*, 264(5156):245–248, 1994.

[120] T. Takeuchi, T. Mizuno, T. Higashi, A. Yamagishi, and M. Date. High-field magnetic orientation of red-blood-cells. *Physica B*, 201:601–605, 1994.

[121] K. Taneda. Geotactic behavior in paramecium-caudatum .1. geotaxis assay of individual specimen. *Zoological Science*, 4(5):781–788, 1987.

[122] J. Torbet. Using magnetic orientation to study structure and assembly. *Trends In Biochemical Sciences*, 12(8):327–330, 1987.

[123] James Torbet. Magnetic orientation in biology:virus structure-blood clot assembly-cell guidance. In H. Wanda and H. J. Schneider-Muntau, editors, *Material Processing in Magnetic Fields*. World Scientific Publishing Co. Pte. Ltd., 2005.

[124] M. A. Tsai, R. S. Frank, and R. E. Waugh. Passive mechanical-behavior of human neutrophils - power-law fluid. *Biophysical Journal*, 65(5):2078–2088, 1993.

[125] O. Valiron, L. Peris, G. Rikken, A. Schweitzer, Y. Saoudi, C. Remy, and D. Job. Cellular disorders induced by high magnetic fields. *Journal of Magnetic Resonance Imaging*, 22(3):334–340, 2005.

[126] J. M. Valles. Model of magnetic field-induced mitotic apparatus reorientation in frog eggs. *Biophysical Journal*, 82(3):1260–1265, 2002.

[127] J. M. Valles, K. Lin, J. M. Denegre, and K. L. Mowry. Stable magnetic field gradient levitation of xenopus laevis: Toward low-gravity simulation. *Biophysical Journal*, 73(2):1130–1133, 1997.

[128] J. M. Valles, S. Wasserman, J. M. Denegre, and K. L. Mowry. Microscope system for use in high magnetic fields. *Review Of Scientific Instruments*, 71(8):3108–3110, 2000.

[129] J. M. Valles, Srrm Wasserman, C. Schweidenback, J. Edwardson, J. M. Denegre, and K. L. Mowry. Processes that occur before second cleavage determine third cleavage orientation in xenopus. *Experimental Cell Research*, 274(1):112–118, 2002.

[130] Aham Van Hoek, V. S. I. Sprakel, T. A. Van Alen, A. P. R. Theuvenet, G. D. Vogels, and J. H. P. Hackstein. Voltage-dependent reversal of anodic galvanotaxis in nyctotherus ovalis. *Journal Of Eukaryotic Microbiology*, 46(4):427–433, 1999.

[131] J. Vanhouten. Membrane-potential changes during chemokinesis in paramecium. *Science*, 204(4397):1100–1103, 1979.

[132] J. Vanhouten, E. Martel, and T. Kasch. Kinetic-analysis of chemokinesis of paramecium. *Journal of Protozoology*, 29(2):226–230, 1982.

[133] A. Vergara, B. Lorber, A. Zagari, and R. Giege. Physical aspects of protein crystal growth investigated with the advanced protein crystallization facility in reduced-gravity environments. *Acta Crystallographica Section D-Biological Crystallography*, 59:2–15, 2003.

[134] H. Weinmann, R. C. Brasch, W. R. Press, and G. E. Wesbey. Characteristics of gadolinium-dtpa complex: A potential nmr contrast agent. *American Journal of Roentgenology*, 142(3):619–24, 1984.

[135] R. Wichterman. *The Biology of Parameicum.* Plenium Press, second edition, 1985.

[136] A. Winkleman, K. L. Gudiksen, D. Ryan, G. M. Whitesides, D. Greenfield, and M. Prentiss. A magnetic trap for living cells suspended in a paramagnetic buffer. *Applied Physics Letters*, 85(12):2411–2413, 2004.

[137] A. Yamagishi, T. Takeuchi, T. Higashi, and M. Date. Diamagnetic orientation of blood-cells in high magnetic-field. *Physica B*, 177(1-4):523–526, 1992.

[138] S. Yanagiya, G. Sazaki, S. D. Durbin, S. Miyashita, K. Nakajima, H. Komatsu, K. Watanabe, and M. Motokawa. Effects of a magnetic field on the growth rate of tetragonal lysozyme crystals. *Journal Of Crystal Growth*, 208(1-4):645–650, 2000.

[139] D. C. Yin, N. I. Wakayama, K. Harata, M. Fujiwara, T. Kiyoshi, H. Wada, N. Niimura, S. Arai, W. D. Huang, and Y. Tanimoto. Formation of protein crystals (orthorhombic lysozyme) in quasi-microgravity environment obtained by superconducting magnet. *Journal of Crystal Growth*, 270(1-2):184–191, 2004.

[140] Q. M. Zhang, M. Tokiwa, T. Doi, T. Nakahara, P. W. Chang, N. Nakamura, M. Hori, J. Miyakoshi, and S. Yonei. Strong static magnetic field and the induction of mutations through elevated production of reactive oxygen species in escherichia coli soxr. *International Journal of Radiation Biology*, 79(4):281–286, 2003.